CAAP Quarterly Report

(Revised on June 29, 2025)

Project Name: Enhancing Knowledge and Technology to Prevent and Mitigate Risks of Stress Corrosion Cracking (SCC) for Pipeline Integrity Management

Contract Number: 693JK32450002CAAP

Prime University: Stevens Institute of Technology

Prepared By: Yi Bao, yi.bao@stevens.edu, 201-216-5223

Reporting Period: [01/01/2025-03/28/2025]

Project Activities for Reporting Period:

In this quarter, we completed the literature review on pipeline Stress Corrosion Cracking (SCC). Based on prior research and current industry standards and practices, a comprehensive review was conducted to integrate knowledge about SCC across three key categories:

- Basic knowledge about pipeline SCC
- Monitoring techniques for pipeline SCC
- Risk mitigation solutions

The review on fundamental knowledge of pipeline SCC primarily focuses on understanding the underlying mechanisms, evolution of SCC over time, and various factors that influence the occurrence and progression of SCC. These topics were briefly discussed in the first quarterly report. In this report, additional insights have been provided to deepen the understanding of the complex interactions involved in pipeline SCC.

Additionally, the applicability of industry standards relevant to pipeline SCC was reviewed. Furthermore, monitoring techniques and mitigation measures were reviewed on three aspects: (1) crack growth rate and remaining life prediction based on empirical data and SCC mechanisms; (2) SCC monitoring techniques, highlighting the latest advancements and the integration of AI-powered methods for enhanced monitoring and predictive analysis; and (3) strategies to mitigate the impact of SCC on the integrity of vintage pipelines. These three aspects complement each other, collectively enhancing pipeline integrity management and reducing the risk of structural failure and associated losses caused by SCC.

Moreover, the literature review greatly facilitates the preparation efforts for Task II, which focuses on experimentally investigating the effects of individual and combined influencing factors on pipeline SCC. First, the literature review helps deepen the understanding of the key challenges in current research on the complex influencing factors and monitoring technologies for pipeline SCC. Second, the literature review provides essential theoretical support and knowledge relevant to the design of experimental methods, selection and preparation of specimens, instrumentation setup, control of influencing factor variables, as well as monitoring and analysis of results.

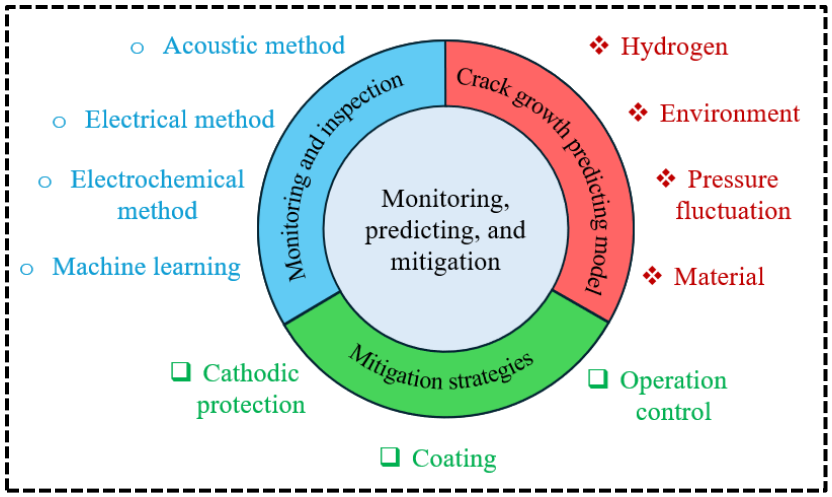

Fig. 1. Monitoring, prediction, and mitigation of pipeline SCC.

This report was written and revised by three graduate students (Ms. Shengju Xie, Mr. Yao Wang, and Mr. Samuel Ajayi) under the guidance of four PI/co-PIs and one consultant. Shengju Xie primarily focused on the SCC mechanisms, influencing factors, and mitigation measures. Yao Wang concentrated on the development of SCC monitoring technologies. Samuel Ajayi contributed to mitigation measures and monitoring technologies. The main reviewed contents on these three aspects are summarized as follows:

1. Introduction

Pipelines are widely used for transporting energy resources such as oil and gas due to their high efficiency and low cost, playing a vital role in meeting public energy demands and supporting the national economy. According to PHMSA's database, by the end of 2023, natural gas pipelines for gathering, transportation, and distribution spanned 2.7 million miles approximately, while liquid commodity pipelines totaled around 228,000 miles [1]. However, despite pipelines being a relatively safe method of energy transportation, the large scale of pipeline systems exposes them to numerous potential damage factors. Over the past two decades, despite significant efforts made to improve pipeline safety, more than 12,000 pipeline incidents occurred, resulting in economic losses exceeding 10 billion USD, as well as pollution and casualties [2]. There is an urgent need to understand the causes of pipeline incidents and develop new feasible pipeline monitoring methods to prevent the disasters caused by pipeline failures.

Pipeline incidents involve various causal factors, such as corrosion, incorrect operation, manufacturing defects, external force damage, and SCC [3]. SCC is regarded as a widespread threat that can cause pipeline leaks and even ruptures [4]. The first three factors have been extensively studied in literature [5–7] and managed in relevant standards [8,9], while SCC has not been fully understood. SCC occurs under synergistic interactions of metallurgical defects, environmental corrosion, and mechanical stress [10]. Its development mechanism encompasses the fields of electrochemistry, metallurgy, and mechanical mechanics. Additionally, the dominant factors in SCC development vary at different stages [11,12]. The complexity of SCC mechanisms and numerous influencing factors have constrained our understanding, impeding further progress in pipeline safety and management.

The development of pipeline SCC has been studied in literature [12–14]. SCC often occurs under certain detrimental environmental conditions and propagates slowly in its early stages; however, once the crack reaches a critical length, its growth rate accelerates, leading to pipeline failure within a short period. Understanding the mechanisms of SCC, monitoring SCC severity, and assessing pipeline health conditions play crucial roles in pipeline integrity management.

Additionally, understanding the mechanisms of SCC enables better control of pipeline SCC. The occurrence of SCC requires three conditions: (1) susceptible metallurgy, (2) a conductive environment, and (3) pipe wall stress [4]. Pipeline SCC typically occurs at locations with defective coating and metallurgical defects which can be aggravated by harsh environments. At a site with defective coating, an electrolyte forms between the coating and the pipeline substrate, facilitating electrochemical corrosion [4]. Metallurgical defects, such as inclusions and surface irregularities are vulnerable areas for crack initiation under the combined effects of corrosion and pipe wall stress [15–17]. Other metallurgical factors, such as steel grade, alloy composition, microstructure (grain size, grain boundary distribution, and texture) also influence the initiation and propagation of SCC [18–20]. Understanding the effects of these factors can help delay the occurrence and decelerate the progression of pipeline SCC.

In practice, effective pipeline SCC monitoring techniques are crucial for assessing pipeline integrity, thereby reducing the risk of incidents such as leaks and ruptures. It also contributes to expanding the data repository for future safety assessment and repair decision-making under varying conditions. Early practices rely on visual inspection, which is inefficient in time and labor. Recently, various techniques have been developed to monitor SCC, such as techniques based on sound waves [21,22], electrical current [23,24], and chemical composition [25,26]. Existing monitoring techniques can be categorized into visual-based, acoustic, electrical, and electrochemical approaches.

The remainder of this quarterly report presents our methodology for screening relevant references, mechanisms and evolution of pipeline SCC, causal factors of pipeline SCC, modelling methods, monitoring methods, and mitigation methods.

2. Methodology

A systematic literature search was conducted to screen references relevant to pipeline SCC. Databases included “Optica”, “ScienceDirect”, “Scopus”, “Web of Science”, “Google Scholar”, “ResearchGate”, “Springer Link”, and “Wiley Online Library”, chosen for their coverage of engineering, materials science, and corrosion studies. The search employed targeted keywords such as “stress corrosion cracking (SCC)”, “pipeline”, “crack growth prediction”, “monitoring technique”, “nondestructive evaluation (NDE)”, “sensors”, “acoustic emission”, “AI-assisted monitoring”, and “mitigation strategies”. Boolean operators like “AND”, “OR”, and “NOT” were used to refine and enhance search accuracy. Inclusion criteria focused on review papers, research papers, conference papers, and book chapters published from 2000 onward, ensuring recent and relevant content. Only relevant publications written in English were reviewed.

Key information from selected publications was organized into themes: SCC mechanisms, monitoring techniques, AI-assisted monitoring, and mitigation strategies. This structured approach helped identify research gaps.

3. Mechanism and evolution of pipeline SCC

3.1 Near-neutral pH SCC

Near-neutral pH SCC typically occurs in diluted groundwater environments with a pH range of approximately 5.5 to 7.5 [4], particularly relevant to pipelines with defective coatings which compromise protection for pipeline steel [27]. Near-neutral pH SCC cracks are predominantly transgranular, characterized by wider crack paths, noticeable corrosion traces on the crack walls, and fracture surfaces that may exhibit quasi-cleavage features [28]. The development of near-neutral pH SCC can be divided into four stages [11]: (1) Stage 0: Incubation stage involving the formation of initial conditions for SCC to occur. (2) Stage 1: Crack initiation stage controlled by anodic dissolution. (3) Stage 2: Crack propagation stage driven by mechanical effects and hydrogen embrittlement (HE), with crack coalescence. (4) Stage 3: Rapid crack growth stage. A bathtub model can be used to describe the time-dependent crack growth of near neutral-pH SCC.

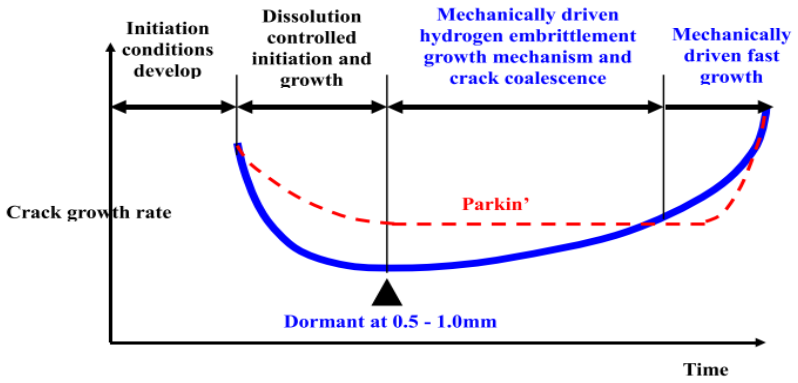

Fig. 2. Bathtub model illustrating the time-dependent crack growth behavior in near-neutral pH SCC of pipelines [11].

Early-stage cracks often initiate at the positions that involve defective coating, metallurgical defects, localized corrosion, and stress concentration on the pipeline surface [29]. In Stage 1, the development of cracks is primarily controlled by the anodic dissolution of the metal, with a higher dissolution rate at the pipeline surface that gradually decreases with increasing crack depth [30]. The anodic dissolution occurring at both the crack surface and crack tip, combined with factors such as the reduction in residual tensile stress toward the pipeline's inner surface can result in a blunted crack tip morphology [31,32]. The blunted crack tip mitigates stress concentration and further decelerates the anodic dissolution, which is beneficial for pipeline SCC resistance [33]. Prior research indicates that approximately 95% of cracks entering a dormant state at a depth of around 0.5 to 1.0 mm, while only 5% of cracks exhibit sustained propagation, potentially resulting in pipeline failure [29,34].

In Stage 2, crack propagation is governed by mechanical loading and HE in the fracture process zone ahead of the crack tip, while the contribution of anodic dissolution is minimal, being approximately an order of magnitude lower than the total crack growth rate [32,35,36]. From the perspective of mechanical loading, crack propagation typically occurs when cyclic loading exceeds a critical threshold, whereas under static loading conditions, crack growth tends to stagnate [37]. However, some studies have shown that in a near-neutral pH environment, SCC can initiate and even propagate if pre-formed corrosion pits reach a critical size, the applied static

load is sufficiently large, and the test duration is appropriate [38]. Moreover, cyclic loading can accelerate SCC development, with the threshold stress required to sustain SCC propagation being lower under cyclic loading than under static loading conditions [38]. In practical oil and gas transportation engineering, pressure fluctuations are inevitable, which makes understanding the effects of cyclic loading on pipeline SCC development particularly important. Depending on the pipeline segment's distance from the compressor station, mechanical factors such as loading type, maximum load, amplitude, frequency, and loading sequence can significantly influence SCC behavior [30].

Hydrogen plays a critical role in the mechanism of near-neutral pH SCC [32,39], with its impact mechanisms being diverse and varying according to environmental conditions. The primary sources of hydrogen in the development of SCC are corrosion reactions and cathodic protection processes [37]. An increase in cathodic protection potential or corresponding changes in the corrosive environment can elevate hydrogen content [40]. Moreover, the presence of a plastic zone facilitates hydrogen ingress and absorption [41,42]. These factors collectively increase the likelihood of hydrogen accumulating at crack tips and defective regions, thereby enhancing the susceptibility of pipeline steel to SCC. The influencing mechanism of hydrogen on SCC involves multiple action modes:

(1) Hydrogen induced cracking (HIC) contributes to the formation of microcracks and weakened steel interfaces, which can promote SCC initiation [43].
(2) Hydrogen-Facilitated Anodic Dissolution (HF-AD) influences crack initiation, which is dependent on the electrochemical potential and is limited to the open circuit potential (OCP) environment [44]. Hydrogen atoms absorb on the metal surface and disrupt the stability of the protective oxide film, reducing the density of corrosion products. This process further accelerates localized anodic dissolution, forming microcracks or pits, particularly in stress-concentrated areas, which can easily trigger SCC crack initiation. However, it is worth noting that its effect on the sustained propagation of SCC is negligible [45,46].
(3) HE promotes SCC progression by reducing material toughness, making cracks more prone to propagation, primarily affecting the crack growth stage of SCC [47,48]. Currently, many studies have indicated that HE synergizes with corrosion fatigue to accelerate near-neutral pH SCC progression, and related crack growth rate models can be found in reference [32,35,36,49].
(4) Hydrogen induced plasticity (HIP) can alter the mechanical properties of the metal matrix by alleviating stress concentration at the crack tip and expanding the local plastic zone, thereby delaying SCC crack initiation and propagation. Experiments have shown that HIP exhibits a positive effect opposite to HE within a specific potential range. Therefore, optimizing the cathodic protection design to harness the HIP effect can significantly enhance the SCC resistance of pipeline steel [50].

3.2 High-pH SCC

High-pH SCC typically occurs in a concentrated carbonate-bicarbonate solution environment with a pH of approximately 9-11, which often forms in areas where the external pipeline coating has defects and under the influence of cathodic protection current [51,52]. High-pH SCC cracks are predominantly characterized by intergranular cracks with sharp crack morphology and

typically lack significant corrosion traces on the crack walls, which differentiates them from low-pH SCC [53]. A bathtub model, as shown in **Fig. 3**, was proposed to describe the development process of high-pH SCC in pipeline steel [13].

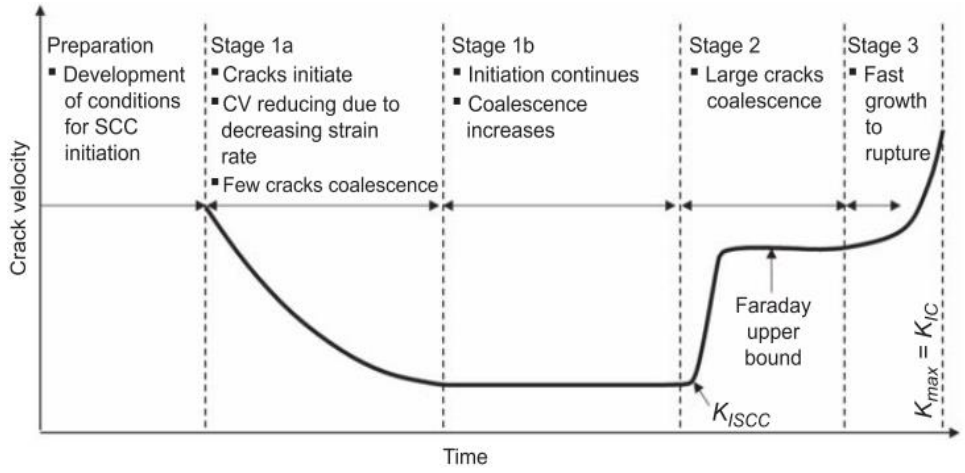

Fig. 3. Bathtub model for crack growth in high-pH SCC of pipelines [54].

The initiation and propagation of buried pipeline high-pH SCC can be divided into five stages [54,55]: (1) Stage 0: Incubation stage involving the formation of a corrosive environment conducive to crack initiation. Key factors include coating degradation, electrolyte accumulation, and inadequate cathodic protection. (2) Stage 1a: Crack initiation stage governed by selective anodic dissolution at grain boundaries and film rupture induced by localized stress. Cracks in this stage are typically sharp and appear as closely spaced microcracks. (3) Stage 1b: The stage of microcrack nucleation and coalescence depends on the initiation and spatial distribution of new cracks. Since the bottom of corrosion pits is a region prone to crack initiation, the probability of crack coalescence is higher in this area. Moreover, this stage is sensitive to loading conditions. The initiation of secondary cracks and their coalescence are promoted by cyclic loads, ultimately accelerating the transition to the next stage. (4) Stage 2: The sustainable crack growth stage is characterized by a crack propagation rate controlled by the increasing stress intensity factor (K). When K exceeds the SCC threshold (K_{ISCC} or ΔK_{th}), continuous crack propagation occurs. The primary mechanism involves anodic dissolution driven by the repeated rupture and re-passivation of the surface film. Prediction models for crack growth rate have been proposed based on this mechanism, with corrosion fatigue effects considered according to the pipeline's function (oil or gas pipeline); further details are available in reference [12,52,56]. (5) Stage 3: Rapid crack growth to rupture stage.

4. Causal factors of pipeline SCC

Pipeline SCC is influenced by metallurgical factors, environmental conditions, and applied stress. The complexity of these interactions has led to extensive research on both individual and combined effects. Metallurgical factors like microstructure and inclusions influence SCC susceptibility, while environmental conditions such as pH, temperature, and aggressive ions impact crack initiation. Applied stress drives crack propagation, especially when exceeding the SCC threshold. Understanding these mechanisms is vital for improving prediction models, optimizing maintenance, and enhancing pipeline safety.

4.1 Materials

It should be noted that metallurgical factors are not controllable for existing pipelines. This project focuses on controllable factors that can be engineered in practices for O&M management. Therefore, metallurgical factors are only briefly reviewed in this report. The emphasis is placed on the other causal factors for pipeline SCC.

4.1.1 Metallurgical properties

The relationships between metallurgical factors, such as the microstructure and mechanical properties and the SCC resistance of pipeline steels, have been investigated in various studies. Chu et al. [18] investigated the SCC initiation process of X65 pipeline steel. Prior to exposure to a near-neutral pH soil environment, the steel underwent cyclic loads simulating the stress levels experienced in operating conditions. The steel remained under loading conditions even after being exposed to the near-neutral pH soil environment. The result revealed that microstructural discontinuities, including grain boundaries, pearlite colonies, and banded phase regions, serve as preferential sites for SCC crack initiation.

Lu et al. [19,20] investigated the correlation between yield strength and SCC resistance in near-neutral pH environments by conducting Slow Strain Rate Tensile (SSRT) tests on API 5L X52, X60, X65, X70, X80, and X100 grade steels. The effect of microstructural changes induced by different heat treatment methods on SCC resistance was considered. The results indicated that SCC resistance generally decreased with increasing steel yielding strength, but this relationship was associated with the microstructural characteristics of pipeline steel. Therefore, assessing SCC resistance requires consideration of both yield strength and microstructural characteristics. This finding was already corroborated by other scholars. Zhu et al. [57] conducted SSRT tests to evaluate the SCC resistance of Chinese X80 pipeline steels with varying yielding strengths and microstructural characteristics in high-pH environments. The results revealed that both strength and microstructure significantly affected the SCC mode.

Fragiel et al. [58] investigated the SCC process of API X65 microalloyed steel with two different microstructures in an acidic H_2S environment at room temperature and 55°C. The results showed that the SCC propagation mode was influenced by both microstructure and temperature. The ferrite-pearlite microstructure primarily exhibited HE as the main cracking mechanism, while the martensitic microstructure experienced a combined effect of anodic dissolution and HE. Anodic dissolution involved the loss of metal ions during electrochemical reactions, while HE resulted from the accumulation and diffusion of hydrogen within the metal, leading to embrittlement and crack propagation [15]. These two mechanisms together cause more pronounced SCC in the martensitic microstructure, particularly at higher temperatures, where the HE effect is more significant.

Fundamentally, the yielding strength and microstructure of steel are influenced by its chemical composition and manufacturing processes [59]. While reducing the carbon content may reduce yielding strength, it improves SCC resistance [60,61]. Additionally, controlling heat treatment to achieve a uniform microstructure, high-angle grain boundaries, and fine grain size can significantly enhance SCC resistance by minimizing stress concentration and restraining crack propagation. Therefore, optimizing composition and refining microstructure are effective strategies for mitigating SCC in newly constructed pipelines [61,62].

4.1.2 Metallurgical defects

The presence of inclusions promotes the initiation of the pipeline SCC. First, the disparity in thermal expansion coefficients between inclusions and the steel matrix induces internal stresses and potential crack initiation due to the inconsistent volume changes under temperature fluctuations [63]. Second, the different Young's moduli and irregular contact surfaces between the inclusions and steel matrix led to high level stress concentration, which could result in the initiation of SCC cracks [63]. Additionally, the micro-crevices between the inclusions and matrix serve as sites for hydrogen penetration. When hydrogen molecules accumulate and reach a certain concentration, the resulting gas pressure generates high local stresses, which can lead to the crack initiation at the weak interfaces within steel [15]. The formation of cracks due to excessive localized stress from hydrogen accumulation is known as HIC. HIC commonly occurs in near-neutral pH environments and can induce defects that promote SCC initiation [37].

The susceptibility of steel to SCC is influenced by surface irregularities. A rough surface (i) enhances stress concentrations, (ii) traps corrosive media, and (iii) increases the likelihood of surface defects, thereby enhancing the risk of hydrogen ingress. Furthermore, concentration gradients of corrosive media between microscopic pits and protrusions accelerates localized corrosion, further compromising the steel's resistance to SCC. To address this issue, appropriate surface treatments and protective coatings can enhance the integrity of the machined surface and isolate corrosive media from steel matrix, thereby effectively improving resistance to SCC [16,17]. Surface treatment methods, such as sand blasting, wire brushing, grit blasting, grinding, milling, and turning, can enhance surface smoothness and improve the adhesion between steel and coatings. However, localized plastic deformation and thermal effects induced by surface treatments cause residual stress and phase transformation [64,65]. Extensive research has been conducted on the influence of surface treatment methods on SCC in steel [66–68].

4.2 Environment

Given the diverse environmental conditions that pipelines are exposed to, understanding the mechanisms and characteristics of SCC in various environments is crucial for effective pipeline management, risk evaluation, and integrity maintenance [69]. Existing studies have shown that both individual and combined environment factors (e.g., temperature, humidity, pH, corrosive deposits, microorganisms, and the concentrations of oxygen and carbon dioxide) influence the electrochemical reactions involved in the steel corrosion process [70–75]. For instance, elevated temperatures accelerate most electrochemical processes [76]. SCC tends to occur in high-temperature regions like pipelines downstream of compressor stations [75].

Gadala et al. [77] demonstrated that environmental factors such as bicarbonate content, purging gas, solution temperature, pH value, and the presence of chloride/sulfate ions affected the SCC behavior of X100 pipeline steel. They found that bicarbonate played a crucial role in passive film formation, promoting the development of a stable protective layer on the steel surface, which effectively reduced corrosion risk. In contrast, the presence of chloride or sulfate ions weakened or even destroyed the stability of the passive film, thereby accelerating corrosion and increasing the likelihood of SCC. Moreover, their research revealed that the corrosion rate of X100 pipeline steel decreased with increasing pH but increased with increasing temperature.

Contreras et al. [78] investigated the influence of pH and temperature on SCC behavior in API X60 pipeline steel. The results revealed that API X60 pipeline steel was susceptible to SCC in low-pH (pH = 3) environments. The impact of temperature on SCC susceptibility was more significant in high-pH environments than in low-pH and near-neutral pH environments [4,78].

In addition to environmental factors, external currents such as cathodic protection (CP) and alternating current (AC) interference have drawn increasing attention. Although CP is widely applied in pipeline corrosion prevention, its improper application may unexpectedly increase SCC susceptibility. Studies have shown that excessive CP may promote HE, increasing the risk of crack initiation and propagation. Liu et al. [79] studied SCC in X70 pipeline steel within acidic soil solutions, demonstrating that shifting the applied potential toward more negative values increases the steel's susceptibility to HE. Contreras et al. [80] investigated SCC behavior in API X52 pipeline steel under controlled electrochemical polarization potentials in a near-neutral pH environment and found that as the applied potential became more negative, the SCC mechanism transitioned from anodic dissolution to HE. When CP potentials exceeded a certain threshold, the fracture morphology gradually shifted to a cleavage-like pattern, indicating a notable increase in crack growth risk [81].

AC interference commonly occurs when pipelines are located near high-voltage transmission lines or AC electrified railways, which can accelerate pitting corrosion and promote SCC development [82]. In recent years, this issue has attracted significant attention due to frequent pipeline leaks attributed to AC corrosion. Wan et al. [82,83] investigated the impact of AC on SCC behavior in X80 steel exposed to near-neutral pH environment and found that SCC susceptibility decreased in the order of negative half-wave AC, full-wave AC, and positive half-wave AC. Negative half-wave AC predominantly promoted hydrogen precipitation, leading to HE, whereas positive half-wave AC was associated with anodic dissolution, encouraging the formation of larger-radius pits [82].

Additionally, non-stable cathodic polarization (NSCP) can accelerate SCC by enhancing localized anodic dissolution (AD) and hydrogen evolution, particularly in near-neutral pH environments [84]. Square wave polarization (SWP) experiments have demonstrated that alternating pulse currents promote localized corrosion, while stable current periods enhance cathodic hydrogen evolution, further increasing SCC susceptibility [84]. These findings highlight the critical importance of precise CP system control and effective mitigation of AC interference in managing pipeline infrastructure.

4.3 Stress

Stress plays a critical role in the growth process of SCC. Since the discovery of pipeline SCC, extensive efforts have been made to study the contribution of stress to its development. Among them, SSRT method, conducted in accordance with the NACE TM0198 standard, has been widely used to evaluate the resistance of alloys in SCC environments [85]. It serves to investigate the influence of strain rate, a factor closely linked to stress, on SCC development.

Lu et al. [86] investigated the effect of strain rate on the SCC behavior of X70 pipeline steel in an acidic soil solution. Experimental results demonstrated that the strain rate plays a dual role in the electrochemical activity of steel under straining. A moderate strain rate increases SCC susceptibility by promoting dislocation activity and enhancing hydrogen permeation, while an

excessively high strain rate reduces SCC susceptibility as the rapid movement of dislocations prevents reactive species in the solution from interacting with the dislocation points. Bueno et al. [47] conducted SSRTs to investigate the SCC susceptibility of API X46 steel in a near-neutral pH environment under different electrode potentials and strain rates. The study also indicated that a lower strain rate extends the exposure time for hydrogen diffusion, making the material more prone to brittle fracture.

However, SSRT results may not accurately reflect real field conditions, as it tends to overestimate the role of hydrogen in crack growth, produce shallow cracks that primarily represent early-stage growth, and yield crack growth rates far exceed those observed in actual pipeline operations. Moreover, as a monotonic loading test, SSRT results show less correlation with crack growth rates under variable amplitude pressure fluctuations encountered in real-world conditions [30].

It is well known that pipelines are subjected to internal cyclic pressure caused by the transport of liquids or gases during operation [87]. Therefore, considering the impact of cyclic loading on SCC is crucial. From this perspective, SCC shares certain similarities with corrosion fatigue. However, SCC occurs at lower frequencies (10^{-1} Hz to 10^{-6} Hz) that fall outside the typical range studied in corrosion fatigue [30]. Numerous studies have shown that cyclic loading promotes crack growth in both near-neutral pH SCC and high-pH SCC, while the absence of cyclic loading more likely to result in crack growth stagnate [12,14,38]. In fact, many current models for predicting SCC crack growth incorporate a superposition model that accounts for the contribution of high-frequency cyclic loading components to the corrosion fatigue-driven crack growth rate [88].

Pressure fluctuations play a crucial role in SCC of pipeline steel, with their impact primarily reflected in parameters such as maximum load, R-ratio, frequency, pressure transients, load type, load composition, and loading history. Studies have shown that a smaller R-ratio and higher frequency can accelerate the transition of cracks from a dormant state to a sustained propagation stage [87,89]. Liquid pipelines are more prone to crack propagation than gas pipelines due to more frequent pressure fluctuations [90].

Specific loading patterns also significantly influence SCC behavior. Pipeline pressure spectra can be categorized into three main types based on their position relative to compressors or pump stations: underload-dominant pressure fluctuations, mean load-dominant pressure fluctuations, and overload-dominant pressure fluctuations [90]. Among these, the underload-dominant spectrum, characterized by high pressure amplitude and frequent fluctuations, has the most significant driving effect on crack propagation [90]. In contrast, overload-type pressure fluctuations (brief increases in stress) may slow down crack growth [30]. Therefore, special attention should be given to pipelines subjected to underload-type pressure fluctuations due to their elevated SCC risk.

Moreover, the combination of underload waveforms and minor cycles has been shown to significantly accelerate crack propagation. Under this combined loading condition, the crack growth rate can reach 2.7 to 5.3 times that observed under constant-amplitude cyclic loading with the same maximum load in either air or near-neutral pH environments [91]. Furthermore, an increase in the R-ratio of both underload cycles and minor cycles is associated with a reduction

in crack growth rate, highlighting the critical influence of load composition and load interaction effects on the crack propagation process. Additionally, studies indicate that pipeline steels previously subjected to large stress cycles exhibit increased susceptibility to crack propagation under subsequent cyclic loading, highlighting the significant impact of pressure fluctuation history on crack behavior [89].

Besides external stress, residual stress is also known to influence crack initiation and propagation. Residual stress can be categorized into three types: macro residual stress, micro residual stress, and atomic-scale residual stress [92]. Among these, macro residual stress mainly results from steel plate bending during pipeline manufacturing, along with uneven cooling rates between the pipe wall and surface during rolling [34]. This type of residual stress is most studied in the context of SCC.

According to the principle of mechanical equilibrium, residual stress within a material must satisfy the conditions of force and moment equilibrium. Consequently, tensile and compressive stress regions alternate along the pipe thickness direction to maintain balance [29]. Studies have shown that residual stress levels are closely related to SCC occurrence and propagation. Beavers et al. [93] found that the average residual stress near SCC cracks is roughly twice as high as that in unaffected regions. Van Boven et al. [34] reported that pitting primarily occurs in areas with the highest tensile residual stress, while SCC tends to develop in regions with moderate residual stress. This may be due to changes in residual stress across the pipe thickness caused by cyclic pressure conditions. Moreover, as high surface tensile stress gradually transitions to lower tensile or compressive stress in deeper regions, the driving force for crack propagation weakens, making cracks more likely to become dormant, typically at a depth of around 1 mm [94]. Zhao et al. [29] further classified the distribution patterns of residual stress along the pipe thickness direction into five types and noted that Type III residual stress exhibited the longest predicted service life, whereas Type II residual stress corresponded to the shortest service life. The five types of residual stress distribution patterns are shown in **Fig. 4**.

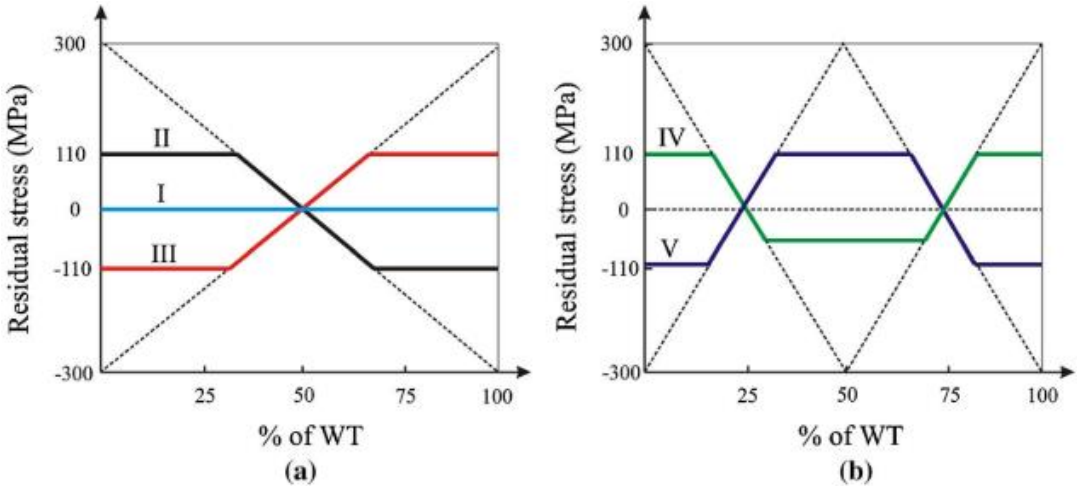

Fig. 4. Five tracks of residual stress versus the percentage of wall thickness (WT): (a) track I to III, and (b) track IV and V [29].

5. Inspection and monitoring techniques

Non-destructive evaluation (NDE) and monitoring techniques for pipeline SCC are classified into sound wave-based, vision-based, electrical, and electrochemical methods, according to their sensing principles. These methods are reviewed in the following subsections.

5.1 Sound wave-based methods

Sound wave-based methods, such as acoustic emission (AE) and ultrasonic testing (UT), are widely used for detecting and evaluating SCC due to their non-destructive nature and ability to evaluate crack initiation and propagation. AE and UT operate on different principles. AE is a passive technique that detects high-frequency (typically 20 kHz – 1 MHz) stress waves emitted by a material when cracks grow or deform under load. AE requires active stress (e.g., pressure, mechanical load) to generate signals and excels at identifying dynamic crack propagation in real time. In contrast, UT is an active method that uses a transducer to send ultrasonic (typically 0.5 – 25 MHz) waves into a material and analyzes reflections from flaws. Unlike AE, UT does not require the crack to be growing and can detect static defects even in unstressed components.

The two methods also differ in sensitivity and application. AE is highly sensitive to micro-level crack activity, making it ideal for early-stage damage detection and continuous monitoring. However, it struggles to achieve high accuracy and reliability due to the relatively low signal-to-noise ratios, and it is also difficult to precisely locate flaws unless multiple AE sensors are used. UT provides superior spatial resolution, allowing for accurate crack sizing, depth measurement, and imaging (e.g., weld inspections, aerospace components). While AE is best for real-time monitoring, UT is suited for precise, on-demand inspections without requiring structural loads.

Representative studies on SCC monitoring using sound wave-based methods are summarized in **Table 1**. In summary, AE was primarily used to investigate the mechanism and propagation process of SCC based on acoustic emission signals, whereas UT was primarily used to evaluate material conditions and construct two-dimensional surface images for estimating the locations and morphology of cracks.

Table 1. Summary of research using sound wave-based methods

Ref.	Material	Specimen type	Specimen size	Method	Sensor type	Crack size	Function
[95]	Cold drawn steel	Strand	-	AE	Broadband PZT	-	Detected SCC
[96]	Stainless steel	Plate	173×16×2 mm	AE	PZT	-	Monitored the whole process of SCC
[97]	Stainless steel	Plate	37.5×36×10 mm	AE	Broadband PZT	-	Detected SCC
[98]	Stainless steel	Pipe	OD: 86 mm W: 7.6 mm L: 150 mm	AE	PZT	-	Detected SCC
[99]	Stainless steel	Plate	280×12×2 mm	AE	-	-	Detected SCC
[100]	Stainless steel	Pipe	OD: 203.2 mm T: 12.7 mm L: 205 mm	AE	PZT	-	Monitored the whole

							process of SCC
[101]	Stainless steel	Plate	24×20×10 mm	AE	-	-	Detected SCC
[102]	Steel	Plate	150×65×5 mm	AE	PZT	-	Detected SCC
[103]	Steel	Strand	R1 = 2.7 mm R2 = 2.6 mm	AE	PZT	-	Monitored the whole process of SCC
[104]	Stainless steel	Plate	31.3×30×12.5 mm	AE	PZT	-	Detected SCC
[105]	Stainless steel	Pipe	OD: 160.2 mm T: 3.9 mm L: 270, 50 mm	UT	EMAT	-	Detected, located, and quantified crack
[106]	SUS 316	Pipe	T: 35 mm L: N/A	UT	EMAT	Depth: 0.5-5.0 mm	Detected and located SCC
[107]	Carbon steel	Dog-bone	L: 254 mm W: 18.5 mm T: 5.1, 3.8 mm	UT	PZT	-	Detected and quantified crack length
[108]	Stainless steel	Pipe	L: 127 mm OD, T: N/A	UT	PZT	-	Detected SCC
[109]	Stainless steel	Washer	50×25×1.4 mm	UT	PZT	L: 830 μm W, depth: N/A	Detected, located, and quantified crack
[110]	-	Pipe	OD: 914.4, 966 mm T: 12.7, 13.0 mm L: N/A	UT	Gas-coupled broadband transducer	L: 60 mm W: 40 mm Depth: 3.7 mm	Detected SCC

Note: T stands for thickness, OD for outer diameter, D for diameter, L for length, and W for width.

5.1.1 Acoustic emission

AE methods have been used to detect and locate cracks by analyzing the characteristics of acoustic signals, as shown in **Fig. 5**. Amplitude is the maximum voltage (unit: dB). Amplitude reflects the energy released by the crack event. Risetime is defined as the time interval from the start of the signal to its peak. Risetime is closely related to the crack type and propagation speed. Duration is the time length from the start to the end of the signal, reflecting the energy release process and the complexity of the crack event. Energy represents the squared integral of the signal amplitude, reflecting the total energy released by the source event. Counts are used to count the number of times the signal exceeds a set threshold, reflecting the oscillation intensity and frequency characteristics of the signal.

The characteristic parameters of AE signals play a crucial role in identifying the state of cracks or defects. The signal duration, when combined with frequency and risetime, can be used to distinguish different types of cracks. The amplitude and energy reflect the severity of the crack, while the time of peak amplitude and the rise time can assist in the preliminary estimation of the crack initiation time and location.

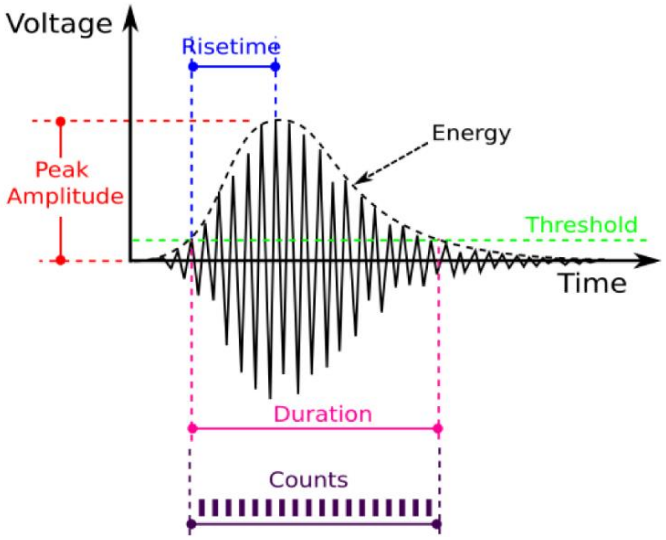

Fig. 5. Schematic of an Acoustic Emission event and related parameters [111].

AE has been applied to monitoring the SCC of pipelines in laboratory testing. Cho et al. [112] produced 25 mm long circumferential SCC at a butt-welded 304 stainless steel pipe by immersing the pipe vertically in a boiling magnesium chloride solution for 410 h. The outer diameter of the pipe was 19 mm. The length and thickness of the pipe were not provided. Lamb wave and cylinder wave were detected using PZT sensors (PAC R3I, PICO) during the heating–cooling cycles. In addition to the pipe specimen, a rectangular carbon-steel plate measured 200 mm in length, 40 mm in width, and 1 mm in thickness was exposed to outdoor weathering and monitored using AE sensors. Waveform simulation revealed crack opening of 1.4×10^{-14} m^3 in the rectangular plate with a rise time of 0.7 μs. Results showed that the AE signals generated by corrosion had higher amplitude than the AE signals generated by cracking.

Park et al. [113] monitored the SCC of a pipe segment using a test setup shown in **Fig. 6**. The pipe was made of 304L stainless steel and measured 203.2 mm in outer diameter, 12.7 mm in thickness, and 205 mm in length. Based on the peak amplitude and energy of AE signals received from PZT sensors (R15i), crack initiation at the inner surface was detected. However, the details of the crack were not reported.

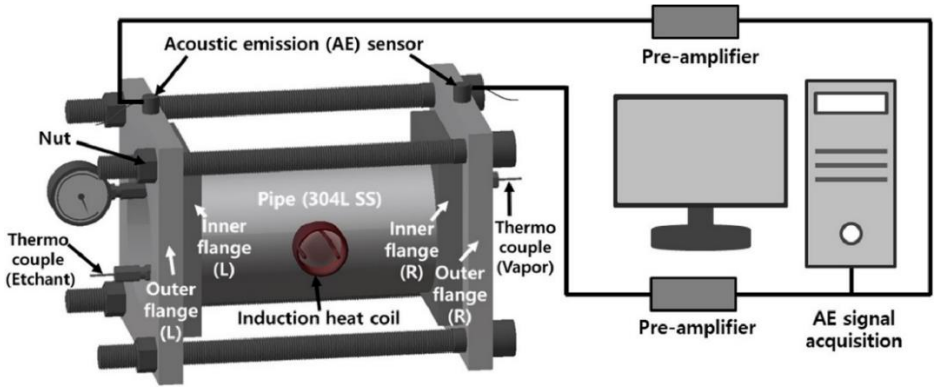

Fig. 6. Pipeline SCC monitoring system [113].

Budano et al. [114] applied AE methods to detect SCC from pipeline steels (API 5L grade X65, X80, and X100), which are commonly used in gas transmission pipes. Specimens were extracted from a pipe used for high pressure gas. The dimensions of the specimens were not provided. PZT sensors were utilized to measure AE signals. The results showed that IG-SCC measuring 100 μm in length was detected by analyzing the energy change of AE signals.

In addition to the applications to pipes, AE has been used to detect SCC in other materials. Du et al. [115] combined the electrochemical noise (EN) method and AE to detect SCC in stainless steel. Plate specimens (173 mm × 16 mm × 2 mm) were tested under mechanical loads. The AE ringdown counts received by PZT sensors showed a staged variation: The first peak corresponding to pitting corrosion appeared at around 16 minutes, and the highest peak associated with cracking occurred at around 33 minutes. After 83 minutes, the AE activity declined, and general surface corrosion was observed. Although the evolution of SCC was recorded, the detailed information of cracks was not reported. Bi et al. [116] extracted steel plates (150 mm × 65 mm × 5mm) from a storage tank. PZT sensors were used to detect AE signals in three-point bending tests. The test results showed that the abrupt increase in AE counts and energy revealed crack propagation. More relevant research on monitoring the SCC by using AE can be found in references [117–120].

AE has been used to advance the understanding of crack mechanisms, crack propagation behavior, and crack interactions. The application of AE for monitoring SCC can be traced back to the 1960s [121–123]. In early research, researchers mainly focused on the macroscopic effects of different materials and environmental factors on AE data. Various alloys, environmental systems, microstructures, and fracturing paths influenced the acoustic signals generated by SCC [124–127]. Later, the focus was shifted to the growth process of SCC. AE counts were used to classify the SCC process into four stages (**Fig. 7**) [128]. In the first stage, homogenization and chemical stabilization occurred in the corrosive solution. Then, SCC initiated and propagated in the second stage. Passive film ruptured, plastic deformation and dissolution happened in the third stage. Finally, the fourth stage is pure crack propagation. Crack initiation, sub-critical crack extension, and stable crack propagation were identified from the AE signals [129]. In the crack initiation and sub-critical crack extension stages, the number of acoustic emission events linearly increased with time. In the stable crack propagation stage, the number of acoustic emission events exponentially increased with time [130].

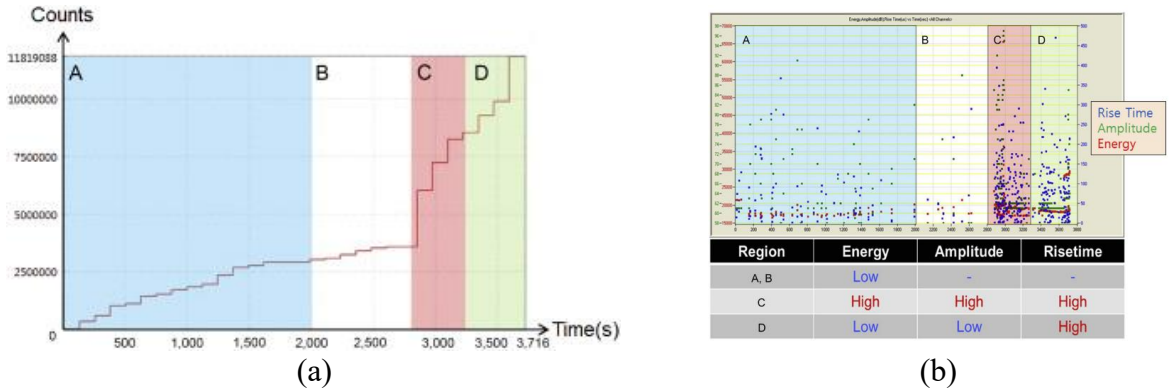

(a) (b)

Fig. 7. Evolution of AE parameters: (a) the number of counts, and (b) the energy, amplitude, and rise time distribution [128].

AE hit energy was also utilized to classify the four stages (**Fig. 8**) [131]. The first stage corresponding to the pre-activation phase of corrosion. The AE hit energy remains relatively low. The second stage represents the onset of material degradation. The cumulative AE energy increases significantly. The third stage involves crack propagation, associated with material dissolution that drives crack extension. In this stage, AE activity remains relatively stable. In the final stage, high-amplitude signals with short rise times are observed, indicating catastrophic failure of the specimen.

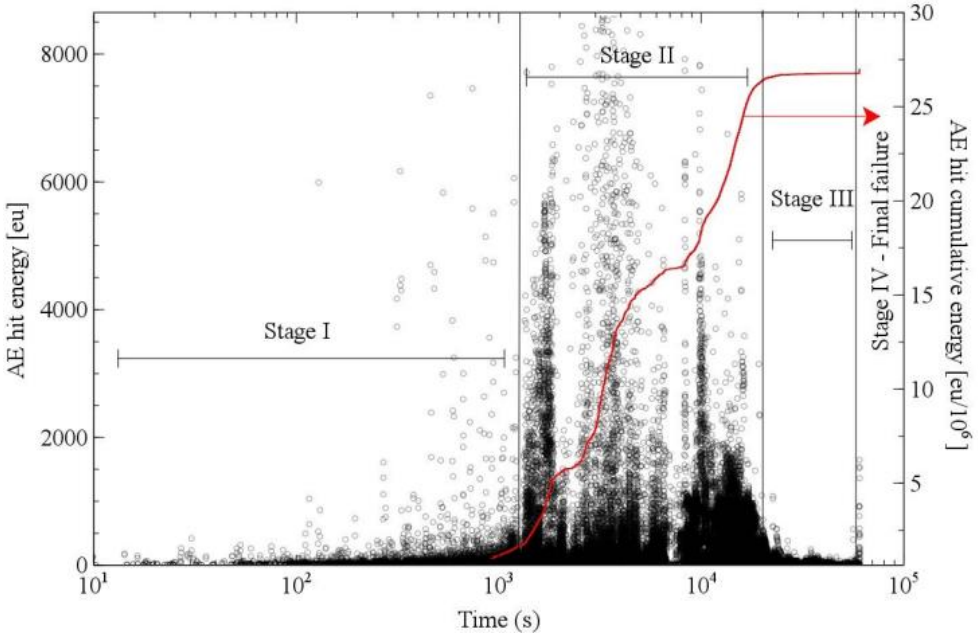

Fig. 8. Evolution of AE hit energy (open circles) and cumulative AE hit energy (continuous line) during time with the identification of four damage stages [132].

During the SCC process, AE signals were generated by multiple events, such as hydrogen evolution, plastic deformation ahead of the crack tip, and cracking of corrosion products [133–137]. AE signals can be divided into two types, which are Type-I and Type-II. Type-I AE signals have high frequency components, which are produced by falling-off of surface grains due to intergranular crack and detected during pit growth. Type-II AE signals have low frequency components, which are produced by cracking of the chromium oxy-hydroxides and detected during SCC propagation [138]. Also, microcrack creep and macrocrack propagation are the most important AE sources in SCC. According to reference [139], microcrack creep was dominant in the early stages when the duration time was up to 80 μs, the frequency range of the signals was 110–190 kHz. The macrocrack propagation was dominant in the latter stages when the duration time was 200-420 μs, with a frequency range of 260-350 kHz. The distinctive duration time and frequency ranges can be used to distinguish the two SCC stages.

AE signals have been analyzed for two types of SCC, which are intergranular SCC (IG-SCC) and transgranular SCC (TG-SCC). IG-SCC is attributed to the interaction of electrochemical and mechanical actions which emit relatively strong AE signals [140,141]. TG-SCC involves stable propagation within the grain interiors, lacking abrupt energy release; thus the AE signal may be weak or undetectable [142,143]. To distinguish these two types of SCC, the ratio of the number

of burst and continuous signal were introduced. This ratio is one for pure TG-SCC and zero for pure IG-SCC. The ratio is between zero and one for a mixture of TG-SCC and IG-SCC [144].

Various indices of acoustic signals have been proposed to characterize the SCC process. Three indices are introduced: (1) Monitoring indicator (MI), which is defined by performing FFT to the maximum amplitude, energy, waveform, and frequency characteristics (range and magnitude) of elastic waves generated by the propagation of SCC, were used for real-time monitoring. The experiment has verified MI's effectiveness for detecting SCC propagation [145]. (2) AE cumulative hits rate (dN/dt, /h) was found to be linear with the SCC crack growth rate (da/dt, mm/h). In practical applications, AE signals can be monitored over a period of time to obtain the cumulative hit rate. Then, empirical formulas can be used to predict the crack growth rate [146]. (3) Energy which defined by the squared integral of the signal amplitude in acoustic signals of AE, was found to be related to the characteristics of crack. Existing research shows that the energy released by the growing crack is linearly proportional to crack depth [147].

Although AE has been proved have outstanding performance on monitoring the evolution of crack and sensitive to the microcrack, AE have low capability to analyze the crack shape or crack location. Meanwhile, the amount of data generated by AE is extremely large, extracting meaningful information from the vast amount of data is highly challenging. Recently, the emergence of machine learning has made this task achievable. The real-time monitoring capability of AE endows it with significant potential for automated pipeline SCC monitoring.

5.2.2 Ultrasonic testing

Linear and nonlinear UT methods have been used to detect, locate, and evaluate the severity of cracks by analyzing the change of ultrasonic waves [148]. There are two primary scenarios, which are through transmission and pulse echo. In through transmission, the transmitter and receiver are two separate transducers. In pulse echo, the same transducer functions both the transmitter and receiver [149].

UT methods can be divided into three modes, which are A-scan, B-scan, and C-scan [150]. Each scanning mode has specific focuses and collects distinctive signals. A-Scan is mainly used to measure the thickness of the material; B-Scan focuses on analyzing the cross-sectional profile and depth of defects; and C-Scan primarily shows the planar shape, size, and distribution of defects [151–155].

UT has been used to monitor pipeline SCC and characterize the geometric features of SCC in laboratory testing. Hernandez-Valle et al. [156] used laser acoustic transducer (LAT) and electromagnetic acoustic transducer (EMAT) to detect and locate the SCC in two stainless steel pipes extracted from a pipeline measuring 160.2 mm in outer diameter and 3.9 mm in thickness. The two pipe specimens respectively measured 270 mm and 50 mm in length. Experiments were performed using a pulsed laser (Nd: YAG, 1064 nm wavelength and 10 ns pulse duration) to generate ultrasound, focused into a point of approximately 500 μm diameter. The laser-LAT system had a scanning step size of 0.67 mm, and the laser-EMAT system had a scanning step size of 1 mm. The exact size of the crack was not reported. Surface maps were constructed by UT, and the geometric alignment of the crack was identified. The laser-LAT system exhibited

higher sensitivity and was capable of distinguishing cracks spaced only a few millimeters apart. Achieving higher resolution requires a finer scanning step size.

Norli et al. [157] tested two pipe specimens: Specimen A (outer diameter: 910 mm, length: 700 mm, wall thickness: 12.7 mm) and Specimen B (outer diameter: 966 mm, length: 700 mm, wall thickness: 13 mm). UT scanners were put inside the pipes, and the maximum resolution was 0.5 mm×0.2° (32 broadband transducers). Ultrasonic waves in the frequency range of 400-1100 kHz was transmitted to the pipes through a 60 bars pressurized gas medium. SCC at depths of 4.3 mm and 2.8 mm were detected. However, the SCC sizes were not determined. The same team [158] also used guided waves and gas-coupled broadband ultrasound to detect cracks. The pipe measured 700 mm in length, 910 mm in outer diameter, and 12.7 mm in wall thickness. Ultrasonic transducers transmitted 0.4-1.2 MHz chirp or sinc pulses and achieved a spatial density of 2×2 mm. A crack at a depth of 4.3 mm was detected.

Nakamura et al. [159] designed a point-focusing electromagnetic-acoustic transducer and used the transducer to detect SCC. Pipes extracted from stainless steel (SUS316) welded pipes were tested. The outer diameter and thickness were 600 mm and 35 mm, respectively. The length was not reported. SV waves with frequencies of 2 MHz and 3 MHz were used to detect cracks with depths ranging from 0.5 mm to 5 mm.

Four advanced UT approaches have been developed to detect SCC, which are gas-coupled UT, liquid-coupled UT, laser UT, and EMAT approaches.

- Gas-coupled UT uses gas as a coupling medium, allowing for non-contact inspection of both the inner and outer walls of pipelines. Since a sound transmits in a gaseous atmosphere, the approach has the potential to inspect pipeline SCC in high-pressure environments. For example, in an environment with a pressure of 60 bar, gas-coupled broadband ultrasound detected pipeline cracks [160–163].
- Liquid-coupled ultrasound was also tested valid for through liquid medium and non-invasive monitoring [164].
- The use of scanning laser doppler vibrometer (SLDV) combined with guided waves also provides new possibilities for SCC detection. This technology captures multidimensional time-space wavefield data through scanning using the SLDV, allowing for accurate assessment of the SCC in thick steel plates [165].
- EMAT and laser ultrasonics have been combined to significantly enhance crack detection capabilities. For instance, the laser generation and EMAT detection technique, by scanning the generation point, can precisely locate cracks on the pipeline surface and provide high-resolution results regarding crack size and shape. By using a dense distribution of EMAT sensors covering the entire pipe circumference and generating ultrasonic shear waves in different modes, high-resolution imaging of the pipe wall is achieved, with sensitivity to the dynamic growth of cracks [166–168].

These advanced UT approaches not only offer precise quantitative information for crack detection in pipelines and structural components, but also improve real-time monitoring and reliability, enabling effective identification of crack shape, size, and distribution, thus providing technological support for the early diagnosis and prevention of SCC.

Conventional linear UT is effective in detecting macro-scale cracks but has exhibited limited sensitivity to micro-scale cracks. In contrast, nonlinear UT has demonstrated superior capability of detecting and characterizing micro-scale cracks. Zeitvogal et al. [169] machined four dog-bone specimens from cold rolled 1018 carbon steel. Three specimens measured 254 mm in length, 18.5 mm in width, and 5.1 mm in thickness. The other specimen had the same length and width but measured 5.1 mm in thickness. A PZT with a center frequency of 2.25 MHz and a diameter of 12.7 mm was fixed to an acrylic wedge clamped to the specimen. Rayleigh waves were generated and detected. By analyzing the nonlinearity parameter β of signals received by the PZT, SCC was revealed by microstructural changes and microcrack initiation.

Doerr et al. [170] welded stainless steel plate (25.4 mm thick) with stainless steel filler material (50.8 mm wide). Nonlinear Rayleigh waves were introduced by a PZT with a center frequency of 2.25 MHz. The signals showed that nonlinearity parameter β increased 200% in the vicinity of the heat-affected zone, which was susceptible to IG-SCC. Although the detailed dimensions of cracks were not reported, the effectiveness of nonlinear UT in monitoring SCC in the early stages was proven.

Although both linear and nonlinear UT have demonstrated the capability to detect SCC and show potential for monitoring pipeline SCC, multi-scale crack detection remains a significant challenge. On the one hand, nonlinear UT has rarely been applied to in-service pipelines. The effectiveness of nonlinear UT in real applications is still unclear. On the other hand, linear UT has been proven to be insensitive to closed cracks and microcracks, which may pose a risk to pipeline safety. Thus, integrating linear and nonlinear UT techniques into a unified multi-scale monitoring approach is important for the effectiveness of monitoring pipeline SCC.

5.2 Vision-based methods

Vision-based methods focus on identifying visual features of SCC from images from various imaging techniques, such as optical cameras, infrared cameras, and microscopes. Early practice involves visual inspection via bare eyes, which is however inefficient and unable to identify fine SCC. To address this issue, advanced techniques, such as digital image correlation (DIC) [171–173] and infrared thermography (IRT) [174,175], have been developed. Representative studies on SCC monitoring using vision-based methods are summarized in **Table 2**. Both DIC and IRT can be used to detect, locate, and quantify the crack. Images are constructed to characterize the state and morphology of the cracks.

Table 2. Summary of research using vision-based methods

Ref.	Material	Specimen type	Specimen size	Method	Sensors	Crack size	Function
[176]	Alloy 600	Plate	117×8×2 mm	DIC	Optical camera	Width: 0.45 μm, length: 55 μm	Detected, located, and quantified crack
[177]	Stainless steel	Plate	36×10×1 mm	DIC	-	-	Detected SCC
[178]	Stainless steel	Plate	42.8×13×0.9 14 mm	DIC	Optical camera	Width: 5 μm, length: 250 μm	Detected, located, and quantified crack

[179]	Aluminum alloys	Plate	L: 10 mm W: 51.46 mm T: N/A	DIC	Microscope	-	Detected, located, and quantified crack
[180]	Fe–13Cr–15Ni alloy	Plate	21×2×1.5 mm	DIC	-	-	Detected, located, and quantified crack
[181]	Aluminum alloy	Plate	T: 8 mm W, L: N/A	DIC	-	-	Detected, located, and quantified crack
[182]	Carbon steel, stainless steel	Pipe	OD: 89 mm T: 7.6 mm L: 150 mm	IRT	Infrared camera,	-	Detected, located, and quantified crack
[183]	Stainless steel	Plate	-	Soni-IR	Infrared camera	Depth: 2.0-4.5mm	Detected, located, and quantified crack

Note: T stands for thickness, OD for outer diameter, D for diameter, L for length, and W for width.

5.2.1 Digital image correlation method

DIC has been used to generate global and localized strain mapping with high resolution by tracking the displacement of speckle patterns on surface of pipes. The strain mapping can be used to evaluate the initiation and propagation of cracks [184–186].

DIC has been applied to steel specimens extracted from pipes in the laboratory. Shirazi et al. [187] extracted a section of API-5L Gr. X52 steel pipe, which measured 406.4 mm in outer diameter and 9.2 mm in wall thickness, from a pipeline that had experienced SCC. Three reduced gauge sections (80 mm × 20 mm × 9.2 mm) with artificial through-thickness notches were designed to evaluate different parameters. The dimensions of the specimens are shown in **Fig. 9**. A DIC method was used to analyze the change of strain fields and cracks under mechanical load. Test results showed that DIC was able to visualize the distribution of strains and stresses. However, the working area of DIC and its performance for detecting SCC were not reported.

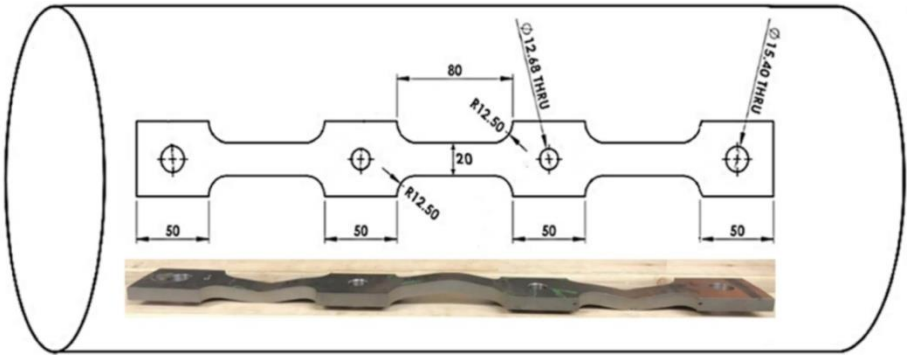

Fig. 9. Dimensions of specimens (unit: mm).

In addition to pipeline steel, DIC has been applied to evaluate the cracks of various materials in laboratory testing, such as stainless steel [188], aluminum alloys [189], nickel-based alloys

[190], concrete [191], and polymers [192]. For example, Cook et al. [193] applied DIC to investigate the growth of SCC in 304L stainless steel. The specimen measured 0.914 mm in thickness, 13 mm in width, and 42.8 mm in length. Two semicircle notches with the radius of 6 mm are cut symmetrically at the central axis. The area of images was 3.9 × 3.9 mm, where one pixel corresponding to 1.85 μm. Test results showed that the DIC method was able to detect surface cracks with lengths of 250 μm and opening width of 5 μm.

Duff et al. [194] studied the performance of DIC in detecting cracks in 304 stainless steel specimens, which measured 5 mm in thickness, 100 mm in length, and 10 mm in width, with intergranular SCC. Test results showed that surface cracks with lengths exceeding 30 μm were identified from images with an area of 3.9 × 3.9 mm, where one pixel corresponded to 1.85 μm.

Bolivar et al. [195] used DIC to analyze the SCC of an alloy plate, which measured 2 mm in thickness, 15 mm in width, and 234 mm in length. Cracks measuring 55 μm in length and 0.45 μm in opening were detected. More relevant research on evaluating SCC by using DIC can be found in references [196–198].

The test results from DIC have been used to advance the understanding of crack initiation mechanisms, crack propagation behavior, and crack interactions. For example, DIC was utilized to identify early signs of cracking and predict crack initiation sites through localized strain measurements from microscopy images. DIC has also been used to analyze the effect of different grain boundary angles on crack initiation, the role of dislocation channels in crack formation, and the dominant mechanisms of corrosion-fatigue cracking [199]. The findings suggest that large-angle grain boundaries are preferred sites for crack initiation, while discontinuous dislocation channels may lead to higher local stresses, promoting crack formation [200–202].

DIC has demonstrated potential for monitoring pipeline SCC. First, DIC can quantitatively measure crack size [203,204]. Second, DIC can be applied not only to optically captured digital images, but also to ultra-high-resolution images obtained from microscopes making it well-suited for detecting SCC [205,206]. Third, recent studies have proposed AI-assisted DIC approaches for underground pipeline monitoring, make it possible to automated SCC detection [207].

However, the performance of DIC also has two primary limitations. First, DIC requires a high-quality surface finish, as a speckle pattern needs to be applied for accurate analysis. Second, the precision of DIC is highly related to the interrogation window size because the window size impacts the resolution of DIC. Third, DIC is sensitive to the light condition. Either low light or high exposure can compromise the quality of images and thereby the quality of DIC results.

5.2.2 Infrared thermography method

IRT has been used to evaluate SCC by analyzing infrared images due to the ability to identify temperature variations associated with crack formation and propagation. When a material undergoes stress and corrosion, localized heating or cooling effects can occur due to friction, oxidation, or electrochemical reactions. Prior research showed that IRT could monitor the initial stage of SCC [208,209].

IRT has been modified and applied to pipes and steel plates extracted from pipes. Park et al. [210] used ultrasound-IRT to detect SCC in a pipe segment which measured 89 mm in diameter, 7.6 mm in thickness, and 150 mm in length. An infrared camera (Silver 480 M) with a noise

equivalent temperature difference of 25 mK was employed in the experiment. The ultrasound generator was set as 250 W in output and 19.8 kHz in frequency. Test results showed that cracks measuring 10 μm in width and over 25 mm in length were detected.

Jama [211] used IRT to detect SCC from 304L stainless steel plate extracted from a pipe. Detailed dimensions about specimens were not reported. An infrared camera (FLIR T640) was used in the experiment. The test results showed that IRT detected the presence of SCC by identifying heat intensity differences at defective locations, which appeared as temperature contrasts compared to defect-free areas.

In addition to the application of pipes, IRT has been applied to steel plates. Sakagami et al. [212] used Sonic-IR to detect SCC in stainless steel plates. The dimensions of plates were not reported. Ultrasonic transducers, whose power ranged from 500 J to 3000 J, were used to generate excitations at frequencies ranging from 10 kHz to 50 kHz. The temperature resolution of the infrared camera was 60 mK in NEDT value. The spatial resolution was 640 × 480 pixels, and the framing rate was 60 Hz. Results showed that a crack (3.7 mm in depth) was detected.

The limitation of IRT can be summarized into two aspects. First, IRT focuses on surface temperature and is insensitive to internal temperature, limiting applications to surface cracks. Second, IRT is sensitive to environmental variables, such as temperature, humidity, and wind, compromising environmental robustness.

5.2.3 Other methods

High-speed imaging techniques have been applied to detect SCC of steel plates [213] and aluminum bars [214], exhibiting unique abilities to capture rapid deformation and crack propagation. By recording high frame rates (even exceeding 10,000 frames per second), the initiation and growth of SCC were visualized in real-time [215,216]. This method is particularly useful in studying dynamic failure, such as crack coalescence, micro-fracture development, and pit-to-crack transition, which occur over very short time [217,218].

In addition to microscale photos, microscale images from various microscopes, such as optical microscopy, scanning electron microscope (SEM), and transmission electron microscopy (TEM), have been used to examine SCC [219–221]. However, the monitoring principle limits microscopy-based methods to laboratory testing and research of small-scale samples.

5.3 Electrical methods

Electrical sensing technology has been used to measure electrical resistance, conductivity, capacitance, and potential, which are used to detect the initiation and development of cracks and corrosion. Eddy Current Testing (ECT) and Direct Current Potential Drop (DCPD) are two representative methods, which have been applied to detect the SCC of pipes and achieved high performance in terms of sensitivity, stability, and environmental adaptability. Representative studies on monitoring SCC using electrical methods are summarized in **Table 3**. Overall, ECT are sensitive to surface, shallow crack, and DCPD can detect deep cracks and quantify the depth of SCC.

Table 3. Summary of research using electrical methods

Ref.	Material	Specimen type	Specimen size	Method	Equipment	Crack size	Function
[222]	Stainless steel	Plate	L: 200 mm W: 100 mm T: N/A	ECT	ECT instrument	-	Detected SCC
[223]	Inconel 600, stainless steel	Welded specimen	L: 300 mm W: 100 mm T: N/A	ECT	ECT instrument	Depth: 9 mm L: 10 mm W: 0.3 mm	Detected SCC and quantified crack size
[224]	Low carbon steel	Plate	600×150×3 mm	ECT	ECT instrument	L: 5-20 mm	Detected SCC and quantify crack length
[225]	Low carbon steel	Plate	-	ECT	-	-	Detected SCC
[226]	Stainless steel	Plate	600×270×25 mm	ECT	ECT instrument	W: 0.01-1.2 mm	Detected SCC and quantified crack width
[227]	-	Pipe	OD: 215.9 mm T: 4.7625 mm L: N/A	ECT	-	Depth: 0.952-3.81 mm	Detected SCC and quantified crack depth
[228]	Stainless steel	Dog-bone	L: 118 mm W: 40 mm T: 2.8 mm	DCPD	DCPD instrument	Depth: 106 μm	Detected SCC and quantified crack depth
[229]	Stainless steel	Plate	T: 20 mm	MICPD	Induction coils, DCPD instrument	Depth: 0.12-9.59 mm	Detected SCC and quantified crack depth
[230]	Stainless steel	Dog-bone	118×40×2.8 mm	DCPD	DCPD instrument	Depth: 106 μm	Detected SCC and quantified crack depth
[231]	Stainless steel	Plate	200×100×10 mm	DCPD	DCPD instrument	W: 0.024 mm Depth: 3.5 mm	Detected SCC and located cracks

Note: T stands for thickness, OD for outer diameter, D for diameter, L for length, and W for width.

5.3.1 Eddy Current Testing

ECT has been used to detect SCC based on electromagnetic induction. ECT operates by inducing alternating electromagnetic fields on the material surface, generating eddy currents, and analyzing their response signals to assess material integrity [232,233]. The working principle of ECT is shown in **Fig. 10**. When defects such as cracks or corrosion exist within the material, the distribution, amplitude, and phase of the eddy currents are altered, resulting in detectable signal variations.

ECT has been applied to detect pipeline SCC in laboratory testing. Taheri et al. [234] applied ECT to detect SCC from steel plates, which were made of AISI 1018 mild carbon and measured 600 mm in length, 150 mm in width, and 3 mm in thickness. SCC in the steel plates were detected, but the dimensions of SCC were not reported.

Moskovkina et al. [235] applied ECT to detect SCC from steel plates, which measured 215 mm in length, 40 mm in width, and 10 mm in thickness. Rectangular defects with an interval of 30 mm were manipulated to simulate SCC, and each defect measured 40 mm in length, 0.2 mm in width, and 10 mm in depth, according to a statistical analysis of the dimensions and locations

of SCC found from a gas pipeline. Test results showed that ECT detected defects but the performance of ECT was limited by the parameter of probes (ferrite core diameter).

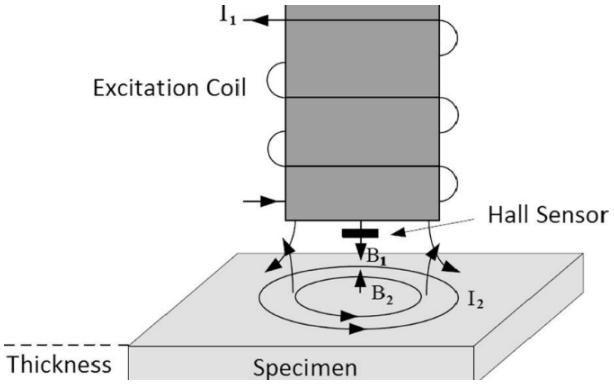

Fig. 10. The basic principle of eddy current testing [236].

Kim et al. [237] applied ECT to detect four types of cracks in a pipe which measured 215.9 mm in outer diameter and 4.76 mm in thickness. The length of the pipe was not reported. The cracks had the same length (25.4 mm) and varying depths (80%, 60%, 40%, and 20% of the pipe wall thickness). The widths of cracks were not provided. Results showed that ECT detected the presence of axially oriented cracks. The accuracy of ECT in crack localization and quantification were not reported.

Butusova et al. [238] applied ECT to detect SCC from four sets of steel plates extracted from gas pipes. The steel plates were placed in a boiling solution of nitrites which simulated an SCC environment and then loaded to generate cracks under bending. Detailed information about the cracks was not provided. Electromagnetic characteristics of the plates were measured using ECT probes at a constant frequency (150 Hz) in the bending test. Results showed that the ECT method was capable of monitoring the incubation stage of SCC. More research on using ECT to evaluate SCC of pipes is available in references [239–246].

Typically, SCC involves heterogenous conductivity distributions. Experiments showed that SCC led to the highest conductivity at the crack tip, reaching up to 17% of the base material's conductivity, while the central conductivity of the crack was about half of that at both ends [247]. Due to the complex conductivity distribution of SCC, reconstructing SCC shape using single-frequency ECT signals presents an ill-posed inverse problem, meaning that multiple local optimal solutions may exist, leading to errors in crack size assessment [248]. Single-frequency ECT signals resulted in significant errors in crack depth and conductivity [249,250]. It is promising to reconstruct SCC shape parameters using multi-frequency ECT signals. High-frequency signals primarily reflect surface conductivity and crack length, while low-frequency signals provide information about the crack's depth [250,251]. Applying regularization methods to process multi-frequency ECT signals effectively improves SCC shape reconstruction accuracy and reduces the impact of multiple solutions [252].

The length and depth of SCC and the conductivity of the material affected ECT signals. Crack length primarily influences the phase of ECT signals, while crack depth and conductivity affect signal amplitude [249]. Numerical methods have been used to study the relationship

between conductivity and SCC [253–255]. For example, a finite element-boundary element (FEM-BEM) hybrid method was utilized for SCC parameter modeling, optimizing crack shape parameters using ECT signals [247]. Regularization methods have been applied to optimize SCC shape reconstruction, making predicted crack depth values closer to real failure test results and improving detection reliability.

Although previous studies have demonstrated the widespread use of ECT in laboratory pipeline testing, the technique is restricted to conductive materials and still faces challenges in detecting subsurface or deeply embedded defects.

5.3.2 Direct Current Potential Drop

DCPD has been applied to detect cracks from metallic materials, with the capability of early detection. DCPD assesses cracks based on the change of electrical resistance. The presence or the propagation of a crack results in a reduction in the cross-sectional area and an increase in the electrical resistance [256]. Based on this phenomenon, DCPD has been used to detect the formation and propagation of cracks.

DCPD has been applied to monitor pipeline SCC in laboratory experiments. Ji et al.[257] used DCPD to monitor SCC in a stainless steel (316L) pipe immersed in the corrosive solution. The pipe was measured 112 mm in outer diameter and 6 mm in thickness. The length of pipe was not provided. The depth of cracks was primarily distributed within the 4-5 mm range. The experiment was conducted using a high-temperature, high-pressure dynamic stainless steel autoclave equipped with a rotating cage. The rotation speed was maintained at 5π rad/s, corresponding to a sample surface flow velocity of 0.5 m/s. In parallel, numerical simulations were carried out using Fluent software under the same inlet flow velocity conditions. Results showed that the initiation of SCC at localized weld defects was attributed to the synergistic interaction of galvanic corrosion, residual stress, and flow velocity.

Zhu et al.[258] applied DCPD to monitor SCC in stainless steel elbow pipe. The elbow pipe measured 355.6 mm in diameter and 45.5 mm in thickness. A compact tensile specimen, which measured 32 mm in length, 30 mm in width, and 12.5 mm in thickness, was extracted from the elbow pipe. The DCPD crack monitoring system consists of a high-precision power supply, a nanovoltmeter, a multiplexer, and a computer. A constant current is applied to the compact tension specimen using the power supply, while the nanovoltmeter measures the potential drop. The multiplexer is used to switch between the primary and reference voltage signals. Due to the symmetrical geometry of the CT specimen, the current input and output electrodes are positioned on opposite sides of the specimen, and the primary voltage measurement points are located on either side of the crack. The experiment monitors changes in crack length by measuring the potential drop across the CT specimen under constant current, and the average of the measurements is taken as the actual stress corrosion crack length. Test results showed the maximum crack length observed in the experiment was 11 mm.

A typical test setup is shown in **Fig. 11**. The test setup consisted of a modular power supply system, a digital nanovoltmeter, and a computer, which were used to provide direct current, measure potential drop, and record data, respectively. A current probe was connected to DC power supply, and a potential probe was connected to the nanovoltmeter [259].

Yoon et al. [260] applied a modified DCPD technique to monitor a pipe, which measured 355 mm in outer diameter, 37 mm in thickness, and 611 mm in length. Results showed that cracks with depths up to 40% of the wall thickness were detected. The minimum detectable crack length was 21.6 mm. The width of the crack was not reported.

Kang et al. [261] used DCPD to monitor SCC in a spiral seam-welded pipe under mechanical loads. The pipe measured 914 mm in outer diameter and 13 mm in thickness. The length of the pipe was not provided. Six cracks were manipulated in the pipe, each measuring 0.3 mm in width, 100 mm in length, and 1.5 mm in depth. The crack growth rate was detected after the maximum pressure was raised up to 95% of the yielding strength of the pipeline steel.

Sato et al. [262] used DCPD to monitor SCC in welded stainless steel plates, which measured 300 mm in length, 150 mm in width, and 20 mm in thickness. Test results showed that DPCD detected backwall SCC in real time when the crack depth was deeper than 4 mm. The length and width of the cracks were not reported.

Fig. 11. Test system of DCPD method[259].

Sun et al. [263] applied DCPD to pipes, which measured 406 mm in outer diameter, 5.8 mm in wall thickness, and 2440 mm in length, extracted from an in-service pipe. Six surface cracks were manipulated, each measuring 60 mm in nominal length. Three cracks were in the base metal, and the other three cracks were in the seam weld. Test results showed that DCPD was able to monitor crack propagation and quantify crack depth. Crack dimensions were not provided.

Prior research showed that the electrical conductivity distribution in SCC regions increased linearly along both crack depth and length directions, with conductivity becoming larger near the crack tip and reaching its minimum at the crack opening position [247,264]. The SCC growth rate decreased with increasing relative humidity and crack depth [265]. Furthermore, research showed that the DCPD technique could monitor back wall SCC propagation, starting from a fatigue pre-crack at a depth of approximately 4 mm and extending until the crack propagates beyond 80% of the specimen thickness [266].

Existing research has confirmed the effectiveness of DCPD in monitoring the crack growth. The quantification of cracks, particularly crack depth, has also been frequently mentioned.

However, accurate defect sizing remains challenging as DCPD techniques generally rely on calibration curves to translate measurement data into depth information. Moreover, existing studies have rarely used DCPD for precise crack quantification.

5.4. Electrochemical approaches

Electrochemical approaches provide critical insights into early-stage crack and corrosion. EN and electrochemical impedance spectroscopy (EIS) are two representative techniques used to evaluate SCC. Representative studies on monitoring SCC using electrochemical approaches are summarized in **Table 4**.

Table 4. Summary of research using electrochemical approaches

Ref.	Material	Specimen type	Specimen size	Method	Equipment	Crack size	Function
[267]	Stainless steel	Plate	280×12×2 mm	EN	-	-	Monitored early-stage SCC
[268]	Stainless steel	Plate	173×16×2 mm	EN	Potentiostat	-	Detected SCC
[269]	Stainless steel	Rod	L: 95 mm D: 6 mm	EN	-	L: 2-420 μm	Detected SCC
[270]	Stainless steel	-	-	EN	Potentiostat	-	Detected SCC
[271]	Low carbon steel	-	-	EN	Potentiostat	-	Detected SCC
[272]	Stainless steel	Dog-bone	-	EN	Potentiostat	-	Detected SCC
[273]	Stainless steel	-	-	EIS	Potentiostat		Detected SCC
[274]	Pipeline steel	-	-	EIS	Potentiostat	-	Detected SCC
[275]	Stainless steel	Tensile specimen	-	EIS	Potentiostat	-	Detected SCC
[276]	Pipeline steel	-	-	EIS	Potentiostat		Detected SCC
[277]	Stainless steel	U-bend	R: 16 mm X: 25 mm Y: 38 mm	EIS	Potentiostat	-	Detected SCC
[278]	Pipeline steel	U-bend	L: 59.07 mm Curvature radius: 15 mm W: 4.9 mm T: 10.4 mm	EIS	Potentiostat	-	Detected SCC
[279]	Stainless steel	Cylindrical	L: 25 mm, D: 5 mm	EIS	-	Depth: 20 μm	Detected SCC
[280]	Pipeline steel	-	-	EIS	Potentiostat	-	Detected SCC

Note: T stands for thickness, OD for outer diameter, D for diameter, L for length, and W for width.

5.4.1 Electrochemical noise

EN is based on spontaneous fluctuations of potential and current on the electrode surface. EN measurements typically use a three-electrode or two-electrode system to record electrochemical potential noise (EPN) and electrochemical current noise (ECN) in the absence of external voltage or current perturbation. These noise signals reflect dynamic changes in the corrosion process, such as the initiation and growth of pitting corrosion, uniform corrosion, and the breakdown of passive films. By employing time-domain, frequency-domain, and statistical analysis methods, such as standard deviation, noise resistance, wavelet transformation, and power spectral density analysis, valuable information related to corrosion mechanisms can be extracted, enabling the identification of different corrosion types and rates, as shown in **Fig. 12**. Since EN is a passive technique, it is suited for online monitoring and can detect localized corrosion, such as pitting and crevice corrosion.

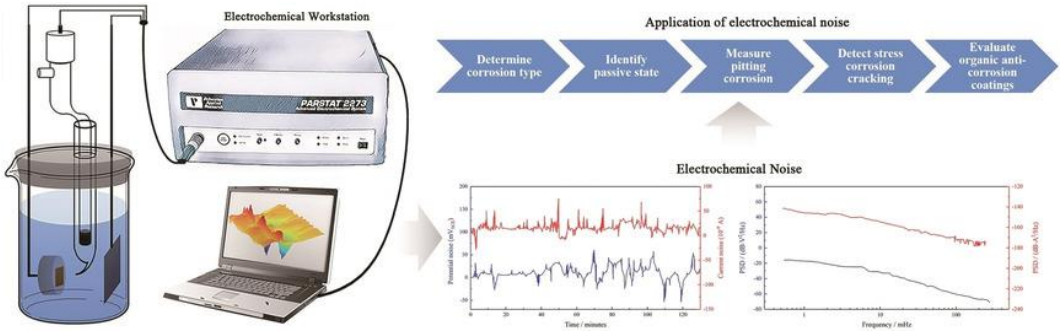

Fig. 12. Typical test setup, representative data, and procedure of the EN approach [281].

EN has been used to detect the initiation of pipeline SCC in limited laboratory studies. Li et al. [282] used EN to investigate the SCC of steel pipes by analyzing EN signals. The evolution of corrosion morphology was detected, but detailed dimensions of the cracks were not provided. Contreras et al. [283] applied EN to detect SCC in low-carbon steel (X52) exposed to synthetic soil solution (NS4) at room temperature with pH values of 5, 8, and 10. Test results showed that the EN was capable of detecting transient activation-passivation events. Crack dimensions were not provided.

EN has been applied to monitor the development of SCC in various materials, demonstrating its effectiveness in detecting crack initiation and propagation. In stainless steels, EN detected early-stage SCC in stainless steels [284–291], with notable applications in H_2S environments and welded structures, where it is often combined with AE techniques for enhanced accuracy. For aluminum alloys, EN detected localized corrosion-induced SCC, with the Hurst exponent used to quantify corrosion behavior [292]. In low-carbon steels, particularly pipeline steel (X52), EN monitored the development of SCC in synthetic soil solutions in real time [293]. Titanium alloys, such as Ti-6Al-4V, benefited from EN monitoring in welded joints, where induction heating treatments enhanced SCC resistance by altering microstructure [294]. Meanwhile, nuclear industry materials, like Alloy 690, leveraged EN signal intensity and frequency shifts to assess SCC initiation [295].

Furthermore, EN has been used to advance the understanding of crack initiation mechanisms, crack propagation behavior, and crack interactions. By analyzing the EN signal, crack initiation,

propagation, and final failure can be identified by specific EN signal patterns, as shown in **Table 5** [296–300].

EN identifies the initiation and propagation of SCC into four stages. In the first stage, the passive film breakdown with pitting or localized corrosion, the EN signals were present as low-frequency, low-amplitude. After that, the initiation of SCC with pitting and micro-crack formation caused high-amplitude current pulses. Third stage is the propagation of SCC with high-intensity EN signals. The final stage is the failure of material, EN signal shows high-amplitude and low-frequency potential fluctuations. Furthermore, the development of SCC can be predicted by analyzing the EN signals. In summary, EN is sensitive to the corrosion and early-stage of SCC according to existing research. However, due to limitations in specimen size, this method is more suitable for laboratory mechanism testing rather than for large-scale or practical applications.

Table 5. Characteristics of EN signal during SCC

SCC stage	Characteristics of EN signal
Initial stage (passive film breakdown)	Low-frequency, low-amplitude noise signals associated with pitting or localized corrosion
Crack initiation stage	Short-term high-amplitude current pulses, typically associated with pitting or micro-crack formation
Crack propagation stage	Middle frequency, high-intensity signals with gradual changes in potential noise
Crack failure stage	High-amplitude, low-frequency potential fluctuations, indicating imminent material failure

5.4.2 Electrochemical impedance spectroscopy

As an electrochemical technique based on small-amplitude sinusoidal voltage or current perturbations, EIS has been used to study the electrode interface and electrochemical reaction kinetics. EIS involves applying an alternating voltage (or current) over a range of frequencies and measuring the corresponding alternating current (or voltage) response to obtain the impedance spectrum of the system. The impedance data are typically analyzed using Nyquist or Bode plots and fitted into equivalent circuit models to extract key parameters such as charge transfer resistance, double-layer capacitance, and Warburg impedance for diffusion process.

EIS has been used to analyze the mechanical behavior of standardized specimens made of different materials. For pipeline steels, EIS has been used to monitor SCC under different environmental conditions in laboratory testing [26,301,302]. For pipeline steels (X70 and X80), EIS was used in high-pH carbonate-bicarbonate solutions, leading to the development of circuit models that simulate SCC-related electrochemical behavior, allowing for early crack detection [209,210]. SCC under disbonded coatings was another major concern for buried pipelines. Research has shown that disbonded coatings create shielding effects, resulting in localized corrosion and SCC [211]. EIS measurements were used to characterize the corrosion behavior beneath coatings and detect variations in charge transfer resistance associated with SCC initiation and growth. Similarly, studies on low-carbon steel (X52) demonstrated that SCC susceptibility increased with higher yield and tensile stress, while cathodic overprotection exacerbated SCC [212].

EIS has been used to study the mechanisms of SCC. EIS has been instrumental in analyzing passive film rupture under mechanical load. Studies using dynamic electrochemical impedance spectroscopy have shown that SCC initiation in stainless steels (304 and 304L) is closely linked to passive film breakdown, especially in chloride-rich environments, where stress-induced phase shifts in impedance spectra correlate with crack propagation [25,203–205]. Furthermore, EIS has been applied to sulfide SCC in stainless steels, revealing a decrease in charge transfer resistance after yielding, indicating SCC initiation [206]. Investigations on nickel-based alloys, including Alloy 600, 182, and 690, demonstrate that SCC susceptibility is strongly influenced by applied potential and film properties [207]. For instance, studies on Alloy 600 in high-temperature NaOH solutions found that SCC rates peak near 0.20 V, with impedance changes correlating to crack depth [208].

EIS has been applied to detect SCC in high-temperature and aggressive environments. For nickel-based Alloy 182 in high-temperature water, EIS distinguished SCC susceptibility near the Ni-NiO transition, revealing impedance variations linked to oxide layer morphologies [207]. Similarly, 304 stainless steels tested in high-temperature acidic solutions (5N H_2SO_4 + 0.1M NaCl) exhibited distinct phase shifts at specific frequencies, which correlated with SCC formation [25]. In hydrogen-induced SCC scenarios, EIS provided valuable insights into HE mechanisms, with significant shifts in impedance spectra confirming hydrogen's role in SCC progression [212]. These applications underscore EIS's capability to provide real-time, non-destructive monitoring of SCC across various materials and environments. EIS is sensitive to early corrosion processes. Nevertheless, the applicability of EIS to field testing is restricted due to size constraints of the specimens and the need for a well-controlled testing environment.

5.5 Comparison and evaluation of techniques

Although conventional monitoring techniques have been proven to be effective for SCC detection, the applicability, sensitivity, accuracy, and effectiveness vary depending on the underlying principles. This section provides a comparative analysis of the mainstream SCC monitoring technologies introduced in previous sections, offering insights into selecting the optimal monitoring approach for specific scenarios.

Firstly, SCC monitoring technologies can be categorized into two parts, suitable for small-scale or large-scale applications. Small-scale SCC monitoring is primarily used for localized defect detection, microscopic material changes, or laboratory research, emphasizing high sensitivity and high resolution. Some localized industrial applications, such as weld inspections or specific corrosion-prone areas, can also fall under this category. In contrast, large-scale SCC monitoring aims for large structures, long-term monitoring, or industrial field applications, prioritizing monitoring coverage, remote detection capabilities, and adaptability to complex environments. Due to constraints in scale and operational requirements, some techniques are not commonly used for in-situ monitoring, though certain electrical and electrochemical methods, like DCPD and EIS, can be adapted for long-term monitoring in specific cases. Additionally, many electrical and electrochemical methods are primarily used for research due to the complexity of equipment layout and measurement requirements, though some, like DCPD, have industrial applications in high-temperature and high-pressure environments. In contrast, acoustic emissions and ultrasonic testing often be used for detecting defects and cracks in-situ. Only a few piezoelectric sensors need to be placed on the metal surface for crack detection.

Secondly, SCC monitoring techniques can be broadly categorized into those focusing on corrosion detection and those emphasizing crack detection. Although electrochemical methods are not effective in accurately measuring crack size, they excel at detecting early-stage corrosion and providing SCC early warnings, which is particularly useful as SCC is primarily initiated by electrochemical corrosion processes before significant crack formation. In contrast, non-destructive monitoring techniques such as DIC, AE, and UT primarily focus on detecting and monitoring crack formation and propagation in SCC. To some extent, these methods can effectively measure crack size and depth, with DIC being suitable for surface deformation analysis, AE for crack propagation monitoring, and UT for crack depth measurement.

Thirdly, SCC monitoring techniques can also be classified based on whether they are intrusive or non-intrusive. DIC and IRT are completely non-contact monitoring techniques, while AE, UT, and ECT require sensors to be attached to the material surface. These techniques do not require sensors to be embedded inside the structure; they only need to be placed on the material surface or at a distance, without significantly affecting the structure's operational performance. In contrast, DCPD, EN, and EIS are intrusive monitoring techniques, as they require sensor placement within or directly on the material. These methods may influence the material's integrity or alter its operational characteristics, depending on the specific application.

Finally, based on existing research, the crack measurement sensitivity, strength, and weakness of various SCC monitoring techniques has been summarized, as shown in **Table 6**. Each method has their strengths and weaknesses, e.g., high sensitivity, sizing capability, and non-intrusive.

Table 6. Comparison between SCC monitoring techniques

Techniques	Sensitivity	Strengths	Weaknesses
DIC	Depending on image resolution and operation object	• Low-cost cameras • Robustness to materials • High resolution • Full-field measurement	• Limited to surface defects • Sensitive to surface textures • Sensitive to lighting conditions
IRT	Depending on image resolution and operation object	• Robustness to materials • High resolution • Full-field measurement	• Limited to surface defects • Sensitive to environmental factors (temperature, humidity)
AE	Depending on signal-to-noise ratio	• Real-time monitoring • Passive measurements	• Low signal-to-noise ratio • Complex post-processing
UT	Slit defects deeper than 0.05 mm [303]	• High sensitivity to fine SCC • Capable of detecting, locating, and quantifying SCC	• Expensive devices • Inefficiency in time and labor • Low accuracy for closed SCC
ECT	Slit defects deeper than 0.1mm [304]	• High sensitivity to fine SCC	• Limited to smooth surfaces
DCPD	Slit defects deeper than 3 mm [305]	• Simple and low cost • Can detect hidden cracks	• Limited to conductive materials • Low spatial resolution
EN	Sensitive to the presence of SCC. Inapplicable to quantify SCC.	• High sensitivity to fine SCC	• Limited to conductive materials • Limited specimen sizes • Sensitive to solution resistance and electrical charges
EIS	Sensitive to the presence of SCC. Inapplicable to quantify SCC.	• High sensitivity to fine SCC	• Limited specimen sizes • Susceptible to environmental influences

However, effective techniques for monitoring multi-scale SCC, ranging from micro-scale to macro-scale, with high sensitivity and high accuracy have yet to be developed. Although previous research has deepened the understanding of pipeline SCC, important knowledge gaps still exist. The effects and underlying mechanisms of key factors, such as pressure cycling, temperature cycling, and metallurgy, have not been sufficiently studied. The knowledge gaps have hindered the advancement of pipeline operation and maintenance (O&M) management, ultimately impacting the pipeline's service life. Additionally, the coupling effect of various factors has not been fully evaluated. In natural environments, the numerous and complex factors influencing pipeline SCC make it challenging to accurately assess their interactions. In experimental settings, research is constrained by available equipment and the long-term nature of SCC development. Furthermore, integrating theoretical mechanisms of SCC with experimental data to gain deeper insight into the effects of coupled factors remains a significant challenge.

5.6 Emerging techniques

Advancements in artificial intelligence (AI) and robotics have provided innovative solutions for SCC monitoring. AI-powered data analysis can efficiently process large volumes of complex data, enhancing detection accuracy and prediction capabilities. Meanwhile, the use of robots helps overcome the limitations of manual inspection, making SCC monitoring more efficient and accurate. Autonomous robots equipped with high-resolution imaging and ultrasonic inspection capabilities can perform inspection tasks in complex environments, and AI algorithms leverage machine learning (ML) and deep learning (DL) techniques for defect detection and prediction.

5.6.1 AI assisted vision detection

Deep learning and computer vision have significantly improved the monitoring of SCC, offering automated, efficient, and highly accurate detection methods. Traditional SCC inspection approaches, such as manual visual examination and basic image processing techniques, suffer from subjectivity, inconsistency, and high labor costs. In contrast, deep learning models, particularly convolutional neural networks (CNN) and residual neural networks (ResNets), have demonstrated superior performance in detecting and classifying SCC features with high precision. These methods have been applied across various materials and structures, including concrete, nuclear fuel storage canisters, gas pipelines, and stainless-steel alloys. For instance, machine learning models were used to evaluate crack patterns [306]. Deep learning-based segmentation techniques automated corrosion detection in nuclear storage canisters [307,308]. Deep learning has been applied to detect SCC, addressing challenges related to nonlinear, multidimensional, and noisy data, although the scarcity of data remains a challenge [309].

Further advancements include the integration of X-ray microscopy and deep learning for detecting SCC in turbine blades, where multi-modal imaging workflows enable precise localization of cracks [310]. Automated segmentation of quasi-brittle fractures in stainless steel using deep encoder-decoder neural networks has significantly improved fracture analysis accuracy, reducing human bias and error [311].

5.6.2 AI assisted signal processing

In SCC monitoring, the introduction of AI technology has significantly improved the efficiency and accuracy of signal processing. Unsupervised learning and deep learning models

were used to analyze the signals related to SCC [312,313]. For example, K-means clustering was used in signal feature analysis and anomaly detection. By clustering AE signals and EN data, different types of corrosion patterns, such as distinguishing normal signals, localized corrosion signals, and crack propagation signals, were automatically classified. The combination of K-means with principal component analysis (PCA) for dimensionality reduction helped reduce computational complexity and improve classification accuracy [314].

Deep learning techniques have demonstrated superior adaptability in signal processing. CNN models were used to analyze ultrasonic signals, avoiding information loss caused by traditional image conversion, and improved classification precision via extracting crack evolution features. Meanwhile, self-supervised learning enabled machine learning models to learn generalized features under limited labeled data conditions, enhancing their adaptability to different environments [315]. Unsupervised learning methods, such as Isolation Forest and One-Class Support Vector Machine, have been used to detect anomalies in SCC signals [316].

5.6.3 Robot assisted monitoring

SCC often occurs in extreme environments or complex regions that are difficult for human inspectors to access. Therefore, robot-assisted monitoring has become a crucial and cutting-edge solution for SCC detection and assessment. Advanced robotic systems integrate multiple non-destructive testing techniques, enabling remote, autonomous, and high-precision detection in hazardous environments, such as oil and gas pipelines [317], nuclear power plants [318], steel bridges [319], and aerospace structures[320].

Several studies have demonstrated the effectiveness of robotic-assisted SCC monitoring systems by combining robotic platforms with various NDT methods: EMAT and Laser-Induced Breakdown Spectroscopy have been successfully deployed in robotic systems like PRINSE for remote SCC detection in nuclear storage canisters, enabling non-contact monitoring of Chloride induced SCC [321]. Climbing robots equipped with sensors allow for autonomous corrosion and crack detection in steel bridges and large structures, effectively maneuvering complex surfaces while reducing manual inspection risks [322]. Laser ultrasonic technology has been integrated into robotic inspection systems, utilizing Rayleigh waves to remotely detect SCC with high precision, making it an effective tool for monitoring hazardous industrial environments [323]. By combining these robotic platforms with advanced NDT techniques, SCC monitoring has become more reliable, efficient, and scalable, significantly improving structural integrity assessment and predictive maintenance in critical industries.

6. Modelling and prediction of SCC

Crack growth rate prediction models with good predictive performance under specific conditions can help assess structural integrity and remaining service life, identify potential failure risks, optimize maintenance strategies, and guide engineering decisions to ensure structural safety and reliability, thus attracting extensive attention in practice. Crack growth rate prediction models focus on two approaches: (1) SCC development mechanism and empirical data, and (2) machine learning. This section discusses crack growth prediction models from these two perspectives.

6.1 Theoretical and empirical models

Since SCC was first reported in the 1960s, it has attracted widespread attention due to the significant failure risks it poses to pipelines [27]. Considerable research has been conducted on the influencing factors and mechanisms of SCC. Based on the current understanding of SCC mechanisms and empirical data, crack growth rate prediction models for pipeline steel exposed to near-neutral pH and high-pH corrosion environments have been developed.

6.1.1 Near-neutral pH SCC

As described in section 3.1, the dominant factors driving the different stages of near-neutral pH SCC development vary. In the early stage, crack growth is mainly controlled by anodic dissolution. Due to the differential dissolution rates at the crack surface and tip, along with the residual stress decreasing with depth in the pipeline, crack passivation and dormancy occur. During the crack propagation stage, the combined effects of HE and mechanical loading govern crack growth. This subsection discusses the crack growth rate prediction models developed for both the initiation and propagation stages.

6.1.1.1 Crack initiation and early-stage growth

Based on the study of crack initiation and early-stage growth mechanisms in near-neutral pH environments, along with the analysis of field crack data from pipelines affected by near-neutral pH SCC, Zhao et al. [29] proposed an equation to describe the early-stage crack growth behavior of pipeline steels, as shown in Equation (1). Model parameters m, r, and h were determined through fitting the data of crack depth-length relationships and experimental measurement of dissolution rates.

$$\frac{da}{dt} = \begin{cases} e^{-\frac{a}{m}} \cdot r, & a \leq 1.0\ mm \\ h, & a > 1.0\ mm \end{cases} \quad (1)$$

where $\frac{da}{dt}$ is the crack depth growth rate (mm/s); a is the crack depth (mm); m is a parameter obtained by data fitting; r is the crack growth rate by dissolution along the pipe surface; and h is the crack depth growth rate caused by the dissolution of the crack tip material when crack depth reaches 1.0 mm.

6.1.1.2 Crack propagation stage

(1) Superposition model

Early crack growth models for pipeline steels in near-neutral pH environments are commonly referred to as superposition models because these models consider the crack growth process as the superposition of corrosion fatigue and SCC [11,31]:

$$\left(\frac{da}{dN}\right)_{total} = \left(\frac{da}{dN}\right)_{fatigue} + \frac{1}{f}\left(\frac{da}{dt}\right)_{SCC} \quad (2)$$

where $\left(\frac{da}{dN}\right)_{total}$ is the total crack growth per cycle in a near-neutral pH solution; $\left(\frac{da}{dN}\right)_{fatigue}$ is the crack growth per cycle in air; f denotes the loading frequency; and $\left(\frac{da}{dt}\right)_{SCC}$ is the crack growth in terms of time in near-neutral pH SCC environment.

(2) Chen et al.'s model

Chen et al. [31] pointed out that the SCC behavior of pipeline steel in near-neutral pH environments shows similarities to corrosion fatigue behavior. They emphasized the importance of calculating the contribution of corrosion fatigue to crack growth. Based on empirical data, they concluded that the Paris law and the crack tip strain rate model are inadequate for describing the crack growth behavior of pipeline steel under cyclic fatigue loading. Instead, they proposed that normalizing the data using Equation (3) could more effectively establish the relationship between crack growth rate, mechanical loading, and environmental corrosion.

$$M = \frac{\Delta K^2 K_{max}}{f^{0.1}} \tag{3}$$

where ΔK is the change in stress intensity at the crack tip due to cyclic loading; K_{max} is the maximum stress intensity at the crack tip; and f is the loading frequency.

(3) Zhao et al.'s model

Zhao et al. [32] further indicated that crack growth under transverse cyclic loading in a near-neutral pH environment can be described by Equation (4):

$$\frac{da}{dN} = A \cdot \left(\frac{\Delta K^{\alpha} K_{max}^{\beta}}{f^{\gamma}} \right)^{n} + h \tag{4}$$

where A, n, α, β, and γ are constants; the relative contributions of ΔK and K_{max} to crack growth are represented by α and β, with $\alpha + \beta = 1$; γ represents the influence of the corrosive environment on the crack growth rate; and h represents the contribution of SCC, which is one order of magnitude lower than the contribution of HE-enhanced corrosion fatigue crack growth.

More specifically, crack growth caused by anodic dissolution in near-neutral pH environment is minimal and can be considered negligible [35]. Current research on predicting Stage 2 crack growth behavior of SCC in near-neutral pH environments primarily emphasizes the role of HE in enhancing the corrosion fatigue mechanism and their combined contribution to crack propagation [324].

(4) Lu et al.'s model

Lu et al. [36] indicated that crack growth of pipelines in near-neutral pH environments is controlled by HE in the fracture process zone ahead of the crack tip. They modified the model in Equation (3) and developed a crack growth model for pipelines in near-neutral pH environments based on a HE-enhanced corrosion fatigue mechanism. The model is expressed as follows:

$$\frac{da}{dN} = B_0 \left[ln\left(\frac{C_{cr}^{L}}{C_B} \right) \right]^{-2} \left(\frac{\Delta K_{eq}}{f^{\frac{1}{24}}} \right)_{th}^{6}; \quad \frac{\Delta K_{eq}}{f^{\frac{1}{24}}} \geq \left(\frac{\Delta K_{eq}}{f^{\frac{1}{24}}} \right)_{th} \tag{5}$$

where $\frac{da}{dN}$ represents the crack growth increment per loading cycle; B_0 is a material constant; C_{cr}^{L} is the critical hydrogen concentration in the fracture process zone required to initiate microcracks; C_B is the concentration of hydrogen dissolved in bulk material; ΔK_{eq} is the equivalent stress intensity factor range; and f is the loading frequency.

(5) Xing et al.' model

Based on Chen et al.'s model, Xing et al. [49] developed a new crack growth model by incorporating the effects of hydrogen potential, diffusivity, crack tip hydrostatic stress, and critical loading frequency, as shown below:

$$\left(\frac{da}{dN}\right)_{total} = \left[\frac{4(1+\nu)\Omega}{3\pi k_B T\sqrt{2\pi} ln(\frac{1}{c_0})}\right]^{2n} \left(\left(\frac{1+R}{1-R}\right)\frac{\Delta K^2}{(f/f_{critical})^{\gamma}}\right)^{n}, f > f_{critical} \quad (6)$$

where $\left(\frac{da}{dN}\right)_{total}$ represents the total crack growth pear cycle; ν is Poisson's ratio; Ω is the partial volume of hydrogen atom (m^3); k_B is the Boltzmann constant (1.3806×10^{-23} m^2 kg s^{-2} K^{-1}); T is the temperature (K); c_0 is the atomic ratio of H/Fe away from the crack tip; $R = K_{min}/K_{max}$ is the stress intensity factor ratio; γ and n are material constants; and $f_{critical}$ represents the minimum loading frequency under which crack growth rate reaches the maximum value and is independent of loading frequency f [324].

(6) Variable amplitude loading fatigue crack growth

During pipeline operation, pressure fluctuations are typically variable amplitude loads rather than constant amplitude cyclic loads. Therefore, studying the crack growth rate under variable amplitude cyclic loading is necessary. The crack growth rate for a variable amplitude loading block can be expressed in Equation (7) [11]. However, the impact of load interactions and loading history on crack growth behavior under variable amplitude pressure fluctuations has not been fully considered [12].

$$\left(\frac{da}{dN}\right)_{block} = N_1\left(\frac{da}{dN}\right)_1 + N_2\left(\frac{da}{dN}\right)_2 + \cdots \quad (7)$$

where $\left(\frac{da}{dN}\right)_{block}$ is the linear summation; $\left(\frac{da}{dN}\right)_i$ represents the constant amplitude crack growth rate at amplitude i, and N_i is the number of cycles in the block with amplitude i.

6.1.2 High-pH SCC

Lu et al. [52] developed a crack growth model for gas and liquid pipelines in high-pH environments, based on the mechanism of repeated rupture of the passive film at the crack tip. For gas pipelines, loading records show that 90% of the stress ratios exceed 0.85, with frequencies below 10^{-3} Hz. As a result, crack growth is predominantly governed by the SCC mechanism, with minimal influence from cyclic loading. The corresponding crack growth rate model is as follows [52]:

$$\dot{a_e} = \dot{a_s} = (A_0 B i_a^*)^{\frac{1}{1-n}}\left[ln\left(\frac{K_m^2 - K^2{}_{ISCC}}{\pi r_0 \sigma_Y^2}\right)\right]^{\frac{N}{N-1}\frac{n}{1-n}}; K_m > K_{ISCC} \quad (8)$$

where $\dot{a_e}$ and $\dot{a_s}$ represent the crack velocity component due to environmental attack and crack velocity component due to SCC under sustained loading, respectively; A_0 is the coefficient correlating crack velocity; B is a material constant; i_a^* is peak current density range immediately after rupture of passive film; n is the exponent of transient current decay; K_m and K_{ISCC} represent the mean stress intensity factor in one stress cycle and threshold of stress corrosion cracking,

respectively; r_0 is the specific length for crack tip strain rate calculation; σ_Y is the yield strength of pipeline steel; and N is strain-hardening exponent.

For liquid pipelines, loading records indicate the presence of stress ratios as low as 0.05, with a relatively higher average loading frequency. Crack growth in these conditions involves the combined effects of SCC, cyclic load-enhanced SCC, and corrosion fatigue, with the corrosion fatigue contribution increasing as environmental corrosiveness decreases. The corresponding crack growth rate model is as follows [52]:

$$\dot{a} = \dot{a_e} + \dot{a_F} = A_0 i_a^* \left\{ B\dot{a} \left[ln\left(\frac{K_m^2 - K_{ISCC}^2}{\pi r_0 \sigma_Y^2} \right) \right]^{\frac{N+1}{N-1}} + \mu(K_m^2 - K_{ISCC}^2) \right\}^n + Cf\left(2\frac{1-R_\sigma}{1+R_\sigma}\right)^{nF} K_m^{nF}; K_m > K_{ISCC} \quad (9)$$

where $\dot{a}$, $\dot{a_e}$, and $\dot{a_F}$ represent the crack velocity, crack velocity component due to environmental attack, and crack velocity component due to fatigue, respectively; A_0 is the coefficient correlating crack velocity; B is a material constant; i_a^* is peak current density range immediately after rupture of passive film; $\dot{a}$ denotes crack velocity; K_m and K_{ISCC} represent the mean stress intensity factor in one stress cycle and threshold of stress corrosion cracking, respectively; r_0 is the specific length for crack tip strain rate calculation; σ_Y is the yield strength of pipeline steel; N is strain-hardening exponent; μ is the coefficient characterizing the effect of cyclic loading; n is the exponent of transient current decay; C is the coefficient of Paris equation; f is loading frequency; R_σ is stress ratio of minimum stress to maximum stress; and F is Faraday's constant.

6.1.3 Summary

Despite some progress that has been made, the understanding of the influencing mechanisms remains incomplete, and the accumulation of empirical data is still limited. This makes it challenging for crack growth rate prediction models to achieve high accuracy. For example, the lack of knowledge regarding the effects of load interaction and loading history on SCC development makes it difficult to adequately account for these factors in existing theoretical and empirical data-based models, thus affecting their prediction accuracy and reliability [12].

6.2 Machine learning assisted prediction

The application of ML in SCC prediction has enhanced the accuracy, efficiency, and robustness of SCC management. Traditional SCC prediction models rely on theoretical models or empirical formulas, which often struggle to capture the complexity of SCC initiation and propagation due to the interactions between stress, environment, and material properties. ML, however, provides data-driven solutions that integrate historical SCC data with advanced algorithms to improve prediction accuracy and automate the analysis of SCC growth rates. In nuclear applications, empirical SCC prediction models are being replaced by ML-based models that integrate real-time monitoring data to predict the probability of SCC initiation and growth [325,326]. Representative research is summarized in **Table 7**.

Datasets are the fundamental part in developing reliable machine learning models. The quality and diversity of the datasets significantly influence the performance of ML models. ML models leverage large datasets to identify hidden patterns among influencing parameters such as stress intensity, temperature, and electrochemical potential [327]. In previous research of SCC prediction, datasets were mainly from experiments. For example, Wang et al. [328] trained ML models to predict the crack propagation rate based on data collected from experiments in relevant publications. A total of 99 data points with 5 input features (cold work, yield strength, vickers hardness, apparent stress intensity factor, and temperature) and 1 output target were used. Collecting the datasets from existing publications is the most common method, Lajevardi et al. [329] also collected data from references. The variables included temperature, chloride ions concentration, applied stress and time of the SCC failure. Furthermore, transfer learning, on the other hand, allows ML models trained on one dataset to be adapted to other SCC environments, reducing the need for extensive new training data [330].

Algorithms are the core of the machine learning models, and each algorithm has its own advantages depending on the nature of the data and the prediction goals. One of the most widely used ML approaches in SCC prediction is artificial neural networks (ANN). ANN models have been successfully developed to predict SCC crack growth rates in nuclear reactor materials and other high-risk environments [337]. Support vector machines (SVM) have also been used to predict SCC, outperforming traditional statistical methods in terms of accuracy and reliability [338]. Tree-based ensemble models, such as Random Forest (RF) and Extreme Gradient Boosting (XGBoost), have shown great promise in SCC risk assessment. These models have been employed to predict SCC susceptibility in various alloy systems, including Fe-Cr-Ni alloys, by incorporating chemical composition and stress parameters [339]. The XGBoost model has demonstrated remarkable accuracy ($R^2 = 0.949$) in predicting SCC susceptibility based on alloy compositions, making it a valuable tool for alloy design and risk assessment [336,340]. CNN and Gaussian Process Regression (GPR) has been utilized to accelerate the physics-based simulation of SCC crack growth [341]. Bayesian neural networks and Dynamic Bayesian Networks (DBN) have been employed to predict SCC growth rates under variable conditions, providing probabilistic estimates for SCC initiation and propagation. Such models are particularly valuable in applications where SCC detection is challenging, such as in buried pipelines or nuclear reactor components [342,343].

Table 7. Machin learning assisted prediction

Ref.	Data source	Dataset size	Feature number	Data analysis	Algorithm	Application	Accuracy
[331]	Experiment	163	8	Normalization	ANN	Predict crack growth rate	$R^2 = 0.98$
[332,333]	Field data	160	12	-	SVM PCA-SVM GBT-SVM	Assess the SCC risk of rock bolts	AUC = 0.81~ 0.86
[334]	Simulation	51,000	4	Normalization	Surrogate model	Predict corrosion and location of SCC	-
[325]	Experiment	99	5	-	RF XGBoost SVR	Predict the SCC crack growth rate	$R^2 = 0.83$

					GPR		
[335]	Experiment	269	37	Minimum, maximum, standard deviation	XGBoost	Assess SCC susceptibility	$R^2 = 0.949$
[336]	ILI data	7000	4	Minimum, maximum, standard deviation, mean	RF SVM Logistic regression	Pipeline defects classification	Accuracy: 67%-99.9%

ML models are utilized to construct component-property relationships, and optimization algorithms are utilized to identify the optimal component that provides the best SCC resistance while satisfying the constraints defined in specific applications. Cao et al. [344] used efficient global optimization algorithms to optimize the design of alloy and found that the Al-6.05Zn-1.46Mg1.32Cu-0.13Zr-0.02Ti-0.50Y-0.23Ce alloy had the best SCC resistance. The results were verified by SSRT. More relevant research on optimizing the material design to get better SCC resistance using ML models is available in references [345,346].

In summary, ML-based SCC prediction models have significantly improved the accuracy and efficiency of SCC risk assessments. Advanced techniques such as physics-informed ML have enhanced the ability to predict SCC susceptibility and growth rates. The continued development of these technologies, combined with improvements in data collection, and model interpretability, will further advance SCC prediction and mitigation strategies, ultimately enhancing the safety and reliability of pipelines and other critical infrastructure.

7. Mitigation strategies

According to Section 4, pipeline SCC is influenced by mechanical, environmental, and material factors, requiring a multifaceted approach for effective mitigation. This section reviews key strategies for delaying the initiation and progression of pipeline SCC, including reducing stresses through optimizing loading conditions and hydrostatic testing, controlling environmental factors by adjusting the composition of the corrosive medium and employing CP, maintaining coatings to prevent debonding and CP shielding, and conducting risk assessment using advanced monitoring and predictive modeling.

7.1 Stress control

The development of pipeline SCC is significantly influenced by stress conditions. Residual tensile stress in the pipeline can promote crack initiation, while cyclic pressure fluctuations may trigger the reactivation of dormant SCC cracks. Optimizing pipeline manufacturing processes and operating conditions can modify stress states, thereby mitigating the occurrence and progression of SCC [30,68].

Applying surface treatment techniques to introduce compressive stress has proven effective in reducing the influence of residual stress on crack propagation, serving as a preventive measure [66,67]. Yang et al. [68] found that surface mechanical grinding treatment enhanced the SCC resistance of AISI 316L stainless steel in high-temperature, chloride-rich environments by inducing a dense ultrafine-grained layer and compressive residual stresses. The dense ultrafine-grained layer enhances the SCC resistance of the machined surface, enabling it to suppress SCC

initiation when the surface tensile stress is below 874 MPa, indicating an improvement in the threshold stress for SCC initiation to some extent. It is worth noting that the optimization of pipeline manufacturing processes and the adoption of appropriate surface treatment techniques are suggested only as potential measures applicable to newly constructed pipelines.

Research on the impact of cyclic pressure fluctuations on SCC in pipeline steel has primarily concentrated on near-neutral pH environments. In contrast, studies investigating their effects on SCC progression in high-pH environments are relatively scarce. Therefore, SCC mitigation measures based on stress parameter control are largely derived from studies conducted in near-neutral pH corrosion environments. By controlling the stress parameters in the pipeline operation, such as maximum load, loading range, frequency, and load composition, the propagation of SCC cracks can be effectively suppressed. However, current research is mainly focused on laboratory testing, and precise stress control in pipelines during actual operation still faces certain challenges. According to Chen et al. [30], reducing K_{max} (maximum stress intensity factor at the crack tip) slowed down SCC propagation. However, since K_{max} is dependent on the volume of transported liquid, it is economically impractical to control K_{max}. Given that a higher R ratio contributes to the mitigation of SCC progression, adjusting the pressure fluctuation range provides a more effective strategy for mitigating SCC [30].

In near-neutral pH environments, low-frequency cyclic loading tends to promote hydrogen evolution, which can induce HE and compromise the long-term performance of pipelines [30]. Conversely, excessively high frequencies may sharpen crack tips, reducing the likelihood of crack dormancy [87]. A loading frequency of approximately 10^{-3} Hz is recommended [30]. In addition to the loading frequency, both the pressurization rate and depressurization rate require attention. Excessively slow pressurization rate should be avoided to prevent the accumulation of hydrogen segregation. A pressurization rate higher than 10^{-3} Hz is recommended [30]. To ensure sufficient time for hydrogen diffusion and redistribution, the depressurization rate should ideally be slower than the pressurization rate [30].

From the perspective of load type and composition, research indicates that underloading can accelerate crack propagation, while overloading may exhibit a retardation effect on crack growth [11]. Therefore, the occurrence of underloading conditions should be minimized. If underloading (large cycle components) is unavoidable, maintaining a high stress ratio (R-ratio) for the smaller cycle components between two large underload cycles or applying constant loading is recommended to mitigate adverse effects [30]. Additionally, hydrostatic testing, a widely used method for detecting critical-sized cracks in pipelines, is essentially a single-cycle overload loading process known to temporarily increase stress levels and delay crack growth. However, optimizing the pressurization rate during hydrostatic testing is crucial to reducing the risk of crack propagation [347]. Furthermore, post-hydrostatic testing underload cycles may limit the test's ability to delay crack growth [30].

7.2 Environmental control

Environmental factors play a significant role in both the initiation stage of SCC and the crack propagation stage under favorable stress conditions. Once coating delamination occurs, the corrosion environment directly interacts with the steel, and in the presence of metallurgical defects and tensile stress, it facilitates the initiation and propagation of SCC. Therefore,

controlling the corrosion environment can help mitigate the initiation and propagation of SCC to some extent. Although environmental factors are complex, involving variables such as pH, humidity, temperature, microbial activity, and the composition of the corrosive medium, targeted mitigation strategies can effectively reduce their impact. The corrosion environment to which a pipeline is exposed can be categorized into internal and external environments [348].The internal environment is primarily influenced by the properties of the transported medium. Measures such as optimizing the medium composition, adding corrosion inhibitors, and adjusting the pH value can effectively reduce corrosion risks [59]. Additionally, temperature has a significant impact on SCC, particularly in high-pH SCC environments. Therefore, in regions with elevated temperatures (e.g., near pump stations), installing cooling towers or other cooling devices can help regulate temperature and mitigate SCC risks [4].

The external environment, influenced by soil composition and climate conditions, not only directly impacts pipeline SCC but also affects the cathodic protection potential. Maintaining an appropriate cathodic protection potential is crucial for mitigating pipeline SCC. However, the cathodic protection potential may vary depending on soil types and moisture content, requiring careful adjustment and monitoring to ensure effective protection [349]. To minimize the impact of external environmental factors on pipeline corrosion, measures such as improving drainage systems and installing insulation layers can effectively slow SCC progression. Furthermore, combining effective environmental and pipeline monitoring techniques not only helps in identifying potential risks in a timely manner but also provides valuable data for SCC mechanism research and the optimization of prevention strategies.

7.3 Coating maintenance and repair

The degradation of coatings and the establishment of a corrosive environment are prerequisites for the occurrence of SCC. Therefore, selecting the appropriate coating for newly constructed pipelines is crucial to prevent SCC. For existing pipelines, identifying the coating types is vital for assessing their susceptibility to SCC [350].

Different coatings exhibit distinct protective properties, which are influenced by factors such as mechanical strength, water permeability, electrical resistance, resistance to disbonding, environmental durability, and compatibility with pipeline materials [4]. To minimize SCC risks, coatings should ideally resist debonding and avoid creating CP shielding effects when debonding occurs, ensuring the CP system remains effective [351]. Common coating types include:

- Asphalt Coating and Coal Tar Enamel: Known for strong adhesion and good weather resistance, but prone to becoming brittle, cracking, and permeable over time, increasing SCC risks. These coatings are commonly found in older pipelines [352,353].
- Fusion-Bonded Epoxy (FBE): Provides excellent mechanical strength, adhesion, and CP permeability, making it widely used in oil and gas pipelines [59,351].
- Liquid Epoxy: Offers robust corrosion protection and adhesion, making it suitable for industrial environments [59].
- Polyurethane (PU): Recognized for its chemical resistance, flexibility, and high adhesion to metal surfaces; however, it has poor resistance to mechanical deformation and high temperature deformation [354].

- Ceramic and Composite Coatings: Known for exceptional durability and high-temperature resistance but are relatively brittle [59].
- Polyethylene (PE) Tape: Prone to wrinkling and debonding under soil stress, which can create electrically shielded areas that weaken CP effectiveness. Disbonded PE Tape coatings have been linked to near-neutral pH SCC environments [352].
- Three-Layer Coating Systems (3LPE/3LPP): Combining the advantages of FBE and PE layers. This multi-layer structure offers excellent resistance to debonding, mechanical damage, corrosion, and oxygen permeation, making them highly effective in protecting oil and gas pipelines [355,356].

When selecting the appropriate coating type for newly constructed pipelines, it is crucial to consider the specific environmental conditions (e.g. corrosive medium, temperature, humidity, pH) and the available budget. This ensures long-term protection of the pipeline and effective prevention of SCC. For existing pipelines, identifying the coating type based on available records and using coating delamination detection technologies helps assess SCC susceptibility and supports coating maintenance decisions. According to the NACE SP0204 standard [350]: In high-pH corrosion environments, SCC is found beneath coal tar, asphalt, and tape coatings. In near-neutral pH conditions, SCC is also associated with tape and asphalt coatings. Advanced technologies such as EMAT technology are now available to effectively detect SCC and disbonded coatings [357].

7.4 Cathodic protection

Cathodic Protection (CP) is a widely used corrosion prevention technique for buried metal pipelines. By applying an electric current, CP reduces the metal surface potential of the pipeline, thereby inhibiting corrosion reactions. Maintaining the CP potential within an appropriate range can effectively prevent and mitigate the occurrence and progression of SCC. However, studies have shown that CP may sometimes have adverse effects under certain conditions.

First, overprotection (i.e., excessively low potential) can lead to negative consequences. On one hand, overprotection may accelerate coating degradation, increasing the likelihood of forming an alkaline environment conducive to high-pH SCC [4]. This elevated alkalinity can further compromise coating integrity, leading to disbondment from the pipe surface. Additionally, research has shown that in high-pH carbonate-bicarbonate solutions, while CP effectively inhibits anodic dissolution, it may also reduce its protective effect due to hydrogen permeation [358]. When the CP potential is set below -900 mV (SCE), hydrogen evolution intensifies, allowing hydrogen atoms to diffuse and accumulate at non-metallic inclusions, voids, and microcracks. This accelerates HE, compromising the ductility and toughness of high-strength pipeline steels such as X80 [358]. On the other hand, in near-neutral pH environments, overprotection also induce HE, thereby promoting SCC initiation and growth [80]. Research indicates that in near-neutral pH conditions, when the CP potential exceeds -1100 mV (SCE), SCC susceptibility increases significantly [44,81]. Therefore, overprotection should be avoided to minimize this risk.

Second, certain types of pipeline coatings (such as PE Tape) may create narrow cavities after debonding, which can hinder the effective penetration of CP current [352]. This shielding effect can lead to localized corrosion environments within these regions, increasing SCC risks. To

ensure CP effectively mitigates SCC risks, it is essential to strictly control CP potential within an appropriate range and adopt monitoring techniques such as Close Interval Survey (CIS) and Direct Current Voltage Gradient (DCVG) to promptly identify and address CP current shielding areas, thereby enhancing the overall effectiveness of the CP system.

7.5 Risk assessment and integrity management

By developing crack growth rate prediction models, in combination with appropriate monitoring technologies, inspection intervals, and integrity management guideline, it is possible to significantly reduce the irreversible economic losses caused by pipeline failures [55]. Several pipeline life prediction models have been proposed, as outlined in section 6. The models with superior predictive performance can offer valuable insights into assessing the remaining lifespan of pipelines and managing their integrity.

Additionally, there are established standards that comprehensively cover the design, materials, construction, inspection, corrosion control, operation, and maintenance of liquid and gas pipeline systems, such as ASME B31.4 (Pipeline Transportation Systems for Liquids and Slurries) [8] and ASME B31.8 (Gas Transmission and Distribution Piping Systems) [9]. Moreover, specific guidelines for SCC direct assessment exist, providing support from pre-assessment to data recording, maintenance decision-making, and selection of proper inspection intervals [350]. According to the NACE SP0204 standard [350], the pre-assessment of pipeline SCC susceptibility areas must consider various factors, including pipeline characteristics, construction information, environmental conditions, corrosion control measures, and operational data. After an initial evaluation to identify vulnerable areas, indirect inspection methods, such as CIS and DCVG data collection, can supplement pre-assessment results to more accurately locate high-risk pipeline sections, improving inspection efficiency and reducing excavation costs. Moreover, In-Line Inspection (ILI) uses advanced inspection tools such as ultrasonic and magnetic flux leakage sensors to assess the internal condition of pipelines. These tools provide vital insights into pipeline defects and potential vulnerable areas, supporting SCC risk assessments and the development of mitigation strategies. During direct excavation inspections, key data such as crack size, location, and corrosion environment should be recorded. The collected information helps determine if mitigation measures are needed and whether adjustments to inspection intervals are required.

Furthermore, hydrostatic testing is vital in pipeline integrity assessment, especially in detecting critical-size cracks [347]. It is applicable in key stages such as new pipeline commissioning, ongoing integrity management, recommissioning of idle pipelines, and pre-decommissioning evaluations.

8. Challenges and opportunities

Despite advancements in understanding, modelling, and mitigating pipeline SCC, significant challenges remain in fully elucidating its mechanisms and developing reliable prevention and rehabilitation strategies. The propagation of SCC is highly complex, driven by the interplay of metallurgical, environmental, and mechanical factors, yet current experimental and predictive methods struggle to capture its long-term, variable behavior under real-world conditions. Additionally, while existing monitoring techniques provide partial insights, limitations in sensitivity, accuracy, and scalability hinder comprehensive SCC detection across micro- and

macro-scale defects. Emerging technologies such as machine learning and robotic inspection offer promising opportunities but face challenges in data quality, real-world validation, and practical implementation. Addressing these gaps is critical to advancing SCC research, enhancing pipeline integrity management, and ensuring the safe and efficient operation and maintenance of pipelines. This section reviews key challenges and future opportunities at both the mechanism and monitoring aspects.

8.1 Mechanism aspect

The complex causes of SCC and its prolonged progression pose significant challenges to related mechanistic studies. Firstly, current experimental methods struggle to accurately replicate SCC development under actual field conditions. As SCC is a slow and cumulative phenomenon, short-term experimental models often fail to capture its true mechanisms. Moreover, monitoring natural SCC progression in field environments is typically time-consuming and labor-intensive, further constraining related research.

Secondly, current research predominantly focuses on the influence of individual variables on SCC behavior under specific environmental conditions, whereas studies exploring the coupled interactions between these factors, including their synergistic or inhibitory effects, remain limited. For instance, research on SCC behavior under variable pressure fluctuation is insufficient. In near-neutral pH environments, the effects of variable pressure fluctuations on SCC progression, as well as the role of load interactions and loading history in crack propagation, remain underexplored. Studies on high-pH environments are even more scarce.

Third, accurately predicting crack growth rates remain a major challenge in current research. Given the complex interplay between electrochemical reactions and mechanical loading responses induced by pressure fluctuations during the SCC process, existing models still have limitations in predicting crack growth rates and require further improvement.

In summary, the complexity of SCC mechanism stems from the interaction of multiple influencing factors, its prolonged development process, the limitations of experimental methods, and the inadequacies of existing predictive models. Future research should focus on the coupled effects of multiple variables, the influence of loading history, and the mechanisms of variable pressure fluctuations. Additionally, integrating field data with experimental validation will be essential to improving the accuracy and practicality of SCC crack growth prediction models.

8.2 Monitoring aspect

Effective techniques for monitoring multi-scale SCC ranging from micro-scale to macro-scale are yet to be developed. The individual techniques have shown various drawbacks: Linear ultrasonic guided wave techniques have high resolution and high sensitivity to macrocracks, but they have low sensitivity to microcracks; nonlinear ultrasonic guided wave techniques achieve higher sensitivity to microcracks but have lower performance in monitoring macrocracks; and acoustic emission techniques offer real-time monitoring data but have low accuracy and low spatial resolution. There is a need for developing an innovative monitoring technique with high sensitivity and high accuracy for monitoring multi-scale pipeline SCC.

Furthermore, although machine learning has been applied in SCC-related research, the effectiveness and availability of high-quality datasets remain key challenges. The complexity of

material characteristics and environmental conditions leads to a lack of well-labeled data, limiting model training and validation. Moreover, current machine learning research in SCC monitoring lacks in-situ industrial validation, making it difficult to assess if it truly effectiveness. Therefore, obtaining effective datasets from real-world environments and validating the accuracy of machine learning-based predictive models remain significant challenges.

In addition, research on robot-assisted monitoring is still in its early stages, and developing robots tailored to different application scenarios remains a critical challenge. Integrating SCC monitoring techniques with robotic systems to enable effective inspection in inaccessible areas and real-time crack detection represents a key future direction. Additionally, incorporating both SCC mitigation and repair strategies into robotic monitoring systems could be a valuable area of research.

9. Conclusions

This report reviews previous research on SCC, including the mechanisms, causal factors, monitoring techniques, prediction methods, current challenges, and new opportunities. The conclusions are summarized as follows:

(1) SCC propagation is governed by metallurgical properties, corrosive environments, and stress, with these factors often interacting in a coupled manner. Its time-dependent nature further complicates the underlying mechanisms.

(2) While extensive research has explored individual factors affecting SCC, studies on the combined effects of multiple variables remain limited. Current experimental methods face limitations in replicating real-world pipeline conditions, particularly in capturing SCC behavior under variable amplitude pressure fluctuations. This limitation is present not only in near-neutral pH environments, where research on the impact of variable pressure fluctuations on SCC progression remains limited, but is even more pronounced in high-pH environments, where such studies are scarce.

(3) Predicting crack growth rates remains a significant challenge due to the complex interplay between electrochemical reactions and mechanical loading responses induced by pressure fluctuations. Existing models, which are largely based on empirical data, require further improvement to better incorporate SCC development mechanisms and improve prediction accuracy.

(4) Various evaluation or monitoring approaches have been developed and demonstrated strengths in laboratory experiments. There is a need to develop an innovative monitoring technique for monitoring multi-scale pipeline SCC.

- The comparison and evaluation of SCC monitoring technologies shows that vision-based techniques, sound wave-based techniques and electrical techniques focused more on the crack propagation while electrochemical concentrated on the corrosion development.
- UT was primarily used to evaluate material conditions and construct two-dimensional surface images for estimating the locations and morphology of cracks. Linear ultrasonic testing can be used for sizing macro-scale cracks, while nonlinear

ultrasonic testing is effective in detecting micro-scale cracks. AE is highly sensitive to the evolution of SCC and has the potential of real-time detection.

- Vision-based methods are the most direct and simplest techniques for monitoring SCC. Both DIC and IRT can be used to detect, locate, and quantify the crack. Images are constructed to characterize the state and morphology of the cracks. However, they are limited to detecting surface cracks.
- Electrical techniques could detect the crack inside the material but only suitable for the conductive materials. ECT are sensitive to surface, shallow crack, and are limited in detect deep crack. DCPD can detect deep cracks and are capable to quantify the depth of SCC. However, accurate defect sizing remains challenging
- Electrochemical techniques can effectively detect the initiation of SCC. Both EN and EIS are sensitive to the corrosion and early-stage of SCC. However, due to limitations in specimen size and the need for a controlled testing environment, these methods are more suitable for laboratory testing rather than for practical applications.
- AI-powered data analysis can efficiently process large volumes of complex data, enhancing detection accuracy and prediction capabilities. However, AI-assisted monitoring still require large, effective datasets and on-site implementation. Robots help overcome the limitations of manual inspection, making SCC monitoring more efficient and accurate.

Project Financial Activities Incurred during the Reporting Period:

The Prime university (Stevens Institute of Technology) fully executed the agreement with the PHMSA and sub-universities (North Dakota State University and Rutgers University).

Project Activities with Cost Share Partners:

There were no major activities that were conducted during this reporting period with cost share partners.

Project Activities with External Partners:

The primary activities that were conducted during this reporting period with external partners or sub-universities include: (1) the kick-off meeting on November 4th, 2024; (2) recruitment of graduate student (Mr. Samuel Ajayi at North Dakota State University); and (3) collaborative effort for the literature review task (Task I).

Potential Project Risks:

We have not identified major projects risks. The project is progressing as planned.

Future Project Work:

In the next 30 days, we aim to make thorough preparations for the experiment to investigate multiple causal factors of pipeline SCC. The samples, equipment, experimental plan and execution process will be proposed based on Task II. In the next 60 days, we aim to conduct experiments and collect results based on Task II. We will also start to design innovative monitoring technologies based on acoustic sensing. In the next 90 days, we aim to write a research paper based on the experiment results. We will also test the effectiveness of the innovative monitoring techniques in Task II.

Potential Impacts on Pipeline Safety:

There are four main impacts: (1) *Improved Understanding of SCC Mechanisms*: The literature review enhances the understanding of SCC mechanisms, including the roles of metallurgical defects, environmental variables, and pipeline stresses. This knowledge contributes to better design experiments for investigating the effects of casual factors of pipeline SCC under various operational and environmental conditions. Insights from reviewed studies on SCC in high-pH, near-neutral pH, and acidic environments directly support the development of effective risk mitigation measures. (2) *Identification of Knowledge Gaps*: By summarizing existing gaps, such as limited understanding of coupled factors (e.g., temperature and pressure cycling), long-term SCC behavior, and the mechanism of variable pressure fluctuation, the project provides a roadmap for targeted research. (3) *Enhancement of Monitoring Techniques*: The review of nondestructive SCC monitoring methods summarizes the applicable scenarios, strengths, and weaknesses of mainstream monitoring technologies. The evaluation and comparison help in selecting appropriate techniques for practical applications based on different scenarios. Meanwhile, by highlighting the weaknesses of existing methods (e.g., limited to surface crack, ineffectiveness in micro-scale crack), the project identifies opportunities for innovative technologies. (4) *Collaborative Efforts for Timely Risk Mitigation*. The biweekly discussions ensure that potential risks, such as delays in the project timeline or test-bed preparation, are monitored and mitigated proactively. This collaborative approach strengthens the project's capacity to maintain alignment with safety-critical milestones and deliver timely recommendations for industry adoption. (5) *Foundation for Advanced Research and Application*: The recruitment of graduate students and initial research efforts provide the human capital and knowledge base needed for subsequent project phases, including experimental studies and advanced risk models. This supports the development of unified safety models for pipelines and long-term improvement in pipeline integrity management practices.

References

[1] Oracle Analytics Interactive Dashboards - Public Reports Portalpages&PortalPath=%2Fshared%2FPDM%20Public%20Website%2F_portal%2FPublic%20Reports&Page=Infrastructure (accessed January 6, 2025).

[2] Oracle Analytics Interactive Dashboards - SC Incident Trend Portalpages&PortalPath=%2Fshared%2FPDM%20Public%20Website%2F_portal%2FSC%20Incident%20Trend&Page=All%20Reported (accessed January 6, 2025).

[3] Xiao R, Zayed T, Meguid MA, Sushama L. Understanding the factors and consequences of pipeline incidents: An analysis of gas transmission pipelines in the US. Engineering Failure Analysis 2023;152:107498.

[4] Cheng YF. Stress corrosion cracking of pipelines. John Wiley & Sons; 2013.

[5] Cheng YF. Pipeline corrosion. Corrosion Engineering, Science and Technology 2015;50:161–2. https://doi.org/10.1179/1478422X15Z.000000000357.

[6] Tomar P, Kaur D, Harron L, Sen M, Fazli S. Quantitative Assessment of Incorrect Operations Threat. International Pipeline Conference, vol. 88582, American Society of Mechanical Engineers; 2024, p. V005T07A025.

[7] Cosham A, Hopkins P. An overview of the pipeline defect assessment manual (PDAM). 4th international pipeline technology conference, vol. 29, 2004, p. 720–45.

[8] Engineers AS of M. B31. 4: pipeline transportation systems for liquids and slurries, ASME; 2016.

[9] Engineers AS of M. B31. 8: gas transmission and distribution piping systems. American Society of Mechanical Engineers; 2016.

[10] Jones RH. Stress-Corrosion Cracking 2003. https://doi.org/10.31399/asm.hb.v13a.a0003633.

[11] Yu M. Crack Growth Behavior of Pipeline Steels under Variable Pressure Fluctuations in a Near-Neutral pH Environment. ERA 2015. https://doi.org/10.7939/R3J679788.

[12] Chen W. Modeling and prediction of stress corrosion cracking of pipeline steels. Trends in Oil and Gas Corrosion Research and Technologies 2017:707–48.

[13] Parkins RN. 1990 plenary lecture: Strain rate effects in stress corrosion cracking. Corrosion 1990;46:178–89.

[14] Niazi H, Eadie R, Chen W, Zhang H. High pH stress corrosion cracking initiation and crack evolution in buried steel pipelines: A review. Engineering Failure Analysis 2021;120:105013.

[15] Elboujdaini M, Revie RW. Metallurgical factors in stress corrosion cracking (SCC) and hydrogen-induced cracking (HIC). J Solid State Electrochem 2009;13:1091–9. https://doi.org/10.1007/s10008-009-0799-0.

[16] Rhouma AB, Sidhom H, Braham C, Lédion J, Fitzpatrick ME. Effects of surface preparation on pitting resistance, residual stress, and stress corrosion cracking in austenitic stainless steels. Journal of Materials Engineering and Performance 2001;10:507–14.

[17] Kentish P. Stress corrosion cracking of gas pipelines – Effect of surface roughness, orientations and flattening. Corrosion Science 2007;49:2521–33. https://doi.org/10.1016/j.corsci.2006.12.014.

[18] Chu R, Chen W, Wang S-H, King F, Jack TR, Fessler RR. Microstructure dependence of stress corrosion cracking initiation in X-65 pipeline steel exposed to a near-neutral pH soil environment. Corrosion 2004;60.

[19] Bulger JT, Lu BT, Luo JL. Microstructural effect on near-neutral pH stress corrosion cracking resistance of pipeline steels. J Mater Sci 2006;41:5001–5. https://doi.org/10.1007/s10853-006-0131-7.
[20] Lu BT, Luo JL. Relationship between yield strength and near-neutral pH stress corrosion cracking resistance of pipeline steels—an effect of microstructure. Corrosion 2006;62:129–40.
[21] Calabrese L, Proverbio E. A review on the applications of acoustic emission technique in the study of stress corrosion cracking. Corrosion and Materials Degradation 2020;2:1–30.
[22] Hernandez-Valle F, Clough AR, Edwards RS. Stress corrosion cracking detection using non-contact ultrasonic techniques. Corrosion Science 2014;78:335–42.
[23] Parkins RN. Predictive approaches to stress corrosion cracking failure. Corrosion Science 1980;20:147–66.
[24] Butusova YN, Mishakin VV, Kachanov M. On monitoring the incubation stage of stress corrosion cracking in steel by the eddy current method. International Journal of Engineering Science 2020;148:103212.
[25] Bosch R-W. Electrochemical impedance spectroscopy for the detection of stress corrosion cracks in aqueous corrosion systems at ambient and high temperature. Corrosion Science 2005;47:125–43.
[26] Shahriari A, Shahrabi T, Oskuie AA. A Study on Stress Corrosion Cracking of X70 Pipeline Steel in Carbonate Solution by EIS. J of Materi Eng and Perform 2013;22:1459–70. https://doi.org/10.1007/s11665-012-0418-6.
[27] Fang BY, Atrens A, Wang JQ, Han EH, Zhu ZY, Ke W. Review of stress corrosion cracking of pipeline steels in “low” and “high” pH solutions. Journal of Materials Science 2003;38:127–32.
[28] Javidi M, Horeh SB. Investigating the mechanism of stress corrosion cracking in near-neutral and high pH environments for API 5L X52 steel. Corrosion Science 2014;80:213–20.
[29] Zhao J, Chen W, Yu M, Chevil K, Eadie R, Van Boven G, Kania R, Been J, Keane S. Crack Growth Modeling and Life Prediction of Pipeline Steels Exposed to Near-Neutral pH Environments: Dissolution Crack Growth and Occurrence of Crack Dormancy in Stage I. Metall Mater Trans A 2017;48:1629–40. https://doi.org/10.1007/s11661-016-3951-3.
[30] Chen W. An Overview of Near-Neutral pH Stress Corrosion Cracking in Pipelines and Mitigation Strategies for Its Initiation and Growth. Corrosion 2016;72:962–77. https://doi.org/10.5006/1967.
[31] Chen W, Sutherby RL. Crack Growth Behavior of Pipeline Steel in Near-Neutral pH Soil Environments. Metall Mater Trans A 2007;38:1260–8. https://doi.org/10.1007/s11661-007-9184-8.
[32] Zhao J, Chen W, Yu M, Chevil K, Eadie R, Been J, Van Boven G, Kania R, Keane S. Crack growth modeling and life prediction of pipeline steels exposed to near-neutral pH environments: stage II crack growth and overall life prediction. Metallurgical and Materials Transactions A 2017;48:1641–52.
[33] Lu BT, Luo JL, Norton PR. Environmentally assisted cracking mechanism of pipeline steel in near-neutral pH groundwater. Corrosion Science 2010;52:1787–95.

[34] Van Boven G, Chen W, Rogge R. The role of residual stress in neutral pH stress corrosion cracking of pipeline steels. Part I: Pitting and cracking occurrence. Acta Materialia 2007;55:29–42.
[35] Cui Z, Wang L, Liu Z, Du C, Li X, Wang X. Anodic Dissolution Behavior of the Crack Tip of X70 Pipeline Steel in Near-Neutral pH Environment. J of Materi Eng and Perform 2016;25:5468–76. https://doi.org/10.1007/s11665-016-2394-8.
[36] Lu BT. Crack growth model for pipeline steels exposed to near-neutral pH groundwater. Fatigue Fract Eng Mat Struct 2013;36:660–9. https://doi.org/10.1111/ffe.12033.
[37] Chen W, Kania R, Worthingham R, Van Boven G. Transgranular crack growth in the pipeline steels exposed to near-neutral pH soil aqueous solutions: the role of hydrogen. Acta Materialia 2009;57:6200–14.
[38] Fang BY, Han EH, Wang JQ, Ke W. Stress corrosion cracking of X-70 pipeline steel in near neutral pH solution subjected to constant load and cyclic load testing. Corrosion Engineering, Science and Technology 2007;42:123–9. https://doi.org/10.1179/174327807X196843.
[39] Carter TJ, Cornish LA. Hydrogen in metals. Engineering Failure Analysis 2001;8:113–21. https://doi.org/10.1016/S1350-6307(99)00040-0.
[40] Eadie RL, Szklarz KE, Sutherby RL. Corrosion Fatigue and Near-Neutral pH Stress Corrosion Cracking of Pipeline Steel and the Effect of Hydrogen Sulfide. Corrosion 2005;61:167–73. https://doi.org/10.5006/1.3278171.
[41] Fang B, Han E-H, Wang J, Zhu Z, Ke W. Hydrogen in stress corrosion cracking of X-70 pipeline steels in near-neutral pH solutions. J Mater Sci 2006;41:1797–803. https://doi.org/10.1007/s10853-006-3944-5.
[42] Cui Z, Liu Z, Wang L, Li X, Du C, Wang X. Effect of plastic deformation on the electrochemical and stress corrosion cracking behavior of X70 steel in near-neutral pH environment. Materials Science and Engineering: A 2016;677:259–73.
[43] Shehata MT, Elboujdaini M, Revie RW. Initiation of Stress Corrosion Cracking and Hydrogen-Induced Cracking in Oil and Gas Line-Pipe Steels. In: Pluvinage G, Elwany MH, editors. Safety, Reliability and Risks Associated with Water, Oil and Gas Pipelines, Dordrecht: Springer Netherlands; 2008, p. 115–29. https://doi.org/10.1007/978-1-4020-6526-2_7.
[44] Zhang C, Wang H, He Y, Zheng W, Wang Y. Electrochemical potential dependence of SCC initiation in X60 pipeline steel in near-neutral pH environment. Journal of Materials Research and Technology 2023;27:4950–61.
[45] Cheng YF. Thermodynamically modeling the interactions of hydrogen, stress and anodic dissolution at crack-tip during near-neutral pH SCC in pipelines. J Mater Sci 2007;42:2701–5. https://doi.org/10.1007/s10853-006-1375-y.
[46] Lu BT, Luo JL, Norton PR, Ma HY. Effects of dissolved hydrogen and elastic and plastic deformation on active dissolution of pipeline steel in anaerobic groundwater of near-neutral pH. Acta Materialia 2009;57:41–9.
[47] Bueno AHS, Moreira ED, Gomes J. Evaluation of stress corrosion cracking and hydrogen embrittlement in an API grade steel. Engineering Failure Analysis 2014;36:423–31.
[48] Barrera O, Bombac D, Chen Y, Daff TD, Galindo-Nava E, Gong P, Haley D, Horton R, Katzarov I, Kermode JR, Liverani C, Stopher M, Sweeney F. Understanding and mitigating hydrogen embrittlement of steels: a review of experimental, modelling and

design progress from atomistic to continuum. J Mater Sci 2018;53:6251–90. https://doi.org/10.1007/s10853-017-1978-5.
[49] Xing X, Chen W, Zhang H. Prediction of crack propagation under cyclic loading based on hydrogen diffusion. Materials Letters 2015;152:86–9.
[50] Liu ZY, Wang XZ, Du CW, Li JK, Li XG. Effect of hydrogen-induced plasticity on the stress corrosion cracking of X70 pipeline steel in simulated soil environments. Materials Science and Engineering: A 2016;658:348–54.
[51] Beavers JA, Harle BA. Mechanisms of high-pH and near-neutral-pH SCC of underground pipelines. International Pipeline Conference, vol. 1, American Society of Mechanical Engineers New York; 1996, p. 555–68.
[52] Lu BT. Further study on crack growth model of buried pipelines exposed to concentrated carbonate–bicarbonate solution. Engineering Fracture Mechanics 2014;131:296–314.
[53] Ryakhovskikh IV, Bogdanov RI, Ignatenko VE. Intergranular stress corrosion cracking of steel gas pipelines in weak alkaline soil electrolytes. Engineering Failure Analysis 2018;94:87–95.
[54] Niazi H, Chevil K, Gamboa E, Lamborn L, Chen W, Zhang H. Effects of loading spectra on high pH crack growth behavior of X65 pipeline steel. Corrosion 2020;76:601–15.
[55] Ryakhovskikh IV, Bogdanov RI. Model of stress corrosion cracking and practical guidelines for pipelines operation. Engineering Failure Analysis 2021;121:105134. https://doi.org/10.1016/j.engfailanal.2020.105134.
[56] Song FM. Predicting the mechanisms and crack growth rates of pipelines undergoing stress corrosion cracking at high pH. Corrosion Science 2009;51:2657–74.
[57] Zhu M, Du C, Li X, Liu Z, Wang S, Zhao T, Jia J. Effect of Strength and Microstructure on Stress Corrosion Cracking Behavior and Mechanism of X80 Pipeline Steel in High pH Carbonate/Bicarbonate Solution. J of Materi Eng and Perform 2014;23:1358–65. https://doi.org/10.1007/s11665-014-0880-4.
[58] Fragiel A, Serna S, Malo-Tamayo J, Silva P, Campillo B, Martínez-Martínez E, Cota L, Staia MH, Puchi-Cabrera ES, Peréz R. Effect of microstructure and temperature on the stress corrosion cracking of two microalloyed pipeline steels in H2S environment for gas transport. Engineering Failure Analysis 2019;105:1055–68.
[59] Vakili M, Koutník P, Kohout J, Gholami Z. Analysis, Assessment, and Mitigation of Stress Corrosion Cracking in Austenitic Stainless Steels in the Oil and Gas Sector: A Review. Surfaces (2571-9637) 2024;7.
[60] Du H, An N, Wang X, Li Y, Liu Z, Jin A, Yang R, Pan Y, Li X. Enhancing the SCC Resistance of the Anchor Steel with Microalloying in a Simulated Mine Environment. Materials (Basel) 2023;16:5965. https://doi.org/10.3390/ma16175965.
[61] Sun J, Tang H, Wang C, Han Z, Li S. Effects of Alloying Elements and Microstructure on Stainless Steel Corrosion: A Review. Steel Research Int 2022;93:2100450. https://doi.org/10.1002/srin.202100450.
[62] Mohtadi-Bonab MA. Effects of different parameters on initiation and propagation of stress corrosion cracks in pipeline steels: a review. Metals 2019;9:590.
[63] Wang L, Xin J, Cheng L, Zhao K, Sun B, Li J, Wang X, Cui Z. Influence of inclusions on initiation of pitting corrosion and stress corrosion cracking of X70 steel in near-neutral pH environment. Corrosion Science 2019;147:108–27.

[64] Ghosh S, Kain V. Microstructural changes in AISI 304L stainless steel due to surface machining: Effect on its susceptibility to chloride stress corrosion cracking. Journal of Nuclear Materials 2010;403:62–7.
[65] Lyon KN, Marrow TJ, Lyon SB. Influence of milling on the development of stress corrosion cracks in austenitic stainless steel. Journal of Materials Processing Technology 2015;218:32–7.
[66] Turnbull A, Mingard K, Lord JD, Roebuck B, Tice DR, Mottershead KJ, Fairweather ND, Bradbury AK. Sensitivity of stress corrosion cracking of stainless steel to surface machining and grinding procedure. Corrosion Science 2011;53:3398–415.
[67] Que Z, Saario T, Toivonen A, Ehrnstén U. Stress corrosion cracking initiation susceptibility of Alloy 182 with different surface treatments. Corrosion Science 2022;196:110037.
[68] Yang C, Jiang X, Zhang W, Wang X. Enhancing stress corrosion cracking resistance of machined surface via surface mechanical grinding treatment for AISI 316 L stainless steel. Materials Characterization 2022;194:112493.
[69] Jack TR, Krist K, Erno B, Fessler RR. Generation of near neutral pH and high pH SCC environments on buried pipelines. NACE CORROSION 2000:NACE-00362.
[70] Sheng X, Ting Y-P, Pehkonen SO. The influence of sulphate-reducing bacteria biofilm on the corrosion of stainless steel AISI 316. Corrosion Science 2007;49:2159–76.
[71] Starosvetsky J, Starosvetsky D, Pokroy B, Hilel T, Armon R. Electrochemical behaviour of stainless steels in media containing iron-oxidizing bacteria (IOB) by corrosion process modeling. Corrosion Science 2008;50:540–7.
[72] Hayashibara H, Mayuzumi M, Mizutani Y, Tani J ichi. Effects of temperature and humidity on atmospheric stress corrosion cracking of 304 stainless steel. NACE CORROSION, NACE; 2008, p. NACE-08492.
[73] Zhang L, Li X, Du C. Effect of environmental factors on electrochemical behavior of X70 pipeline steel in simulated soil solution. Journal of Iron and Steel Research, International 2009;16:52–7.
[74] Cundong YE, Dejun K, Lei Z. Effects of temperature on stress corrosion of X70 pipeline steel in solution with oxygen. J Cent South Univ(Sci Technol) 2015;46:2432–8.
[75] Abubakar SA, Mori S, Sumner J. A review of factors affecting SCC initiation and propagation in pipeline carbon steels. Metals 2022;12:1397.
[76] Kritzer P. Corrosion in high-temperature and supercritical water and aqueous solutions: a review. The Journal of Supercritical Fluids 2004;29:1–29. https://doi.org/10.1016/S0896-8446(03)00031-7.
[77] Gadala IM, Alfantazi A. Electrochemical behavior of API-X100 pipeline steel in NS4, near-neutral, and mildly alkaline pH simulated soil solutions. Corrosion Science 2014;82:45–57.
[78] Contreras A, Hernández SL, Galván-Martínez R. Effect of pH and temperature on stress corrosion cracking of API X60 pipeline steel. MRS Online Proceedings Library (OPL) 2010;1275:S3-P28.
[79] Liu ZY, Li XG, Du CW, Zhai GL, Cheng YF. Stress corrosion cracking behavior of X70 pipe steel in an acidic soil environment. Corrosion Science 2008;50:2251–7.
[80] Contreras A, Sosa E, Espinosa-Medina MA. Cathodic protection effect on the assessment of SCC susceptibility of X52 pipeline steel. MRS Online Proceedings Library (OPL) 2009;1242:S4-53.

[81] Luo S, Yuan R, Wang J, He W, Xue Y, Liu M. Effect of Cathodic Polarization on SCC Behavior of a X52 Pipeline Steel in Service for 20 Years. J of Materi Eng and Perform 2023;34:1–11. https://doi.org/10.1007/s11665-023-09088-6.
[82] Wan H, Song D, Cai Y, Du C. The AC corrosion and SCC mechanism of X80 pipeline steel in near-neutral pH solution. Engineering Failure Analysis 2020;118:104904. https://doi.org/10.1016/j.engfailanal.2020.104904.
[83] Wan H, Song D, Liu Z, Du C, Zeng Z, Wang Z, Ding D, Li X. Effect of negative half-wave alternating current on stress corrosion cracking behavior and mechanism of X80 pipeline steel in near-neutral solution. Construction and Building Materials 2017;154:580–9.
[84] Li Z, Sun B, Liu Q, Yu Y, Liu Z. Fundamentally understanding the effect of Non-stable cathodic potential on stress corrosion cracking of pipeline steel in Near-neutral pH solution. Construction and Building Materials 2021;288:123117.
[85] TM0198 N. Slow strain rate test method for screening corrosion-resistant alloys (CRAs) for stress corrosion cracking in sour oilfield service. Houston, TX: Nace 2004.
[86] Liu ZY, Li XG, Du CW, Cheng YF. Local additional potential model for effect of strain rate on SCC of pipeline steel in an acidic soil solution. Corrosion Science 2009;51:2863–71. https://doi.org/10.1016/j.corsci.2009.08.019.
[87] Beavers JA, Jaske CE, Fessler RR. Effect of Pressure Fluctuations on the Propagation and Dormancy of Near Neutral pH Stress Corrosion Cracks in Underground Petroleum Pipelines. Proceedings of 15th EPRG-PRCI Joint Technical Meeting on Pipeline Research, Orlando, USA, 2005.
[88] Lambert SB, Beavers JA, Delanty B, Sutherby R, Plumtree A. Mechanical Factors Affecting Stress Corrosion Crack Growth Rates in Buried Pipelines, American Society of Mechanical Engineers Digital Collection; 2016. https://doi.org/10.1115/IPC2000-219.
[89] Wang S, Lamborn L, Chen W. Pre-cyclic-loading-enhanced Stage-1b stress corrosion crack growth of pipeline steels. Corrosion Science 2022;208:110693.
[90] Zhao J, Chevil K, Yu M, Been J, Keane S, Van Boven G, Kania R, Chen W. Statistical Analysis on Underload-Type Pipeline Spectra. J Pipeline Syst Eng Pract 2016;7:04016007. https://doi.org/10.1061/(ASCE)PS.1949-1204.0000241.
[91] Yu M, Chen W, Kania R, Van Boven G, Been J. Crack propagation of pipeline steel exposed to a near-neutral pH environment under variable pressure fluctuations. International Journal of Fatigue 2016;82:658–66.
[92] Withers PJ, Bhadeshia HKDH. Residual stress. Part 1 – Measurement techniques. Materials Science and Technology 2001;17:355–65. https://doi.org/10.1179/026708301101509980.
[93] Beavers JA, Johnson JT, Sutherby RL. Materials Factors Influencing the Initiation of Near-Neutral pH SCC on Underground Pipelines, 2000. https://doi.org/10.1115/IPC2000-221.
[94] Chen W, Van Boven G, Rogge R. The role of residual stress in neutral pH stress corrosion cracking of pipeline steels–Part II: Crack dormancy. Acta Materialia 2007;55:43–53.
[95] Ramadan S, Gaillet L, Tessier C, Idrissi H. Detection of stress corrosion cracking of high-strength steel used in prestressed concrete structures by acoustic emission technique. Applied Surface Science 2008;254:2255–61. https://doi.org/10.1016/j.apsusc.2007.09.011.
[96] Du G, Li J, Wang WK, Jiang C, Song SZ. Detection and characterization of stress-corrosion cracking on 304 stainless steel by electrochemical noise and acoustic emission

techniques. Corrosion Science 2011;53:2918–26. https://doi.org/10.1016/j.corsci.2011.05.030.
[97] Shaikh H, Amirthalingam R, Anita T, Sivaibharasi N, Jaykumar T, Manohar P, Khatak HS. Evaluation of stress corrosion cracking phenomenon in an AISI type 316LN stainless steel using acoustic emission technique. Corrosion Science 2007;49:740–65. https://doi.org/10.1016/j.corsci.2006.06.007.
[98] Hwang W, Bae S, Kim J, Kang S, Kwag N, Lee B. Acoustic emission characteristics of stress corrosion cracks in a type 304 stainless steel tube. Nuclear Engineering and Technology 2015;47:454–60. https://doi.org/10.1016/j.net.2015.04.001.
[99] Kovac J, Alaux C, Marrow TJ, Govekar E, Legat A. Correlations of electrochemical noise, acoustic emission and complementary monitoring techniques during intergranular stress-corrosion cracking of austenitic stainless steel. Corrosion Science 2010;52:2015–25. https://doi.org/10.1016/j.corsci.2010.02.035.
[100] Park J, Kim JS, Lee DY, Lee SH. Real-time monitoring of stress corrosion cracking in 304 L stainless steel pipe using acoustic emission. Journal of Nuclear Materials 2022;571:154009. https://doi.org/10.1016/j.jnucmat.2022.154009.
[101] Xu J, Wu X, Han E-H. Acoustic emission response of sensitized 304 stainless steel during intergranular corrosion and stress corrosion cracking. Corrosion Science 2013;73:262–73. https://doi.org/10.1016/j.corsci.2013.04.014.
[102] Bi H, Li H, Zhang W, Wang L, Zhang Q, Cao S, Toku-Gyamerah I. Evaluation of the acoustic emission monitoring method for stress corrosion cracking on aboveground storage tank floor steel. International Journal of Pressure Vessels and Piping 2020;179:104035. https://doi.org/10.1016/j.ijpvp.2019.104035.
[103] Djeddi L, Khelif R, Benmedakhene S, Favergeon J. Reliability of Acoustic Emission as a Technique to Detect Corrosion and Stress Corrosion Cracking on Prestressing Steel Strands. International Journal of Electrochemical Science 2013;8:8356–70. https://doi.org/10.1016/S1452-3981(23)12894-X.
[104] Zhang Z, Wu X, Tan J. In-situ monitoring of stress corrosion cracking of 304 stainless steel in high-temperature water by analyzing acoustic emission waveform. Corrosion Science 2019;146:90–8. https://doi.org/10.1016/j.corsci.2018.10.022.
[105] Hernandez-Valle F, Clough AR, Edwards RS. Stress corrosion cracking detection using non-contact ultrasonic techniques. Corrosion Science 2014;78:335–42. https://doi.org/10.1016/j.corsci.2013.10.018.
[106] Nakamura N, Ashida K, Takishita T, Ogi H, Hirao M. Inspection of stress corrosion cracking in welded stainless steel pipe using point-focusing electromagnetic-acoustic transducer. NDT & E International 2016;83:88–93. https://doi.org/10.1016/j.ndteint.2016.06.005.
[107] Zeitvogel DT, Matlack KH, Kim J-Y, Jacobs LJ, Singh PM, Qu J. Characterization of stress corrosion cracking in carbon steel using nonlinear Rayleigh surface waves. NDT & E International 2014;62:144–52. https://doi.org/10.1016/j.ndteint.2013.12.005.
[108] Hogg SM, Anderson BE, Le Bas P-Y, Remillieux MC. Nonlinear resonant ultrasound spectroscopy of stress corrosion cracking in stainless steel rods. NDT & E International 2019;102:194–8. https://doi.org/10.1016/j.ndteint.2018.12.007.
[109] Remillieux MC, Kaoumi D, Ohara Y, Stuber Geesey MA, Xi L, Schoell R, Bryan CR, Enos DG, Summa DA, Ulrich TJ, Anderson BE, Shayer Z. Detecting and imaging stress corrosion cracking in stainless steel, with application to inspecting storage canisters for

spent nuclear fuel. NDT & E International 2020;109:102180. https://doi.org/10.1016/j.ndteint.2019.102180.
[110] Norli P, Vallée E, Aanes M, Prieur F, Bjåstad TG, Standal ØK-V, Brende OM, Frijlink M. Ultrasonic detection of stress corrosion cracks in pipe samples in gaseous atmosphere. 2019 IEEE International Ultrasonics Symposium (IUS), 2019, p. 1624–7. https://doi.org/10.1109/ULTSYM.2019.8925831.
[111] Calabrese L, Proverbio E. A review on the applications of acoustic emission technique in the study of stress corrosion cracking. Corrosion and Materials Degradation 2020;2:1–30.
[112] Cho H, Takemoto M. Acoustic Emission from Rust in Stress Corrosion Cracking 2004.
[113] Park J, Kim JS, Lee DY, Lee SH. Real-time monitoring of stress corrosion cracking in 304 L stainless steel pipe using acoustic emission. Journal of Nuclear Materials 2022;571:154009. https://doi.org/10.1016/j.jnucmat.2022.154009.
[114] Budano S, Giunta G, Lucci A. Acoustic Emission data analysis to evaluate damage mechanisms in pipeline carbon steels 2011.
[115] Du G, Li J, Wang WK, Jiang C, Song SZ. Detection and characterization of stress-corrosion cracking on 304 stainless steel by electrochemical noise and acoustic emission techniques. Corrosion Science 2011;53:2918–26. https://doi.org/10.1016/j.corsci.2011.05.030.
[116] Bi H, Li H, Zhang W, Wang L, Zhang Q, Cao S, Toku-Gyamerah I. Evaluation of the acoustic emission monitoring method for stress corrosion cracking on aboveground storage tank floor steel. International Journal of Pressure Vessels and Piping 2020;179:104035. https://doi.org/10.1016/j.ijpvp.2019.104035.
[117] Goldaran R, Turer A, Kouhdaragh M, Ozlutas K. Identification of corrosion in a prestressed concrete pipe utilizing acoustic emission technique. Construction and Building Materials 2020;242:118053. https://doi.org/10.1016/j.conbuildmat.2020.118053.
[118] Xu J, Wu X, Han E-H. Acoustic emission response of sensitized 304 stainless steel during intergranular corrosion and stress corrosion cracking. Corrosion Science 2013;73:262–73. https://doi.org/10.1016/j.corsci.2013.04.014.
[119] Zhang Z, Wu X, Tan J. In-situ monitoring of stress corrosion cracking of 304 stainless steel in high-temperature water by analyzing acoustic emission waveform. Corrosion Science 2019;146:90–8. https://doi.org/10.1016/j.corsci.2018.10.022.
[120] Matsuo T, Sano K, Sakakibara Y, Nakayama G. Estimation of Stress Corrosion Cracking Initiation and Propagation in High-Pressure, High-Temperature Water Environment Utilizing Acoustic Emission. Mater Trans 2015;56:327–32. https://doi.org/10.2320/matertrans.M2014357.
[121] Beck T. Stress corrosion cracking of titanium alloys-Potential transients at open circuit during SCC and pitting corrosion, and chloride absorption during formation of TiO sub 2 Quarterly progress report, Jul. 1-30 Sep. 1967. 1967.
[122] Ferrer F, Schille E, Verardo D, Goudiakas J. Sensitivity of acoustic emission for the detection of stress corrosion cracking during static U-bend tests on a 316L stainless steel in hot concentrated magnesium chloride media 2002.
[123] Katz Y. Micro-mechanical Approach to Stress Corrosion Cracking in Titanium Alloys 1969.
[124] Craig I, Parkins R. Stress corrosion cracking of 18 Ni maraging steel in chloride solutions. British Corrosion Journal 1984;19:3–16.

[125] Kumosa M. Acoustic emission monitoring of stress corrosion cracks in aligned GRP. Journal of Physics D: Applied Physics 1987;20:69.
[126] Pollock W, Hardiet D, Holroyd N. Monitoring sub-critical crack growth due to stress corrosion or hydrogen embrittlement by acoustic emission. British Corrosion Journal 1982;17:103–11.
[127] Yuyama S, Kishi T. AE analysis during corrosion, stress corrosion cracking and corrosion fatigue processes. J Acoust Emiss; (United States) 1AD;2.
[128] Hwang W, Bae S, Kim J, Kang S, Kwag N, Lee B. Acoustic emission characteristics of stress corrosion cracks in a type 304 stainless steel tube. Nuclear Engineering and Technology 2015;47:454–60. https://doi.org/10.1016/j.net.2015.04.001.
[129] Calabrese L, Bonaccorsi L, Proverbio E, Di Pietro D, Cappuccini F. SCC damage evolution on martensitic stainless steel by using acoustic emission technique. Corrosion Engineering, Science and Technology 2015;50:364–71.
[130] Megel M, Kumosa L, Ely T, Armentrout D, Kumosa M. Initiation of stress-corrosion cracking in unidirectional glass/polymer composite materials. Composites Science and Technology 2001;61:231–46.
[131] Calabrese L, Proverbio E. A Review on the Applications of Acoustic Emission Technique in the Study of Stress Corrosion Cracking. CMD 2020;2:1–30. https://doi.org/10.3390/cmd2010001.
[132] Calabrese L, Bonaccorsi L, Galeano M, Proverbio E, Di Pietro D, Cappuccini F. Identification of damage evolution during SCC on 17-4 PH stainless steel by combining electrochemical noise and acoustic emission techniques. Corrosion Science 2015;98:573–84.
[133] Djeddi L, Khelif R, Benmedakhene S, Favergeon J. Reliability of Acoustic Emission as a Technique to Detect Corrosion and Stress Corrosion Cracking on Prestressing Steel Strands. International Journal of Electrochemical Science 2013;8:8356–70. https://doi.org/10.1016/S1452-3981(23)12894-X.
[134] Shaikh H, Amirthalingam R, Anita T, Sivaibharasi N, Jaykumar T, Manohar P, Khatak H. Evaluation of stress corrosion cracking phenomenon in an AISI type 316LN stainless steel using acoustic emission technique. Corrosion Science 2007;49:740–65.
[135] Wu K, Ito K, Shinozaki I, Chivavibul P, Enoki M. A Comparative Study of Localized Corrosion and Stress Corrosion Cracking of 13Cr Martensitic Stainless Steel Using Acoustic Emission and X-ray Computed Tomography. Materials 2019;12:2569. https://doi.org/10.3390/ma12162569.
[136] Yonezu A, Cho H, Takemoto M. Monitoring of stress corrosion cracking in stainless steel weldments by acoustic and electrochemical measurements. Measurement Science and Technology 2006;17:2447.
[137] Yonezu A, Cho H, Takemoto M. Detection of stress corrosion cracking of Type 304 stainless steel using acoustic emission and corrosion potential fluctuation. Advanced Materials Research 2006;13:243–50.
[138] Yonezu A, Cho H, Ogawa T, Takemoto M. Simultaneous monitoring of acoustic emission and corrosion potential fluctuation for mechanistic study of chloride stress corrosion cracking. Key Engineering Materials 2006;321:254–9.
[139] Bi H, Li H, Zhang W, Wang L, Zhang Q, Cao S, Toku-Gyamerah I. Evaluation of the acoustic emission monitoring method for stress corrosion cracking on aboveground

storage tank floor steel. International Journal of Pressure Vessels and Piping 2020;179:104035. https://doi.org/10.1016/j.ijpvp.2019.104035.
[140] Jones R, Friesel M, Pathania R. Evaluation of stress corrosion crack initiation using acoustic emission. Corrosion 1991;47:105–15.
[141] Yonezu A, Kusano R, Chen X. On the mechanism of intergranular stress corrosion cracking of sensitized stainless steel in tetrathionate solution. Journal of Materials Science 2013;48:2447–53.
[142] Cho H, Takemoto M. Acoustic emission from rust in stress corrosion cracking, 2004, p. 605–15.
[143] Fujimoto S, Takemoto M, Ono K. AE monitoring of chloride stress corrosion cracking of austenitic stainless steel 2000.
[144] Zhang Z, Wu X, Tan J. In-situ monitoring of stress corrosion cracking of 304 stainless steel in high-temperature water by analyzing acoustic emission waveform. Corrosion Science 2019;146:90–8. https://doi.org/10.1016/j.corsci.2018.10.022.
[145] Park J, Kim JS, Lee DY, Lee SH. Real-time monitoring of stress corrosion cracking in 304 L stainless steel pipe using acoustic emission. Journal of Nuclear Materials 2022;571:154009.
[146] Zhang Z, Zhang Z, Tan J, Wu X. Quantitatively related acoustic emission signal with stress corrosion crack growth rate of sensitized 304 stainless steel in high-temperature water. Corrosion Science 2019;157:79–86.
[147] Shao Y, Yu Y, Zhang Y, Wei S, Li X. Analysis of acoustic emission signal characteristics based on the crack pattern of stress corrosion cracking, IEEE; 2016, p. 1–5.
[148] Odor EG, Adekeye MS, Owunna IB, Agbonze NG, Salman MB, Salman AO. Advanced Non-Destructive Testing Techniques For Pipeline Integrity Assessment. Path of Science 2024;10:2068–75.
[149] Hamdan H, Alsit A, Al Tahhan AB, Mughieda O, Mourad A-HI, Shehadeh MA, Alkhedher M. Prognosis methods of stress corrosion cracking under harsh environmental conditions. Heliyon 2024.
[150] Marr J, Ginzel R, Pennie J. Hand Held Ultrasonic Sizing of Stress Corrosion Cracking, 2005.
[151] Hasiotis T, Badogiannis E, Tsouvalis NG. Application of ultrasonic C-scan techniques for tracing defects in laminated composite materials. Strojniški Vestnik-Journal of Mechanical Engineering 2011;57:192–203.
[152] Kolkoori S, Hoehne C, Prager J, Rethmeier M, Kreutzbruck M. Quantitative evaluation of ultrasonic C-scan image in acoustically homogeneous and layered anisotropic materials using three dimensional ray tracing method. Ultrasonics 2014;54:551–62.
[153] Li S, Poudel A, Chu TP. Ultrasonic defect mapping using signal correlation for nondestructive evaluation (NDE). Research in Nondestructive Evaluation 2015;26:90–106.
[154] Iyer S, Schokker AJ, Sinha SK. Ultrasonic C-Scan imaging: Preliminary evaluation for corrosion and void detection in posttensioned tendons. Transportation Research Record 2003;1827:44–52.
[155] Sandhu JS, Wang H, Popek WJ, Sincebaugh PJ. Acoustography: It could be a practical ultrasonic NDE tool for composites. vol. 4336, SPIE; 2001, p. 129–34.

[156] Hernandez-Valle F, Clough AR, Edwards RS. Stress corrosion cracking detection using non-contact ultrasonic techniques. Corrosion Science 2014;78:335–42. https://doi.org/10.1016/j.corsci.2013.10.018.
[157] Norli P, Vallée E, Aanes M, Prieur F, Bjåstad TG, Standal ØK-V, Brende OM, Frijlink M. Ultrasonic detection of stress corrosion cracks in pipe samples in gaseous atmosphere. 2019 IEEE International Ultrasonics Symposium (IUS), 2019, p. 1624–7. https://doi.org/10.1109/ULTSYM.2019.8925831.
[158] Norli P, Frijlink M, Standal ØK-V, Bjåstad TG, Prieur F, Vallée E. Ultrasonic Detection of Stress Corrosion Cracks in Pipe Samples Using Guided Waves. 2018 IEEE International Ultrasonics Symposium (IUS), 2018, p. 1–4. https://doi.org/10.1109/ULTSYM.2018.8579864.
[159] Nakamura N, Ashida K, Takishita T, Ogi H, Hirao M. Inspection of stress corrosion cracking in welded stainless steel pipe using point-focusing electromagnetic-acoustic transducer. NDT & E International 2016;83:88–93. https://doi.org/10.1016/j.ndteint.2016.06.005.
[160] Norli P, Vallée E, Aanes M, Prieur F, Bjåstad TG, Standal ØK-V, Brende OM, Frijlink M. Ultrasonic detection of stress corrosion cracks in pipe samples in gaseous atmosphere, IEEE; 2019, p. 1624–7.
[161] Norli P, Vallée E, Aanes M, Spilde A, Duerud H, Prieur F, Bjåstad T, Standal Ø, Frijlink M. Ultrasonic detection of stress corrosion cracks in gaseous atmosphere using Broadband transducers. vol. 38, AIP Publishing; 2019.
[162] Norli P, Vallée E, Aanes M, Prieur F, Bjåstad TG, Standal ØK-V, Brende OM, Frijlink M. Ultrasonic detection of crack defects in pipe samples with a 132-channel test scanner in gas, IEEE; 2020, p. 1–4.
[163] Norli P, Frijlink M, Standal ØK-V, Bjåstad TG, Prieur F, Vallée E. Ultrasonic detection of stress corrosion cracks in pipe samples using guided waves, IEEE; 2018, p. 1–4.
[164] Ashworth B, Uzelac N, Willems H, Barbian O. Detection and Verification of SCC in a Gas Transmission Pipeline. vol. 40252, American Society of Mechanical Engineers; 2000, p. V002T06A004.
[165] Ma Z, Yu L, Chao YJ, Lam P-S, Sindelar RL, Duncan AJ, Truong T-T, Verst C, Sun P-K, Campbell A. Nondestructive evaluation of stress corrosion cracking in a welded steel plate using guided ultrasonic waves. Journal of Nondestructive Evaluation, Diagnostics and Prognostics of Engineering Systems 2022;5:031003.
[166] Tandon S, Gao M, Krishnamurthy R, Kania R, Piazza M. SCC in-field inspection technology evaluation and its application to EMAT based pipeline integrity management programs. vol. 46117, American Society of Mechanical Engineers; 2014, p. V002T06A079.
[167] Hernandez-Valle F, Clough A, Edwards RS. Stress corrosion cracking detection using non-contact ultrasonic techniques. Corrosion Science 2014;78:335–42.
[168] Hilvert M, Beuker T. High-Resolution EMAT as a Diagnostic Tool for Analysis of SCC and Crack-Like Pipelines Defects. vol. 56468, American Society of Mechanical Engineers; 2015, p. V001T04A005.
[169] Zeitvogel DT, Matlack KH, Kim J-Y, Jacobs LJ, Singh PM, Qu J. Characterization of stress corrosion cracking in carbon steel using nonlinear Rayleigh surface waves. NDT & E International 2014;62:144–52. https://doi.org/10.1016/j.ndteint.2013.12.005.

[170] Doerr C, Lakocy A, Kim J-Y, Singh PM, Wall JJ, Qu J, Jacobs LJ. Evaluation of the heat-affected zone (HAZ) of a weld joint using nonlinear Rayleigh waves. Materials Letters 2017;190:221–4. https://doi.org/10.1016/j.matlet.2017.01.021.
[171] Bolivar J, Fregonese M, Réthoré J, Duret-Thual C, Combrade P. Evaluation of multiple stress corrosion crack interactions by in-situ Digital Image Correlation. Corrosion Science 2017;128:120–9.
[172] Fujii T, Hisada Y, Tohgo K, Shimamura Y. Investigation on nucleation of intergranular stress corrosion cracking in austenitic stainless steel by in situ strain measurement. Materials Science and Engineering: A 2020;773:138858. https://doi.org/10.1016/j.msea.2019.138858.
[173] Shin JH, Kim SW, Kim DJ. In-situ analysis of SCC initiation on Alloy 600 surface in primary water environment using digital image correlation with electron backscatter diffraction. Nuclear Engineering and Design 2024;421:113095.
[174] Cadelano G, Bortolin A, Ferrarini G, Molinas B, Giantin D, Zonta P, Bison P. Corrosion Detection in Pipelines Using Infrared Thermography: Experiments and Data Processing Methods. J Nondestruct Eval 2016;35:49. https://doi.org/10.1007/s10921-016-0365-5.
[175] Rao B p. c., Raj B. NDE Methods for Monitoring Corrosion and Corrosion-assisted Cracking. Non-Destructive Evaluation of Corrosion and Corrosion-assisted Cracking, John Wiley & Sons, Ltd; 2019, p. 101–21. https://doi.org/10.1002/9781118987735.ch4.
[176] Bolivar J, Frégonèse M, Réthoré J, Duret-Thual C, Combrade P. Evaluation of multiple stress corrosion crack interactions by in-situ Digital Image Correlation. Corrosion Science 2017;128:120–9. https://doi.org/10.1016/j.corsci.2017.09.001.
[177] Fujii T, Hisada Y, Tohgo K, Shimamura Y. Investigation on nucleation of intergranular stress corrosion cracking in austenitic stainless steel by *in situ* strain measurement. Materials Science and Engineering: A 2020;773:138858. https://doi.org/10.1016/j.msea.2019.138858.
[178] Cook AB, Duff J, Stevens N, Lyon S, Sherry A, Marrow J. Preliminary Evaluation of Digital Image Correlation for In-situ Observation of Low Temperature Atmospheric-Induced Chloride Stress Corrosion Cracking in Austenitic Stainless Steels. ECS Trans 2010;25:119. https://doi.org/10.1149/1.3407553.
[179] Esteves R, Ghosh R, Raghavan S. Quantifying Stress Corrosion Cracking Performance of Additively Manufactured Aluminum Alloys Via Micro Digital Image Correlation 2024. https://doi.org/10.2139/ssrn.4896387.
[180] McMurtrey MD, Cui B, Robertson I, Farkas D, Was GS. Mechanism of dislocation channel-induced irradiation assisted stress corrosion crack initiation in austenitic stainless steel. Current Opinion in Solid State and Materials Science 2015;19:305–14. https://doi.org/10.1016/j.cossms.2015.04.001.
[181] Stermann L, Simon G, Fulcrand R, Vanel L, Tanguy D. An experimental set up to study the micro-mechanisms of stress corrosion cracking. Congrès Français de Mécanique, Brest, France: Association française de mécanique; 2019.
[182] Park H, Choi M, Park J, Kim W. A study on detection of micro-cracks in the dissimilar metal weld through ultrasound infrared thermography. Infrared Physics & Technology 2014;62:124–31. https://doi.org/10.1016/j.infrared.2013.10.006.
[183] Sakagami T, Kuroki K, Kubo S. Detection of Stress Corrosion Cracking by Sonic-IR Technique 2009.

[184] Ghorbani R, Matta F, Sutton MA. Full-Field Deformation Measurement and Crack Mapping on Confined Masonry Walls Using Digital Image Correlation. Exp Mech 2015;55:227–43. https://doi.org/10.1007/s11340-014-9906-y.
[185] Yates JR, Zanganeh M, Tai YH. Quantifying crack tip displacement fields with DIC. Engineering Fracture Mechanics 2010;77:2063–76. https://doi.org/10.1016/j.engfracmech.2010.03.025.
[186] Jiang R, Pierron F, Octaviani S, Reed PAS. Characterisation of strain localisation processes during fatigue crack initiation and early crack propagation by SEM-DIC in an advanced disc alloy. Materials Science and Engineering: A 2017;699:128–44. https://doi.org/10.1016/j.msea.2017.05.091.
[187] Shirazi H, Wang S, Chen W, Eadie R. Pipeline circumferential corrosion fatigue failure under the influence of bending residual stress in the near-neutral pH environment. Engineering Failure Analysis 2024;166:108887. https://doi.org/10.1016/j.engfailanal.2024.108887.
[188] Sriba A, Bouquerel J, Vogt J-B. DIC-aided analysis of the fatigue behaviour of a welded 316L stainless steel. Weld World 2022;66:1915–27. https://doi.org/10.1007/s40194-022-01355-9.
[189] The Application of DIC Technique to Evaluate Residual Tensile Strength of Aluminum Alloy Plates with Multi-Site Damage of Collinear and Non-Collinear Cracks 2019. https://www.mdpi.com/2075-4701/9/2/118 (accessed March 25, 2025).
[190] Jiang J, Yang J, Zhang T, Zou J, Wang Y, Dunne FPE, Britton TB. Microstructurally sensitive crack nucleation around inclusions in powder metallurgy nickel-based superalloys. Acta Materialia 2016;117:333–44. https://doi.org/10.1016/j.actamat.2016.07.023.
[191] Allain M, Ple O, Prime N, Roux E, Vacher P. In situ DIC method to determine stress state in reinforced concrete structures. Measurement 2023;210:112483. https://doi.org/10.1016/j.measurement.2023.112483.
[192] Jerabek M, Major Z, Lang RW. Strain determination of polymeric materials using digital image correlation. Polymer Testing 2010;29:407–16. https://doi.org/10.1016/j.polymertesting.2010.01.005.
[193] Cook AB, Duff J, Stevens N, Lyon S, Sherry A, Marrow J. Preliminary Evaluation of Digital Image Correlation for In-situ Observation of Low Temperature Atmospheric-Induced Chloride Stress Corrosion Cracking in Austenitic Stainless Steels. ECS Trans 2010;25:119. https://doi.org/10.1149/1.3407553.
[194] Cook AB, Duff J, Stevens N, Lyon S, Sherry A, Marrow J. Preliminary Evaluation of Digital Image Correlation for In-situ Observation of Low Temperature Atmospheric-Induced Chloride Stress Corrosion Cracking in Austenitic Stainless Steels. ECS Trans 2010;25:119. https://doi.org/10.1149/1.3407553.
[195] Bolivar J, Frégonèse M, Réthoré J, Duret-Thual C, Combrade P. Evaluation of multiple stress corrosion crack interactions by in-situ Digital Image Correlation. Corrosion Science 2017;128:120–9. https://doi.org/10.1016/j.corsci.2017.09.001.
[196] Kovac J, Alaux C, Marrow TJ, Govekar E, Legat A. Correlations of electrochemical noise, acoustic emission and complementary monitoring techniques during intergranular stress-corrosion cracking of austenitic stainless steel. Corrosion Science 2010;52:2015–25. https://doi.org/10.1016/j.corsci.2010.02.035.

[197] Fujii T, Hisada Y, Tohgo K, Shimamura Y. Investigation on nucleation of intergranular stress corrosion cracking in austenitic stainless steel by *in situ* strain measurement. Materials Science and Engineering: A 2020;773:138858. https://doi.org/10.1016/j.msea.2019.138858.
[198] Kovač J, Marrow TJ, Govekar E, Legat A. Detection and characterisation of intergranular stress-corrosion cracking on austenitic stainless steel. Materials and Corrosion 2012;63:664–73. https://doi.org/10.1002/maco.201106182.
[199] Ho Shin J, Woo Kim S, Jin Kim D. In-situ analysis of SCC initiation on Alloy 600 surface in primary water environment using digital image correlation with electron backscatter diffraction. Nuclear Engineering and Design 2024;421:113095. https://doi.org/10.1016/j.nucengdes.2024.113095.
[200] McMurtrey MD, Cui B, Robertson I, Farkas D, Was G. Mechanism of dislocation channel-induced irradiation assisted stress corrosion crack initiation in austenitic stainless steel. Current Opinion in Solid State and Materials Science 2015;19:305–14.
[201] Fujii T, Yamakawa R, Tohgo K, Shimamura Y. Strain-based approach to investigate intergranular stress corrosion crack initiation on a smooth surface of austenitic stainless steel. Materials Science and Engineering: A 2019;756:518–27.
[202] Fujii T, Hisada Y, Tohgo K, Shimamura Y. Investigation on nucleation of intergranular stress corrosion cracking in austenitic stainless steel by in situ strain measurement. Materials Science and Engineering: A 2020;773:138858.
[203] The application of digital image correlation (DIC) in fatigue experimentation: A review - Hebert - 2023 - Fatigue & Fracture of Engineering Materials & Structures - Wiley Online Library 2023. https://onlinelibrary.wiley.com/doi/full/10.1111/ffe.13931 (accessed March 25, 2025).
[204] Carroll JD, Abuzaid W, Lambros J, Sehitoglu H. High resolution digital image correlation measurements of strain accumulation in fatigue crack growth. International Journal of Fatigue 2013;57:140–50. https://doi.org/10.1016/j.ijfatigue.2012.06.010.
[205] Kagalwala F, Kanade T. Reconstructing specimens using DIC microscope images. IEEE Transactions on Systems, Man, and Cybernetics, Part B (Cybernetics) 2003;33:728–37. https://doi.org/10.1109/TSMCB.2003.816924.
[206] Cogswell CJ, Sheppard CJR. Confocal differential interference contrast (DIC) microscopy: including a theoretical analysis of conventional and confocal DIC imaging. Journal of Microscopy 1992;165:81–101. https://doi.org/10.1111/j.1365-2818.1992.tb04307.x.
[207] Oguntoye KS, Laflamme S, Sturgill R, Eisenmann DJ. Review of Artificial Intelligence Applications for Virtual Sensing of Underground Utilities. Sensors 2023;23:4367. https://doi.org/10.3390/s23094367.
[208] Park H, Choi M, Park J, Kim W. A study on detection of micro-cracks in the dissimilar metal weld through ultrasound infrared thermography. Infrared Physics & Technology 2014;62:124–31.
[209] Sakagami T, Kuroki K, Kubo S, Katsumata R, Matsumoto Y, Harada Y. Detection of stress corrosion cracking by sonic-IR technique. vol. 1215, 2009.
[210] Park H, Choi M, Park J, Kim W. A study on detection of micro-cracks in the dissimilar metal weld through ultrasound infrared thermography. Infrared Physics & Technology 2014;62:124–31. https://doi.org/10.1016/j.infrared.2013.10.006.

[211] Jama B, Wilson GJ, Gryzagoridis J. Benchmarking Induction Thermography with Magnetic Particle and Dye Penetrant NDT Techniques .
[212] Sakagami T, Kuroki K, Kubo S. Detection of Stress Corrosion Cracking by Sonic-IR Technique 2009.
[213] Ren X, Xu X, Jiang C, Huang Z, He X. Strain distribution and fatigue life estimation for steel plate weld joint low cycle fatigue based on DIC. Optics and Lasers in Engineering 2020;124:105839. https://doi.org/10.1016/j.optlaseng.2019.105839.
[214] Pierron F, Sutton MA, Tiwari V. Ultra High Speed DIC and Virtual Fields Method Analysis of a Three Point Bending Impact Test on an Aluminium Bar. Exp Mech 2011;51:537–63. https://doi.org/10.1007/s11340-010-9402-y.
[215] Everton SK, Hirsch M, Stravroulakis P, Leach RK, Clare AT. Review of in-situ process monitoring and in-situ metrology for metal additive manufacturing. Materials & Design 2016;95:431–45. https://doi.org/10.1016/j.matdes.2016.01.099.
[216] Moore S, Burrows R, Kumar D, Kloucek MB, Warren AD, Flewitt PEJ, Picco L, Payton OD, Martin TL. Observation of stress corrosion cracking using real-time in situ high-speed atomic force microscopy and correlative techniques. Npj Mater Degrad 2021;5:1–10. https://doi.org/10.1038/s41529-020-00149-y.
[217] Zhu LK, Yan Y, Li JX, Qiao LJ, Volinsky AA. Stress corrosion cracking under low stress: Continuous or discontinuous cracks? Corrosion Science 2014;80:350–8.
[218] Chen X, Karasz E, Badwe N, Sieradzki K. Dynamic fracture and dealloying induced stress-corrosion cracking. Corrosion Science 2021;187:109503.
[219] Nisbet W, Lorimer G, Newman R. A transmission electron microscopy study of stress corrosion cracking in stainless steels. Corrosion Science 1993;35:457–69.
[220] Sennour M, Laghoutaris P, Guerre C, Molins R. Advanced TEM characterization of stress corrosion cracking of Alloy 600 in pressurized water reactor primary water environment. Journal of Nuclear Materials 2009;393:254–66.
[221] Thomas LE, Bruemmer SM. High-resolution characterization of intergranular attack and stress corrosion cracking of Alloy 600 in high-temperature primary water. Corrosion 2000;56:572–87.
[222] Yusa N, Perrin S, Mizuno K, Chen Z, Miya K. Eddy current inspection of closed fatigue and stress corrosion cracks. Meas Sci Technol 2007;18:3403. https://doi.org/10.1088/0957-0233/18/11/021.
[223] Yusa N, Janousek L, Rebican M, Chen Z, Miya K, Dohi N, Chigusa N, Matsumoto Y. Caution when applying eddy current inversion to stress corrosion cracking. Nuclear Engineering and Design 2006;236:211–21. https://doi.org/10.1016/j.nucengdes.2005.06.016.
[224] Taheri H, Jones C, Taheri M. Assessment and detection of stress corrosion cracking by advanced eddy current array nondestructive testing and material characterization. Journal of Natural Gas Science and Engineering 2022;102:104568. https://doi.org/10.1016/j.jngse.2022.104568.
[225] Butusova YeN, Mishakin VV, Kachanov M. On monitoring the incubation stage of stress corrosion cracking in steel by the eddy current method. International Journal of Engineering Science 2020;148:103212. https://doi.org/10.1016/j.ijengsci.2019.103212.
[226] Yusa N, Hashizume H. Evaluation of stress corrosion cracking as a function of its resistance to eddy currents. Nuclear Engineering and Design 2009;239:2713–8. https://doi.org/10.1016/j.nucengdes.2009.08.032.

[227] Kim D, Udpa L, Udpa S. Remote field eddy current testing for detection of stress corrosion cracks in gas transmission pipelines. Materials Letters 2004;58:2102–4. https://doi.org/10.1016/j.matlet.2004.01.006.
[228] Zhang Y, Cook AJMC, Padovani C, Zhou S, Turnbull A. Atmospheric stress corrosion crack growth rates of 316 L stainless steel for nuclear waste containment. Corrosion Science 2020;177:109008. https://doi.org/10.1016/j.corsci.2020.109008.
[229] Sato Y, Atsumi T, Shoji T. Continuous monitoring of back wall stress corrosion cracking growth in sensitized type 304 stainless steel weldment by means of potential drop techniques. International Journal of Pressure Vessels and Piping 2007;84:274–83. https://doi.org/10.1016/j.ijpvp.2007.01.004.
[230] Zhang Y, Cook AJMC, Padovani C, Zhou S, Turnbull A. Atmospheric stress corrosion crack growth rates of 316 L stainless steel for nuclear waste containment. Corrosion Science 2020;177:109008. https://doi.org/10.1016/j.corsci.2020.109008.
[231] Cai W, Xie S, Jomdecha C, Wang X, Pei C, Li Y, Chen Z, Yusa N. Assessment of local conductivity distribution in stress corrosion crack region using direct current potential drop method. Corrosion Science 2017;123:197–208. https://doi.org/10.1016/j.corsci.2017.01.019.
[232] Machado MA. Eddy currents probe design for NDT applications: A review. Sensors (Basel, Switzerland) 2024;24:5819.
[233] Sophian A, Tian G, Taylor D, Rudlin J. Electromagnetic and eddy current NDT: a review. Insight 2001;43:302–6.
[234] Taheri H, Jones C, Taheri M. Assessment and detection of stress corrosion cracking by advanced eddy current array nondestructive testing and material characterization. Journal of Natural Gas Science and Engineering 2022;102:104568. https://doi.org/10.1016/j.jngse.2022.104568.
[235] Moskovkina VN, Zagidulin RV. The Study of Possibility of Stress-Corrosion Cracks Group Resolution by Eddy-Current Flaw Detector. IOP Conf Ser: Earth Environ Sci 2020;459:042010. https://doi.org/10.1088/1755-1315/459/4/042010.
[236] Coramik M, Ege Y. Discontinuity inspection in pipelines: A comparison review. Measurement 2017;111:359–73. https://doi.org/10.1016/j.measurement.2017.07.058.
[237] Kim D, Udpa L, Udpa S. Remote field eddy current testing for detection of stress corrosion cracks in gas transmission pipelines. Materials Letters 2004;58:2102–4. https://doi.org/10.1016/j.matlet.2004.01.006.
[238] Butusova YeN, Mishakin VV, Kachanov M. On monitoring the incubation stage of stress corrosion cracking in steel by the eddy current method. International Journal of Engineering Science 2020;148:103212. https://doi.org/10.1016/j.ijengsci.2019.103212.
[239] Dobmann G. Electromagnetic Nondestructive Evaluation (VII). IOS Press; 2006.
[240] Lutfallah MH, Hammali AY, Felemban TO, Alismail MA. Digital Generation of Eddy Current Testing (ECT) for Inspection of Surface and Near-Surface Defects, 2023.
[241] Yusa N, Hashizume H. Evaluation of stress corrosion cracking as a function of its resistance to eddy currents. Nuclear Engineering and Design 2009;239:2713–8. https://doi.org/10.1016/j.nucengdes.2009.08.032.
[242] Chen Z, Janousek L, Yusa N, Miya K. A Nondestructive Strategy for the Distinction of Natural Fatigue and Stress Corrosion Cracks Based on Signals From Eddy Current Testing. Journal of Pressure Vessel Technology 2006;129:719–28. https://doi.org/10.1115/1.2767365.

[243] Sirois M, Bouchard M. Recent Advances in Depth Assessment of Stress Corrosion Cracking Using Tangential Eddy Current Array on Carbon Steel Pipelines, 2022.
[244] Sirois M, Bouchard M, Sweedy A. Advanced Eddy Current Array Tools for Stress Corrosion Cracking Direct Assessment on Pipelines, 2020. https://doi.org/10.1115/IPC2020-9335.
[245] Raude A, Bouchard M, Sirois M. Stress Corrosion Cracking Direct Assessment of Carbon Steel Pipeline Using Advanced Eddy Current Array Technology, 2018.
[246] Yusa N, Chen ,Zhenmao, and Miya K. Sizing of stress corrosion cracking on austenitic stainless piping in a nuclear power plant from eddy current NDT signals. Nondestructive Testing and Evaluation 2005;20:103–14. https://doi.org/10.1080/10589750500209554.
[247] Cai W, Jomdecha C, Zhao Y, Wang L, Xie S, Chen Z. Quantitative evaluation of electrical conductivity inside stress corrosion crack with electromagnetic NDE methods. Philosophical Transactions of the Royal Society A 2020;378:20190589.
[248] Wang L. Ill-posedness of reconstruction of stress corrosion cracking and a regularization method using multifrequency eddy current signals. AIP Advances 2021;11.
[249] Cheng W, Kanemoto S, Komura I, Shiwa M. Depth sizing of partial-contact stress corrosion cracks from ECT signals. Ndt & E International 2006;39:374–83.
[250] Wang L, Xie S, Chen Z, Li Y, Wang X, Takagi T. Reconstruction of stress corrosion cracks using signals of pulsed eddy current testing. Nondestructive Testing and Evaluation 2013;28:145–54.
[251] Wang L, Chen Z. A Multiple Frequency Strategy for Reconstruction of Stress Corrosion Crack from ECT Signals. Electromagnetic Nondestructive Evaluation (XII), IOS Press; 2009, p. 313–20.
[252] Wang L, Chen Z. Reconstruction of Stress Corrosion Cracking Based on a Regularization Method Using Multi-Frequency Eddy Current Signals. Electromagnetic Non-Destructive Evaluation (XXI), IOS Press; 2018, p. 229–36.
[253] Chen Z, Rebican M, Yusa N, Miya K. Fast simulation of ECT signal due to a conductive crack of arbitrary width. IEEE Transactions on Magnetics 2006;42:683–6.
[254] Jomdecha C, Cai W, Xie S, Chen Z, Li P. A numerical study on eddy current signal characteristics of imitative stress corrosion cracks. International Journal of Applied Electromagnetics and Mechanics 2017;55:257–69.
[255] Jomdecha C, Cai W, Xie S, Li Y, Chen Z. Analysis of magnetic flux perturbation due to conductivity variation in equivalent stress-corrosion crack. International Journal of Applied Electromagnetics and Mechanics 2019;59:1385–92.
[256] Arrieta S, Perosanz FJ, Barcala JM, Ruiz ML, Cicero S. Using Direct Current Potential Drop Technique to Estimate Fatigue Crack Growth Rates in Solid Bar Specimens under Environmental Assisted Fatigue in Simulated Pressurized Water Reactor Conditions. Metals 2022;12:2091. https://doi.org/10.3390/met12122091.
[257] Ji C, Zheng Z, Qin Z, Xue H. Investigation of Multi-Factor Stress Corrosion Cracking Failure of Safe-End Feedwater Lines of Submarine Power System. Materials 2024;17:1381. https://doi.org/10.3390/ma17061381.
[258] Ruolin ZHU LZ. Stress Corrosion Crack Propagation Behavior of Elbow Pipe of Nuclear Grade 316LN Stainless Steel in High Temperature High Pressure Water. Journal of Chinese Society for Corrosion and protection 2018;38:54–61. https://doi.org/10.11902/1005.4537.2017.006.

[259] Sun D, Li H, Feng H, Li Y, Li Q. Calibrating Johnson's formula for applying DCPD method to an axial through-wall crack in a pipe. Engineering Fracture Mechanics 2021;242:107461. https://doi.org/10.1016/j.engfracmech.2020.107461.
[260] Yoon J, Kim Y, Choi S, Nam W, Hwang I, Bromberg L, Stahle P, Ballinger R. On-line monitoring of environment-assisted cracking in nuclear piping using array probe direct current potential drop. Journal of Nondestructive Evaluation 2016;35:1–11.
[261] Kang J, Bibby D, Blanchard R, Zheng W. Full-Scale Stress Corrosion Crack Growth Testing of an X70 Spiral-Welded Pipe in Near-Neutral pH Soil Environment, 2016. https://doi.org/10.1115/IPC2016-64443.
[262] Sato Y, Atsumi T, Shoji T. Continuous monitoring of back wall stress corrosion cracking growth in sensitized type 304 stainless steel weldment by means of potential drop techniques. International Journal of Pressure Vessels and Piping 2007;84:274–83. https://doi.org/10.1016/j.ijpvp.2007.01.004.
[263] Sun H, Yan L, Bibby D, Gravel J-P, Kang J, Zhou W. Full-scale testing of near-neutral pH stress corrosion cracking growth behavior of a vintage X52 oil pipe. Fatigue & Fracture of Engineering Materials & Structures 2024;47:1638–55. https://doi.org/10.1111/ffe.14261.
[264] Cai W, Xie S, Jomdecha C, Wang X, Pei C, Li Y, Chen Z, Yusa N. Assessment of local conductivity distribution in stress corrosion crack region using direct current potential drop method. Corrosion Science 2017;123:197–208.
[265] Zhang Y, Cook A, Padovani C, Zhou S, Turnbull A. Atmospheric stress corrosion crack growth rates of 316 L stainless steel for nuclear waste containment. Corrosion Science 2020;177:109008.
[266] Sato Y, Atsumi T, Shoji T. Continuous monitoring of back wall stress corrosion cracking growth in sensitized type 304 stainless steel weldment by means of potential drop techniques. International Journal of Pressure Vessels and Piping 2007;84:274–83.
[267] Kovac J, Alaux C, Marrow TJ, Govekar E, Legat A. Correlations of electrochemical noise, acoustic emission and complementary monitoring techniques during intergranular stress-corrosion cracking of austenitic stainless steel. Corrosion Science 2010;52:2015–25. https://doi.org/10.1016/j.corsci.2010.02.035.
[268] Du G, Li J, Wang WK, Jiang C, Song SZ. Detection and characterization of stress-corrosion cracking on 304 stainless steel by electrochemical noise and acoustic emission techniques. Corrosion Science 2011;53:2918–26. https://doi.org/10.1016/j.corsci.2011.05.030.
[269] Breimesser M, Ritter S, Seifert H-P, Suter T, Virtanen S. Application of electrochemical noise to monitor stress corrosion cracking of stainless steel in tetrathionate solution under constant load. Corrosion Science 2012;63:129–39. https://doi.org/10.1016/j.corsci.2012.05.017.
[270] Anita T, Pujar MG, Shaikh H, Dayal RK, Khatak HS. Assessment of stress corrosion crack initiation and propagation in AISI type 316 stainless steel by electrochemical noise technique. Corrosion Science 2006;48:2689–710. https://doi.org/10.1016/j.corsci.2005.09.007.
[271] Contreras A, Salazar M, Carmona A, Galván-Martínez R. Electrochemical Noise for Detection of Stress Corrosion Cracking of Low Carbon Steel Exposed to Synthetic Soil Solution1. Mat Res 2017;20:1201–10. https://doi.org/10.1590/1980-5373-MR-2016-0183.
[272] Calabrese L, Galeano M, Proverbio E. Data Mining Applied to the Electrochemical Noise Technique in the Time/Frequency Domain for Stress Corrosion Cracking Recognition.

Corrosion and Materials Degradation 2023;4:659–79. https://doi.org/10.3390/cmd4040034.
[273] Bosch R-W. Electrochemical impedance spectroscopy for the detection of stress corrosion cracks in aqueous corrosion systems at ambient and high temperature. Corrosion Science 2005;47:125–43. https://doi.org/10.1016/j.corsci.2004.05.018.
[274] Oskuie AA, Shahrabi T, Shahriari A, Saebnoori E. Electrochemical impedance spectroscopy analysis of X70 pipeline steel stress corrosion cracking in high pH carbonate solution. Corrosion Science 2012;61:111–22. https://doi.org/10.1016/j.corsci.2012.04.024.
[275] Darowicki K, Orlikowski J, Arutunow A. Investigations of the passive layer cracking by means of Dynamic Electrochemical Impedance Spectroscopy. Electrochimica Acta 2003;48:4189–96. https://doi.org/10.1016/S0013-4686(03)00604-2.
[276] Shahriari A, Shahrabi T, Oskuie AA. A Study on Stress Corrosion Cracking of X70 Pipeline Steel in Carbonate Solution by EIS. J of Materi Eng and Perform 2013;22:1459–70. https://doi.org/10.1007/s11665-012-0418-6.
[277] Neshati J, Adib B, Sardashti A. Stress Corrosion Cracking Detection of Sensitized Stainless Steel 304 in Chloride Media by Using Electrochemical Impedance Spectroscopy (EIS). Journal of Petroleum Science and Technology 2012;2:55–60. https://doi.org/10.22078/jpst.2012.94.
[278] Li MC, Cheng YF. Corrosion of the stressed pipe steel in carbonate–bicarbonate solution studied by scanning localized electrochemical impedance spectroscopy. Electrochimica Acta 2008;53:2831–6. https://doi.org/10.1016/j.electacta.2007.10.077.
[279] Monnot M, Roche V, Estevez R, Mantel M, Nogueira RP. Molybdenum effect on the Sulfide Stress Corrosion of a super martensitic stainless steel in sour environment highlighted by Electrochemical Impedance Spectroscopy. Electrochimica Acta 2017;252:58–66. https://doi.org/10.1016/j.electacta.2017.08.165.
[280] Mishra P, Yavas D, Bastawros AF, Hebert KR. Electrochemical impedance spectroscopy analysis of corrosion product layer formation on pipeline steel. Electrochimica Acta 2020;346:136232. https://doi.org/10.1016/j.electacta.2020.136232.
[281] Lv J, Yue Q, Ding R, Wang X, Gui T, Zhao X. The application of electrochemical noise for the study of metal corrosion and organic anticorrosion coatings: a review. ChemElectroChem 2021;8:337–51.
[282] Li X, Song J, Gan K, Xia D-H, Gao Z, Liu C, Liu Y. Identifying sulfide stress cracking stages on a HSLA pipeline steel in H2S environment by electrochemical noise. Journal of Electroanalytical Chemistry 2020;876:114480. https://doi.org/10.1016/j.jelechem.2020.114480.
[283] Contreras A, Salazar M, Carmona A, Galván-Martínez R. Electrochemical Noise for Detection of Stress Corrosion Cracking of Low Carbon Steel Exposed to Synthetic Soil Solution1. Mat Res 2017;20:1201–10. https://doi.org/10.1590/1980-5373-MR-2016-0183.
[284] Watanabe Y, Shoji T, Kondo T. Electrochemical noise characteristics of IGSCC in stainless steels in pressurized high-temperature water, NACE; 1998, p. NACE-98129.
[285] Zhang W, Dunbar L, Tice D. Monitoring of stress corrosion cracking of sensitised 304H stainless steel in nuclear applications by electrochemical methods and acoustic emission. Energy Materials 2008;3:59–71.
[286] Du G, Li J, Wang W, Jiang C, Song S. Detection and characterization of stress-corrosion cracking on 304 stainless steel by electrochemical noise and acoustic emission techniques. Corrosion Science 2011;53:2918–26.

[287] Luo J, Qiao L. Application and evaluation of processing methods of electrochemical noise generated during stress corrosion cracking. Corrosion 1999;55:870–6.
[288] Zhao R, Zhang Z, Shi J, Tao L, Song S. Characterization of stress corrosion crack growth of 304 stainless steel by electrochemical noise and scanning Kelvin probe. Journal of Central South University of Technology 2010;17:13–8.
[289] Park J, Kim JS, Lee DY, Lee SH. Real-time monitoring of stress corrosion cracking in 304 L stainless steel pipe using acoustic emission. Journal of Nuclear Materials 2022;571:154009.
[290] Alonso CO, Lucio-Garcia M, Hermoso-Diaz I, Chacon-Nava J, Martínez-Villafañe A, Gonzalez-Rodriguez J. Detection of sulfide stress cracking in a supermartensitic stainless steel by using electrochemical noise. International Journal of Electrochemical Science 2014;9:6717–33.
[291] Calabrese L, Bonaccorsi L, Galeano M, Proverbio E, Di Pietro D, Cappuccini F. Identification of damage evolution during SCC on 17-4 PH stainless steel by combining electrochemical noise and acoustic emission techniques. Corrosion Science 2015;98:573–84.
[292] Rathod R, Sapate S, Raman R, Rathod W. Stress corrosion cracking study of aluminum alloys using electrochemical noise analysis. Journal of Materials Engineering and Performance 2013;22:3801–9.
[293] Quej-Ake LM, Rivera-Olvera JN, Domínguez-Aguilar Y del R, Avelino-Jiménez IA, Garibay-Febles V, Zapata-Peñasco I. Analysis of the physicochemical, mechanical, and electrochemical parameters and their impact on the internal and external SCC of carbon steel pipelines. Materials 2020;13:5771.
[294] Liu Y, Feng J, Tan S, Cheng Y, Hu J. Application of electrochemical noise to investigate role of microstructural evolution on inhibiting stress corrosion cracking of Ti–6Al–4V weldment. Metals and Materials International 2021;27:5034–45.
[295] Gonzalez-Rodriguez J, Casales M, Salinas-Bravo V, Espinosa-Medina M, Martinez-Villafañe A. Electrochemical noise generated during the stress corrosion cracking of sensitized alloy 690. Journal of Solid State Electrochemistry 2004;8:290–5.
[296] Kovac J, Alaux C, Marrow TJ, Govekar E, Legat A. Correlations of electrochemical noise, acoustic emission and complementary monitoring techniques during intergranular stress-corrosion cracking of austenitic stainless steel. Corrosion Science 2010;52:2015–25.
[297] Calabrese L, Bonaccorsi L, Galeano M, Proverbio E, Di Pietro D, Cappuccini F. Identification of damage evolution during SCC on 17-4 PH stainless steel by combining electrochemical noise and acoustic emission techniques. Corrosion Science 2015;98:573–84.
[298] Liu Y, Feng J, Tan S, Cheng Y, Hu J. Investigation of inhibition of stress corrosion cracking of welded Ti-6Al-4V alloy using electrochemical noise. International Journal of Electrochemical Science 2020;15:9204–22.
[299] Zhang Z, Wu X. Interpreting electrochemical noise signal arising from stress corrosion cracking of 304 stainless steel in simulated PWR primary water environment by coupling acoustic emission. Journal of Materials Research and Technology 2022;20:3807–17.
[300] Calabrese L, Galeano M, Proverbio E. Data Mining Applied to the Electrochemical Noise Technique in the Time/Frequency Domain for Stress Corrosion Cracking Recognition. Corrosion and Materials Degradation 2023;4:659–79.

[301] Galván-Martínez R, Orozco-Cruz R, Carmona-Hernández A, Mejía-Sánchez E, Morales-Cabrera MA, Contreras A. Corrosion Study of Pipeline Steel under Stress at Different Cathodic Potentials by EIS. Metals 2019;9:1353. https://doi.org/10.3390/met9121353.
[302] Maocheng Y, Jin X, Libao Y, Tangqing W, Cheng S, Wei K. EIS analysis on stress corrosion initiation of pipeline steel under disbonded coating in near-neutral pH simulated soil electrolyte. Corrosion Science 2016;110:23–34.
[303] Takishita T, Ashida K, Nakamura N, Ogi H, Hirao M. Development of shear-vertical-wave point-focusing electromagnetic acoustic transducer. Japanese Journal of Applied Physics 2015;54:07HC04.
[304] Jiao S, Cheng L, Li X, Li P, Ding H. Monitoring fatigue cracks of a metal structure using an eddy current sensor. EURASIP Journal on Wireless Communications and Networking 2016;2016:1–14.
[305] Sato Y, Atsumi T, Shoji T. Continuous monitoring of back wall stress corrosion cracking growth in sensitized type 304 stainless steel weldment by means of potential drop techniques. International Journal of Pressure Vessels and Piping 2007;84:274–83. https://doi.org/10.1016/j.ijpvp.2007.01.004.
[306] Jacobsen C, Zscherpel U, Perner P. A Comparison between Neural Networks and Decision Trees. In: Perner P, Petrou M, editors. Machine Learning and Data Mining in Pattern Recognition, Berlin, Heidelberg: Springer; 1999, p. 144–58. https://doi.org/10.1007/3-540-48097-8_12.
[307] Bayar G, Bilir T. A novel study for the estimation of crack propagation in concrete using machine learning algorithms. Construction and Building Materials 2019;215:670–85.
[308] Papamarkou T, Guy H, Kroencke B, Miller J, Robinette P, Schultz D, Hinkle J, Pullum L, Schuman C, Renshaw J. Automated detection of corrosion in used nuclear fuel dry storage canisters using residual neural networks. Nuclear Engineering and Technology 2021;53:657–65.
[309] Hussain M, Zhang T, Chaudhry M, Jamil I, Kausar S, Hussain I. Review of prediction of stress corrosion cracking in gas pipelines using machine learning. Machines 2024;12:42.
[310] Bale H, Kothari M, Holwell A, Phaneuf M, Gray S, Legget J. Investigation of Stress Corrosion Cracking in CMSX-4 Turbine Blade Alloys Using Deep Learning Assisted X-ray Microscopy. Microscopy and Microanalysis 2022;28:2052–3.
[311] Haboub A, Tariq M, De Sa JDS, Aljaradli M, Farhat H. Deep Learning for Automated Identification of Quasi-Brittle Fractures in 316l Stainless Steel. Available at SSRN 5012225 2024.
[312] Du G, Li J, Wang W, Jiang C, Song S. Detection and characterization of stress-corrosion cracking on 304 stainless steel by electrochemical noise and acoustic emission techniques. Corrosion Science 2011;53:2918–26.
[313] Wu K, Ito K, Shinozaki I, Chivavibul P, Enoki M. A comparative study of localized corrosion and stress corrosion cracking of 13Cr martensitic stainless steel using acoustic emission and X-ray computed tomography. Materials 2019;12:2569.
[314] Calabrese L, Campanella G, Proverbio E. Identification of corrosion mechanisms by univariate and multivariate statistical analysis during long term acoustic emission monitoring on a pre-stressed concrete beam. Corrosion Science 2013;73:161–71.
[315] Zou X. Machine Learning in stress corrosion crack characterisation from full matrix capture ultrasonic signal 2022.

[316] Bayane I, Leander J, Karoumi R. An unsupervised machine learning approach for real-time damage detection in bridges. Engineering Structures 2024;308:117971.
[317] Daniyan I, Balogun V, Ererughurie OK, Daniyan L, Oladapo BI. Development of an inline inspection robot for the detection of pipeline defects. Journal of Facilities Management 2021;20:193–217. https://doi.org/10.1108/JFM-01-2021-0010.
[318] Iqbal J, Tahir AM, ul Islam R, Riaz-un-Nabi. Robotics for Nuclear Power Plants — Challenges and future perspectives. 2012 2nd International Conference on Applied Robotics for the Power Industry (CARPI), 2012, p. 151–6. https://doi.org/10.1109/CARPI.2012.6473373.
[319] La HM, Dinh TH, Pham NH, Ha QP, Pham AQ. Automated robotic monitoring and inspection of steel structures and bridges. Robotica 2019;37:947–67. https://doi.org/10.1017/S0263574717000601.
[320] Santos KR da S, Villani E, de Oliveira WR, Dttman A. Comparison of visual servoing technologies for robotized aerospace structural assembly and inspection. Robotics and Computer-Integrated Manufacturing 2022;73:102237. https://doi.org/10.1016/j.rcim.2021.102237.
[321] Lissenden CJ, Jovanovic I, Motta AT, Xiao X, Le Berre S, Fobar D, Cho H, Choi S. Remote detection of stress corrosion cracking: Surface composition and crack detection. vol. 1949, AIP Publishing; 2018.
[322] Rui W. Study on Non-Destructive Testing System for Corrosion and Crack Inspection of Steel Bridge Based on Magnetic Sensor and Climbing Robot 2016.
[323] Hasanian M, Choi S, Lissenden C. Laser ultrasonics toward remote detection of stress corrosion cracking. Materials Evaluation 2019;77:1089–98.
[324] Sun H, Zhou W, Kang J. A review of crack growth models for near-neutral pH stress corrosion cracking on oil and gas pipelines. J Infrastruct Preserv Resil 2021;2:28. https://doi.org/10.1186/s43065-021-00042-1.
[325] Wang P, Wu H, Liu X, Xu C. Machine Learning-Assisted Prediction of Stress Corrosion Crack Growth Rate in Stainless Steel. Crystals 2024;14:846.
[326] Li Z, Lu Y, Wang X. Modeling of stress corrosion cracking growth rates for key structural materials of nuclear power plant. Journal of Materials Science 2020;55:439–63.
[327] Shi J, Wang J, Macdonald DD. Prediction of primary water stress corrosion crack growth rates in Alloy 600 using artificial neural networks. Corrosion Science 2015;92:217–27.
[328] Wang P, Wu H, Liu X, Xu C. Machine Learning-Assisted Prediction of Stress Corrosion Crack Growth Rate in Stainless Steel. Crystals 2024;14:846.
[329] Lajevardi SA, Shahrabi T, Baigi V, Shafiei M A. Prediction of time to failure in stress corrosion cracking of 304 stainless steel in aqueous chloride solution by artificial neural network. Prot Met Phys Chem Surf 2009;45:610–5. https://doi.org/10.1134/S2070205109050207.
[330] Jiang P. Machine learning methods for corrosion and stress corrosion cracking risk analysis of engineered systems 2018.
[331] Shi J, Wang J, Macdonald DD. Prediction of primary water stress corrosion crack growth rates in Alloy 600 using artificial neural networks. Corrosion Science 2015;92:217–27.
[332] Jiang P, Craig P, Crosky A, Maghrebi M, Canbulat I, Saydam S. Risk assessment of failure of rock bolts in underground coal mines using support vector machines. Appl Stoch Models Bus & Ind 2018;34:293–304. https://doi.org/10.1002/asmb.2273.

[333] Jiang P. Machine learning methods for corrosion and stress corrosion cracking risk analysis of engineered systems. PhD Thesis. UNSW Sydney, 2018.
[334] Qian G, Tantratian K, Chen L, Hu Z, Todd MD. A probabilistic computational framework for the prediction of corrosion-induced cracking in large structures. Scientific Reports 2022;12:20898.
[335] Bakhtiari S, Aldrich C, Calo VM, Iannuzzi M. XGBoost model for the quantitative assessment of stress corrosion cracking. Npj Materials Degradation 2024;8:126.
[336] Ismail MFH, May Z, Asirvadam VS, Nayan NA. Machine-learning-based classification for pipeline corrosion with monte carlo probabilistic analysis. Energies 2023;16:3589.
[337] Rao AY. Development of an artificial neural network model for predicting the stress corrosion cracking behaviors of nucler reactor internal structural materials 2021.
[338] Jiang P, Craig P, Crosky A, Maghrebi M, Canbulat I, Saydam S. Risk assessment of failure of rock bolts in underground coal mines using support vector machines. Applied Stochastic Models in Business and Industry 2018;34:293–304.
[339] Bakhtiari S, Wang K, Calo VM, Iannuzzi M. Revisiting the Copson Curve Using Data Science. Journal of The Electrochemical Society 2023;170:061501.
[340] Bakhtiari S, Aldrich C, Calo VM, Iannuzzi M. XGBoost model for the quantitative assessment of stress corrosion cracking. Npj Materials Degradation 2024;8:126.
[341] Qian G, Tantratian K, Chen L, Hu Z, Todd MD. A probabilistic computational framework for the prediction of corrosion-induced cracking in large structures. Scientific Reports 2022;12:20898.
[342] Najera-Flores DA, Qian G, Hu Z, Todd MD. Corrosion morphology prediction of civil infrastructure using a physics-constrained machine learning method. Mechanical Systems and Signal Processing 2023;200:110515.
[343] Lee D, Huang Y, Achenbach JD. Probabilistic analysis of stress corrosion crack growth and related structural reliability considerations. Journal of Applied Mechanics 2016;83:021003.
[344] Xinyu C, Yingbo Z, Jiaheng L, Hui C. Composition design of 7XXX aluminum alloys optimizing stress corrosion cracking resistance using machine learning. Mater Res Express 2020;7:046506. https://doi.org/10.1088/2053-1591/ab8492.
[345] Bhargava S, Dulikravich ,George S., Murty ,Gollapudi S., Agarwal ,Arvind, and Colaço MJ. Stress Corrosion Cracking Resistant Aluminum Alloys: Optimizing Concentrations of Alloying Elements and Tempering. Materials and Manufacturing Processes 2011;26:363–74. https://doi.org/10.1080/10426914.2010.536938.
[346] Jiang L, Fu H, Zhang Z, Zhang H, Zhang X, Feng X, Xu X, Mao M, Xie J. Synchronously enhancing the strength, toughness, and stress corrosion resistance of high-end aluminum alloys via interpretable machine learning. Acta Materialia 2024;270:119873. https://doi.org/10.1016/j.actamat.2024.119873.
[347] Kang Y, Chen W, Kania R, Boven GV, Worthingham R. Simulation of crack growth during hydrostatic testing of pipeline steel in near-neutral pH environment. Corrosion Science 2011;53:968–75. https://doi.org/10.1016/j.corsci.2010.11.029.
[348] Quej-Ake LM, Rivera-Olvera JN, Domínguez-Aguilar Y del R, Avelino-Jiménez IA, Garibay-Febles V, Zapata-Peñasco I. Analysis of the physicochemical, mechanical, and electrochemical parameters and their impact on the internal and external SCC of carbon steel pipelines. Materials 2020;13:5771.

[349] Quej LM, Míreles MJ, Galvan-Martinez R, Contreras A. Electrochemical Characterization of X60 Steel Exposed to Different Soils from South of México. In: Pérez Campos R, Contreras Cuevas A, Esparza Muñoz R, editors. Materials Characterization, Cham: Springer International Publishing; 2015, p. 101–16. https://doi.org/10.1007/978-3-319-15204-2_11.
[350] SP0204 N. Stress corrosion cracking (SCC) direct assessment methodology. Houston, TX: NACE 2008.
[351] Kuang D, Cheng YF. Study of cathodic protection shielding under coating disbondment on pipelines. Corrosion Science 2015;99:249–57.
[352] Wilmott M, Erno B, Jack T, Worthingham R. The role of coatings in the development of corrosion and stress corrosion cracking on gas transmission pipelines. International Pipeline Conference, vol. 40221, American Society of Mechanical Engineers; 1998, p. 399–408.
[353] Thompson I, Saithala JR. Review of pipe line coating systems from an operators perspective. NACE CORROSION 2013:NACE-2013.
[354] Yatsenko EA, Li W, Izvarin AI, Goltsman BM, Ryabova AV, Kurdashov VM. Review of protective coatings for pipelines. International Journal of Hydrogen Energy 2024;110:656–63.
[355] Hardy SB, Marr JE, Willmot M, Norman D, Khera A. Addressing stress corrosion cracking on multi layer pipeline coating systems 2005.
[356] Samimi A, Zarinabadi S, Samimi S, SETOUDEH M, BARATI A. An analysis of polyethylene coating corrosion in oil and gas pipelines 2012.
[357] Beuker T, Alers R, Brown B, Alers G. SCC detection and coating disbondment detection improvements using the high resolution EMAT ILI-technology. International Pipeline Conference, vol. 41766, 2004, p. 957–61.
[358] Zhao W, Zou Y, Xia DX, Zou ZD. Effects Of Anodic Protection On SCC Behavior Of X80 Pipeline Steel In High-pH Carbonate-Bicarbonate Solution. Archives of Metallurgy and Materials 2015;Vol. 60, iss. 2A. https://doi.org/10.1515/amm-2015-0251.